Early Active Zone Assembly in *Drosophila*

PhD Thesis

in partial fulfillment of the requirements
for the degree “Dr. rer. nat.”
in the Neuroscience Program
at the Georg August University Göttingen,
Faculty of Biology

submitted by

David Owald

born in

Wolfenbüttel

2010

Thesis Committee:

Professor Dr. Erwin Neher, MPI für biophysikalische Chemie Göttingen
Professor Dr. Stephan J. Sigrist, Freie Universität Berlin
Professor Dr. Evgeni Ponimaskin, Medizinische Hochschule Hannover

I hereby declare that this thesis has been written independently and with no other sources and aids than quoted**.**

Göttingen, March 2010

………..………………………

David Owald

Acknowledgements

I would like to begin by thanking my instructor, Professor Dr. Stephan Sigrist, who gave me the opportunity to conduct this work in his laboratory, shared his expertise, and guided me through this PhD thesis.

Likewise, I thank Prof. Dr. Erwin Neher and Prof. Dr. Evgeni Ponimaskin for their guidance and for sharing their expertise with me.

Special thanks to Dr. Robert Kittel, not only for teaching me *Drosophila* electrophysiology, and to Dr. Carolin Wichmann, not only for teaching me electron microscopy. Thanks to Dr. Manuela Schmidt for starting the DSyd-1 project. I would also like to thank Dr. Wernher Fouquet and Omid Khorramshahi for productive discussions and collaborations. Likewise, thanks to Frauke Cristiansen, Harald Depner, Till Andlauer, Peter Engerer, Sara Mertel, Jorg Körner, Dr. Christina Zube, Franziska Zehe, Anastasia Stawrakakis, Madeleine Brünner, Claudia Wirth, along with all further present or past members of the Sigrist lab, and especially Christine Quentin.

I thank Prof. Dr. Albert Sickmann for successful collaboration on BRP interaction partners, and Prof Dr. Hermann Aberle for successfully collaborating on the Neuroligin project.

I wish to thank the members of the Göttingen IMPRS, especially Prof. Dr. Michael Hörner and Sandra Drube, along with my fellow students, for their support.

I would like to further thank members of the Rudolf-Virchow-Center and the Biozentrum in Würzburg, of the ENI and the Max-Planck-Institute for Biophysical Chemistry in Göttingen, and of the NeuroCure in Berlin for great discussions and a great working atmosphere.

I acknowledge all members of the scientific community who shared reagents with us.

Finally, I would like to especially thank my parents, my sister, and Kerstin for their unconditional support.

Contents

1. Introduction 8

1.1. Modules of Chemical Synapses 9
1.2. Modularity of Synapse Assembly 10
1.3. Assembly of the Presynaptic Active Zone 11
1.3.1. Defining the Location 11
1.3.2. Downstream of Cell Adhesion Molecules 12
1.3.3. Continuing towards Maturation 13
1.3.4. A Digital Nature of Active Zone Assembly and Structure? 14
1.3.5. Providing the Backbone 15
1.4. The Synaptic Vesicle Exo/Endo-Cycle Machinery 16
1.4.1. Exocytosis 16
1.4.2. Endocytosis 17
1.5. Transsynaptic Signaling and the Postsynaptic Density 18
1.5.1. Cell Adhesion Molecules 18
1.5.2. Diffusible Retrograde Signals 19
1.5.3. The Postsynaptic Density 20
1.6. Synapse Disassembly 21
1.7. The *Drosophila* Neuromuscular Junction 22
1.8. The Scope of this Thesis 25

2. Material and Methods 27

2.1. Co-Immunoprecipitations and Mass Spectrometry 27
2.2. Antibody Production 27
2.3. Western Blotting 28
2.4. Molecular Cloning 28
2.5. Pulldowns from *Drosophila* Schneider Cells 30
2.6. Yeast Two-Hybrid 30
2.7. Genetics 32
2.7.1. Generation of *dsyd-1* Mutants 32
2.7.2. Other Single and Double Mutants 32
2.7.3. Synthesis of Other Genetic Combinations 33
2.8. Image Acquisition 34
2.9. Immunostainings of Larval and Embryonic NMJs 34
2.10. *In Vivo* Live Imaging of NMJs 35
2.11. Image Processing 35
2.12. Quantifications of AZ/PSD Size and Intensity 36
2.13. Two Electrode Voltage Clamp Recordings 36
2.14. Transmission Electron Microscopy 37
2.15. Behavioral Analysis 38
2.16. Statistics 39

3. Results 40

3.1. BRP is an Integral Element of the Electron Dense Body 40
3.1.1. Truncated BRP gives Truncated T bars 42
3.1.2. Functional Analysis of a New Severe *brp* Allele 42

3.2. DSyd-1 Regulates Initial Active Zone Formation 44

3.2.1. *Drosophila* Syd-1 is a BRP-associated Protein 44
3.2.2. Reduced Lifespan and Impaired Behavior of *dsyd-1* Deficient Flies 45
3.2.3. DSyd-1 Localizes to Active Zones 48
3.2.4. Reduced Evoked Current Amplitudes at *dsyd-1* Mutant NMJs 49
3.2.5. Reduced Numbers of Synaptic Release Sites at *dsyd-1* Mutant NMJs 51
3.2.6. Defective Active Zone Assembly and Ectopic BRP Accumulations at *dsyd-1* Mutant Terminals 53
3.2.7. Dense Body Morphology at *dsyd-1* Mutant AZs 56
3.2.8. DSyd-1 Regulates AZ Morphology Dependent on DLiprin-α 57

3.3. DSyd-1 in the Assembly of Nascent Active Zones 60
3.3.1. DSyd-1 and DLiprin-α Arrive Early at Nascent Active Zones 60
3.3.2. Dynamic, Often Reversible Assembly of DLiprin-α and DSyd-1 during Initial Active Zone Assembly 61
3.3.3. DSyd-1 is Needed for Proper Active Zone Localization of DLiprin-α - but Not *Vice Versa* 64
3.3.4. DSyd-1 Stalls DLiprin-α at Nascent Synaptic Sites 66

3.4. Presynaptic DSyd-1 Controls the Composition of Postsynaptic Glutamate Receptor Fields 68
3.4.1. Shifted Glutamate Receptor Composition in *dsyd-1* Mutants 68
3.4.2. Presynaptically Differentiated Boutons Lacking Postsynaptic Glutamate Receptors in *dsyd-1* Mutants 71
3.4.3. *Drosophila* Neuroligin1 localizes adjacent to glutamate receptor fields. 73
3.4.4. Mutants for *Drosophila* Nlg1 Show Presynaptically Differentiated Boutons Lacking Postsynaptic Differentiation 75
3.4.5. eEJC Amplitudes are Reduced in *dnlg1* Mutants 75
3.4.6. DNlg1 Localization is Affected in *dsyd-1* Mutants 76

3.5. Components of the Exo/Endo-Machinery Interact with BRP 78
3.5.1. BRP and Dynamin Physically Interact 79

4. Discussion **82**

4.1. The BRP Protein Shapes the Electron Dense Specialization at *Drosophila* Synapses 83
4.2. DSyd-1 Stalls DLiprin-α at Nascent AZs 86
4.3. Premature "Precipitation" of BRP in *dsyd-1* Mutants 87
4.4. Both DSyd-1 and DLiprin-α promote synapse assembly but are not fully essential 90
4.5. DSyd-1 and DLiprin-α Define a Novel Subcompartment at the AZs Edge 91
4.6. Timing of Synaptic Assembly 91
4.7. Early AZ Assembly Appears Reversible at *Drosophila* NMJs 93
4.8. Potential Modes of DSyd-1 Regulation 95
4.9. DSyd-1 Regulates the Postsynaptic Compartment 96
4.10. *Drosophila* Neurexin is a Potential Second Substrate for DSyd-1 97
4.11. A Possible Link to Autism Spectrum Diseases? 99
4.12. Does the CAZ Interact with the Exo/Endo-Cycle? 100

5. Summary **103**

6. References **105**

7. Figure Index 126

8. Abbreviations.. 129

9. *Curriculum Vitae* 132

10. Scientific Abstracts at International Conferences.. 132

11. Publications 133

1. Introduction

In 400 B.C., Aristotle developed the concept of the *vital pneuma*, which is transmitted to muscles via the blood stream. Here, the muscle's *psyche* was said to mediate contraction leading to locomotion (Bennett, 1999). In the 17th century, Descartes coined the term *animal spirit*: particles that are transmitted via nerves during transmission (Bennett, 1999). These were later shown to be of electrical nature by Galvani (Bennett, 1999; Galvani, 1791). Helmholtz and others finally showed that nerves possessed a potential which could be transmitted to muscles at a specialized site. This was named *synapse* by Sherrington at the end of the 19th century (Bennett, 1999; Foster, 1897; Helmholtz, 1850). Neuroanatomic studies by y Cajal showed that nerve endings were not continuous with their targets (y Cajal, 1894), while for example Golgi believed in the existence of a continuous syncytium of nervous tissue (Sotelo, 2003).

It was up to Loewi to then reveal that the gap between nerve endings and targets was bridged by chemical compounds [neurotransmitters, (Friedman, 1971)]. Subsequently, the work of Hodgkin and Huxley showed that electrical potentials were transduced via action potentials [APs, (Hodgkin and Huxley, 1952)] and Bernhard Katz discovered that neurotransmitter release was Ca^{2+}-dependent (Katz and Miledi, 1965). Moreover, neurotransmitters were discovered to be released in a quantal manner (Del Castillo and Katz, 1954): a single quantum was found to correspond to the amount of neurotransmitter stored in a single synaptic vesicle (SV). With the advent of the patch clamp technique, it became clear that presynaptically released neurotransmitters would open single ion channels at the postsynaptic site (Neher and Sakmann, 1976).

Finally, both nerve endings, not continuous (chemical synapses) and continuous (electrical synapses) with their targets, co-exist. Electrical synapses, allowing for direct cell to cell coupling consist of intercellular channels that mediate direct and fast conductance of ionic signals and small second messenger molecules (e.g. cAMP). These gap junctions thus allow for rapid synchronization of cell ensembles (Hormuzdi et al., 2004). The following will deal exclusively with chemical synapses.

1.1. Modules of Chemical Synapses

At chemical synapses electrical information gets relayed into chemical intermediates and back into electrical signals. Thus, electrical activity arriving at the presynaptic terminal triggers the release of neurotransmitter molecules, which activate postsynaptic receptors, leading to a change in membrane potential.

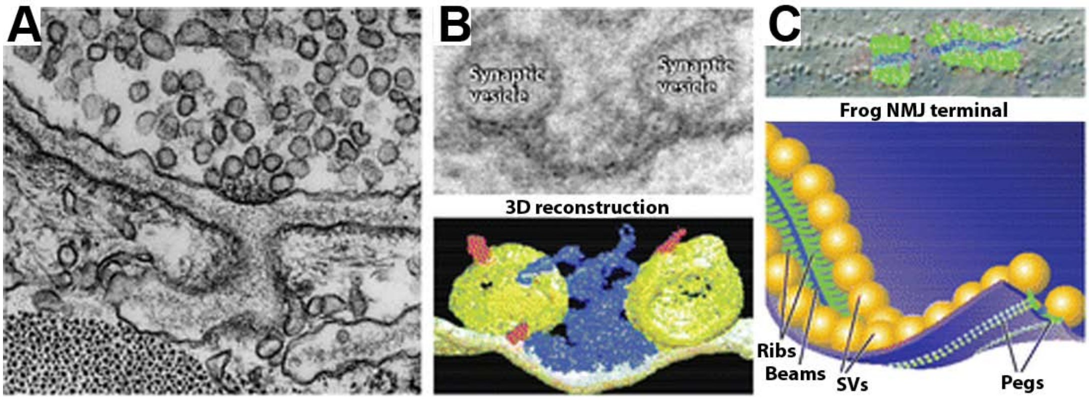

Fig. 1 AZ ultrastructure
A) Electron micrograph of the frog NMJ shows electron dense material (CAZ) at the presynaptic membrane opposing the postsynaptic compartment. This proteinacious material is surrounded by SVs. **B**) Docked SVs at the presynaptic membrane. Tomography reveals electron dense projections in close proximity to SVs. **C**) Freeze fracture replica shows pegs which might reflect Ca^{2+} channels. These are connected by Ribs (green) emerging from beams (blue), which might represent individual AZ building blocks (Harlow et al., 2001). SVs (yellow) are organized along the ribs in close proximity to pegs. Modified from Jin and Garner (2008).

For functionality, chemical synapses depend on the proper interplay of several “modules” (highlighted in *italics*). At the presynaptic site, the *active zone* [AZ, (Couteaux and Pecot-Dechavassine, 1970)] provides the platform for rapid fusion of neurotransmitter-filled SVs after Ca^{2+} influx. The AZ membrane is decorated by a proteinacious cytomatrix (cytoplasmic matrix at the active zone – CAZ, Fig. 1A-C), which is characterized by a set of specialized proteins (Owald and Sigrist, 2009). In electron micrographs the CAZ appears electron dense and is easily visible, contrasting the cytoplasm, the presynaptic membrane and SVs. While CAZs display variable morphologies at different synapse types, they are likely to be critical for the effective organization of the associated SV *exo/endo-cycle* machinery (Siksou et al., 2007; Zhai and Bellen, 2004). Moreover, AZ-resident electron dense material often appears filamentous and in direct contact with SVs, suggesting a possible involvement in SV tethering. It is thus to be expected that a certain degree of synaptic precision depends on molecular interactions of CAZ proteins.

Between the pre- and postsynaptic membrane, a synaptic cleft of defined width is found. This cleft is meant to be organized by *transsynaptic* pairs of cell adhesion molecules. As released neurotransmitters need to bridge this gap, mechanisms involving neurotransmitter clearance and degradation give rise to regulatory mechanisms.

At the postsynaptic site, neurotransmitter receptors accumulate within another electron dense compartment, the *postsynaptic density* (PSD). Here, the stability and dynamic regulation of neurotransmitter receptor populations is regulated (Renner et al., 2008). Thus, ionotropic receptors with differing conductivity or ion specificity contribute to defining the precise characteristics of a synapse. Additionally, metabotropic seven transmembrane receptors can come into play. These activate G-proteins upon ligand-binding, which can then either directly regulate ionotropic receptors or second messenger pathways (Woehler and Ponimaskin, 2009).

1.2. Modularity of Synapse Assembly

Under physiological conditions it is to be expected that synaptic modules closely communicate to fine-tune the synapse assembly process. In order to understand the composition of the mentioned modules, it will, however, be important to know whether one may study them as autonomous entities. In other words, are synaptic modules independent units of assembly or does their formation require the presence of a synaptic site, assembling the other modules parallel to it?

Multiple findings argue in favor of units being able to self-assemble (at least to some degree). Vesicle fusion activity can be reconstituted *in vitro*, in the absence of cytomatrix scaffolds and even of Ca^{2+} (Holt et al., 2008). In immature neurons, mobile moving clusters of SVs have been observed (Krueger et al., 2003), exchanging with the neuronal plasma membrane in the absence of postsynaptic differentiation. Furthermore, in genetically engineered *Drosophila* embryos, presynaptic AZs can form in the complete absence of postsynaptic partner cells and thus of any postsynaptic specializations (Prokop et al., 1996).

Notably, presynaptic differentiation, including the formation of AZs in cultured neurons, can be induced by the presentation of single postsynaptic cell adhesion proteins (Neuroligin, SynCAM1) expressed on non-neuronal cells (Akins and Biederer, 2006; Scheiffele et al., 2000). *Vice versa*, postsynaptic differentiation is inducible by the Neuroligin-interactor Neurexin (Graf et al., 2004). Additionally, postsynaptic differentiation can occur prior to formation of a detectable functional presynaptic AZ in young hippocampal neurons (Gerrow et al., 2006).

Thus, vesicle release machinery, AZ matrix and to some degree the postsynaptic specialization can (under certain experimental circumstances) display intrinsic assembly propensities and form “in isolation”. This intrinsic assembly propensity might become dominating when physiological signals from other synaptic modules are missing after genetic intervention (Owald and Sigrist, 2009).

1.3. Assembly of the Presynaptic Active Zone

Proteins organizing AZ assembly are likely part of the CAZ themselves. Due to the low solubility of AZ material, the biochemical identification of AZ proteins has lagged behind the characterization of ion channels and SV proteins, with fundamental components still awaiting a functional characterization. Recently, however, unbiased genetic approaches [especially studies from the *C. elegans* HSNL synapse and the *Drosophila* NMJ (Collins and DiAntonio, 2007; Margeta et al., 2008)] have identified several presynaptic proteins as important for AZ assembly [Fig. 2, (Owald and Sigrist, 2009)]. In the following, the role of these proteins will be looked into in more detail.

1.3.1. Defining the Location

Up high in a hierarchy of assembly events, a membrane district suitable for the formation of a new AZ needs to be defined. In *C. elegans*, the immunoglobulin containing cell adhesion molecules Unc 40/DCC, as well as the heterophilic interaction pair Syg-1/Neph1 and Syg-2/Nephrin have been shown to be important in this respect, though at different synapse populations (Chao and Shen, 2008; Colon-Ramos et al., 2007; Shen et al., 2004). As other IgCAMs might take over similar functions in *Drosophila* and mice, it appears that cell adhesion codes triggering initial assembly have diverged between synapse types as well as between species (Fig. 2).

Along with defining the location where synapses form, pre- and postsynaptic cell adhesion molecules might coordinate the formation of postsynaptic structures (see 1.5.1), tightly coupled to ongoing clustering of AZ components (Owald and Sigrist, 2009).

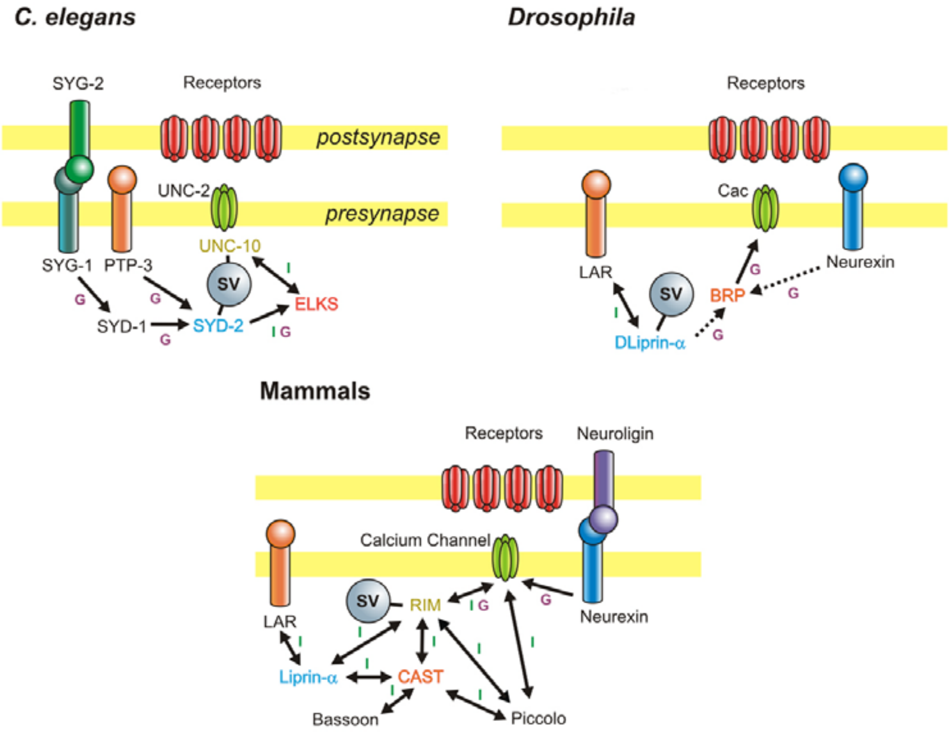
C. elegans
SYG-2
Receptors
postsynapse
UNC-2
presynapse
UNC-10
SYG-1
PTP-3
SV
ELKS
SYD-1
SYD-2
Drosophila
Receptors
Cac
LAR
SV
BRP
Neurexin
DLiprin-α
Mammals
Receptors
Neuroligin
Calcium Channel
SV
RIM
LAR
Neurexin
Liprin-α
CAST
Bassoon
Piccolo

Fig. 2 Proteins implicated in AZ assembly
A summary of proteins considered to be important players for AZ assembly. Results from different model organisms are depicted in separated panels. Syd-2/Liprin-α family proteins are highlighted in blue, ELKS/BRP/CAST in red and Unc 10/Rim in yellow. The type of interaction is indicated by letters above the arrows: I = direct physical interaction, G = genetic interaction/ regulation inferred from genetic findings. Dashed lines indicate indirect evidence of interaction from imaging data. Modified from Owald and Sigrist (2009).

1.3.2. Downstream of Cell Adhesion Molecules

Downstream of cell adhesion molecules, Syd-2/Liprin-α was found to be crucial for AZ assembly and SV clustering in *C. elegans* and *Drosophila* (Dai et al., 2006; Kaufmann et al., 2002; Miller et al., 2005; Patel et al., 2006). The Syd-2/Liprin-α family is characterized by alpha-helical coiled coil and SAM domains, and has been implicated in both pre- and postsynaptic assembly by recruiting and interacting with a multitude of synaptic proteins and by regulating synaptic cargo transport (Spangler and Hoogenraad, 2007). Thus, Syd-2/Liprin-α might guide transport of further components to the AZs, with its described binding partners being prime candidates to be relevant cargo (see Fig. 2).

In addition to Syd-2/Liprin-α, a C2-domain and putative RhoGAP-domain containing protein named Syd-1 was found to be essential for AZ assembly at the HSNL synapse of *C. elegans* (Dai et al., 2006; Patel et al., 2006). There, Syd-1 seems to help the functional recruitment of Syd-2/Liprin-α, since a gain of function allele of *syd-2* [a missense mutation in a coiled coil domain of Syd-2, *syd-2(gf)*], allows the suppression of Syd-1 requirement (Dai et al., 2006; Owald and Sigrist, 2009).

1.3.3. Continuing towards Maturation

Which other AZ proteins interact functionally with Syd-2/Liprin-α throughout AZ assembly? Among the Syd-2/Liprin-α binding partners, Rim/Unc 10s are specific AZ proteins. However, Rim/Unc 10s so far appear dispensable for principal AZ assembly in both mouse and worm (Calakos et al., 2004; Patel et al., 2006), though they are important to functionally anchor neurotransmitter-containing vesicles in the vicinity of voltage-operated Ca^{2+} channels (Kiyonaka et al., 2007) and to target SVs to the AZ membrane (Weimer et al., 2006).

Notably, the activity of Syd-2(gf) in *C. elegans* does not depend on Rim/Unc 10 or Ca^{2+} channels (Unc 2), but instead requires ELKS 1, a member of the CAST/ERC family (Dai et al., 2006). CAST (CAZ-associated structural protein) was originally identified biochemically as an AZ associated coiled coil domain protein (Ohtsuka et al., 2002), which interacts with Bassoon, Piccolo, Rim 1 and Liprin-α (Ko et al., 2003; Ohtsuka et al., 2002; Takao-Rikitsu et al., 2004). *Drosophila* Bruchpilot (BRP), whose N-terminal half encodes the *Drosophila* CAST homologue (Kittel et al., 2006; Wagh et al., 2006), proved to be crucial for proper clustering of Ca^{2+} channels within AZs, CAZ formation and efficient neurotransmitter release (Kittel et al., 2006).

Two further large scaffolding molecules, Piccolo and Bassoon, were among the first AZ specific proteins to be identified (Cases-Langhoff et al., 1996; tom

Dieck et al., 1998). Not conserved in *Drosophila* or *C. elegans*, they turned out to be specific to vertebrate synapses. While Piccolo seems dispensable for principal AZ assembly at glutamatergic synapses [however, important for function, (Leal-Ortiz et al., 2008)], Bassoon is reported to play an important role in the assembly and functioning of various types of synapses (Schoch and Gundelfinger, 2006), and to be amongst the first proteins that appear at newly forming AZs (Owald and Sigrist, 2009; Regus-Leidig et al., 2009).

1.3.4. A Digital Nature of Active Zone Assembly and Structure?

A principal question arising is whether preassembled units of AZ proteins are shipped to prospective AZs, or whether AZs assemble *de novo* from diffuse pools of the relevant proteins. Additionally, after AZ assembly, would the strength of an individual synapse (Atwood and Karunanithi, 2002) be regulated by the addition or subtraction of individual modules? In fact, presynaptic proteins have been suggested to be transported in specialized 80 nm dense core transport vesicles positive for the mammalian AZ markers Piccolo and Bassoon [and were thus named Piccolo-and-Bassoon transport vesicles, PTVs, (Garner et al., 2006)]. It was suggested that PTVs carry a comprehensive set of AZ materials [including CAST as well as Rim 1/Unc 10, Munc 13/Unc 13 and Munc 18/Unc 18 (Shapira et al., 2003; Zhai et al., 2001)], providing unitary building blocks for AZs.

However, the situation appears to be more complex. Immuno-electron microscopic analysis could validate that in fact Piccolo and Bassoon decorate both small clear and dense core vesicles, whereas SV proteins are mostly confined to small clear vesicles (Tao-Cheng, 2007). Both dense core and SVs seem to be transported in a preassembled multi-vesicle transport aggregate (Tao-Cheng, 2007), with the potential to rapidly form functional presynaptic sites. Notably, extra-vesicular electron dense material and filaments connecting SVs are observed at multi-vesicle transport aggregates as well.

Potentially reflecting a modular mode of synapse assembly, an electron tomography study of rat neocortical synapses (Zampighi et al., 2008) indicated that AZ architecture might be arranged from several “synaptic units”. Polyhedral cages surrounded by a subset of SVs are shown to be associated with cytomatrix filaments. Surprisingly, these polyhedral cages (“syndesomes”) resemble Clathrin cages, which so far have only been discussed in the context of vesicular endocytosis.

At mammalian ribbon synapses, AZ components form electron dense precursors, instead of being transported to AZs by membranous compartments (Regus-Leidig et al., 2009). Here, Bassoon and Piccolo assemble early together with RIBEYE and Rim, whereas other synaptic players, such as Munc 13, Ca^{2+} channels or CAST, accumulate late during synapse assembly (Regus-Leidig et al., 2009), probably marking a later maturation process. Thus, at least at this specialized synapse, not all players seem preassembled but rather arrive in a sequential fashion (Owald and Sigrist, 2009).

1.3.5. Providing the Backbone

Changes in the synaptic protein composition form a basis for synaptic plasticity. With the advent of live fluorescent imaging, a picture of high protein flux at synapses (Renner et al., 2008), with dynamic proteins often exchanging on a minutes time scale, has emerged.

The CAZ is resistant to chemical extraction procedures (Phillips et al., 2001), making it a candidate for a “core scaffold” that specifies and maintains the position of membrane-associated molecules as well as the exo/endocytic-machinery and SV clusters (Tsuriel et al., 2009). Interestingly, at mammalian AZs, the priming factor Munc 13 shows rapid exchange (Kalla et al., 2006), while Bassoon exhibits high retention times in cultured hippocampal neurons (Tsuriel et al., 2009) and remains static after stimulation (Tao-Cheng, 2006). This indicates that Bassoon might be part of a relatively static core scaffold in contrast to Munc 13, which is directly associated with the process of neurotransmitter exocytosis. Thus, presynaptic tenacity, to a large degree, might be based on the tenacity of the CAZ. The CAZ might be constructed of a more or less static backbone (e.g. Bassoon) and mobile machinery (e.g. Munc 13). It appears likely that such cooperative protein scaffolds with stable interactions provide nucleation zones (meaning hot spots for synaptic proteins to associate) for the clustering of less static synaptic proteins in a dynamic equilibrium (Owald and Sigrist, 2009).

1.4. The Synaptic Vesicle Exo/Endo-Cycle Machinery

Assembled AZs provide the framework for the process of neurotransmitter release to function in a precise and highly specific manner, and thus for the core proteins of the secretory release machinery to exert their action.

1.4.1. Exocytosis

For exocytosis to take place, SVs, filled with neurotransmitters, need to fuse with the presynaptic plasma membrane. Therefore, SVs need to be tethered to the (C)AZ, and subsequently docked to the presynaptic plasma membrane. The molecular basis for the docking step at AZs has remained enigmatic so far (Rizo and Rosenmund, 2008). Work from *C. elegans* synapses and chromaffin cells, however, indicated that the docking step might be regulated by the t-SNARE Syntaxin in concert with SM (Sec 1/Unc 18/Munc 18-1) as well as Munc 13 proteins (Rizo and Rosenmund, 2008; Toonen and Verhage, 2007).

The v-SNARE Synaptobrevin, residing on SVs, associates with the plasma membrane t-SNARES (Syntaxins and SNAP-25) via alphahelical stretches. Interaction starts at the N-term of the proteins and is transduced (“zippered”) to the C-term (Fang et al., 2008; Sorensen et al., 2006). This process transfers energy, needed for the membranes to fuse. The release probability of a SV increases via further transitions, including molecular and positional priming [Fig. 3A, (Neher and Sakaba, 2008)]. Along with the Rab3 effector Rim (Castillo et al., 2002; Schoch et al., 2002), and more recently ELKS (Kaeser et al., 2009), Unc 13/Munc 13s (Betz et al., 1998) are considered to be crucial for the molecular priming of vesicle release (Rosenmund et al., 2003), potentially via opening Syntaxins (Guan et al., 2008). Complexins also associate with SNARES and appear to be able to both facilitate and inhibit SV fusion (Xue et al., 2009).

However, the crucial signal needed for fusion of the membranes is the local influx of Ca^{2+} at AZs. Ca^{2+} binds to SV-resident Synaptotagmin (Sudhof, 2004; Takamori et al., 2006), which functions as a rapid Ca^{2+} sensor, further facilitating membrane fusion. The release probability of a single vesicle was shown to depend on the amount of Ca^{2+} ions in its direct vicinity (Wadel et al., 2007). Thus, the distance that separates a Ca^{2+} channel [approximately 20 per AZ at the calyx of Held synapse (Meinrenken et al., 2003; Satzler et al., 2002)] and its corresponding

Ca^{2+} nanodomain from the molecularly primed vesicle is regarded as a key parameter controlling release probability.

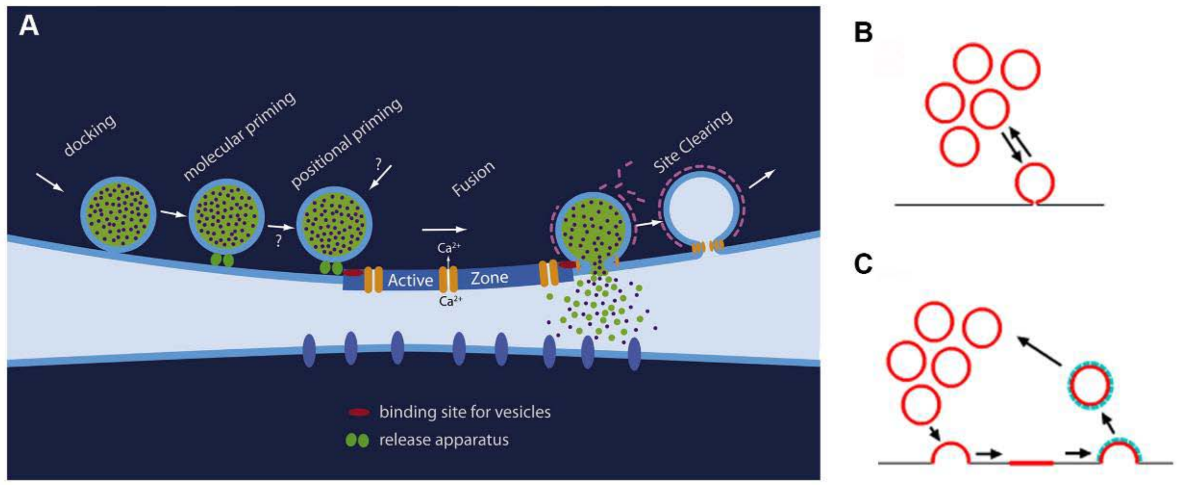

Fig. 3 The SV exo/endo-cycle
A) A schematic overview of SV exocytosis including docking, molecular priming and positional priming. How vesicles are tethered and positionally primed, remains to be investigated. After SV fusion, release sites need to be cleared of SV membranes and proteins. Adapted from Neher and Sakaba (2008). **B-C**) Two modes of endocytosis. B) depicts the heavily debated mechanism of kiss and run. In this model, SV do not fully collapse into the presynaptic plasma membrane, but rather release neurotransmitters via a narrow fusion pore. The intact (but empty) SV hereafter is pinched off at the site of neurotransmitter release and can be reused (after refilling) rapidly. C) Classical endocytosis involves full collapse of the SV membrane into the presynaptic plasma membrane. Lipids and proteins diffuse laterally to the periactive zone, where Clathrin coated vesicle pits are taken up. This mode of endocytosis is widely agreed on. B-C) are modified from Rizzoli and Jahn (2007). Further possible modes of endocytosis, e.g. bulk uptake are not shown here.

1.4.2. Endocytosis

After SVs have released their neurotransmitters into the synaptic cleft, both SV lipids and proteins need to be retrieved and recycled to form new neurotransmitter-filled SVs (Fig. 3B and C). Following Heuser and Reese, who observed an increase in coated vesicles after stimulation on ultramicrographs (Heuser and Reese, 1973), studies of the last decades came up with one prime model of vesicle recycling, comprising the full collapse of the SV membrane into the plasma membrane and lateral diffusion of SV components to periactive compartments. Here, adaptor proteins recruit Clathrin to the plasma membrane, and SV precursors bud, while fission of the membranes is mediated by the GTPase Dynamin. Overwhelming evidence (Rizzoli and Jahn, 2007) suggests that this is a major mode of vesicle recycling (Fig. 3C). However, certain findings have argued for the necessity of a more rapid mode of recycling. This model comprises a transient formation of a fusion pore and subsequent pinching-off of the SV for rapid reuse (Fig. 3B). Many studies have indicated the existence of such a mechanism [e.g. (Zhang et al., 2009), also see (He and Wu, 2007)]. These include mutant analyses of the endocytic proteins Endophilin and Synaptojanin (Pawlu et al., 2004; Verstreken et al., 2002), which, however, were challenged afterwards (Dickman et al., 2005). Especially work on temperature sensitive mutants of *Drosophila* Dynamin (*shibire*^{TS} alleles) has indicated a role of the protein in endocytosis at AZs. Here, membrane invaginations at AZs were observed after recovery from non-permissive temperature (Koenig et al., 1998). Along with the classical non-AZ mode of endocytosis, a distinct endocytic pathway operating within AZs is proposed in these studies (Koenig et al., 1998). However, further work on *shibire*^{TS} also suggested a role of Dynamin in release site replenishment (Kawasaki et al., 2000).

1.5. Transsynaptic Signaling and the Postsynaptic Density

Transsynaptic signals emanating from pre- and postsynaptic cell adhesion molecules seem to coordinate the assembly of postsynaptic structures in tight coupling to ongoing clustering of AZ components. Moreover, synaptic strength (Atwood and Karunanithi, 2002) and maintenance appear to be dependent on transsynaptic signaling pathways.

1.5.1. Cell Adhesion Molecules

Transsynaptic protein complexes can play major roles during synapse assembly (see 1.3.1.); they have, nonetheless, also been implicated in synapse maintenance and function. Dissecting roles in assembly, maturation and function has, however, remained difficult. For example, N-cadherins have been reported necessary for target selection in the *Drosophila* optic neuropil (Prakash et al., 2009), while in vertebrates they have rather been implicated in synapse maturation and function (Akins and Biederer, 2006).

The complex formed by Neurexins and Neuroligins (Ichtchenko et al., 1995) has made them prototypical candidates for synaptic cell adhesion molecules due to the molecular asymmetry of their heterophilic binding, reflecting the asymmetric nature of the synapse. Their role in synapse function and structure has been explored in knockout mice and in cell culture assays (Caroni and Scheiffele, 2008). Overall, the findings in Neurexin- and Neuroligin-deprived or -manipulated situations have shown dramatic impairments in both the structural and functional assembly of synapses (Garner et al., 2006; Li et al., 2007; Missler et al., 2003; Varoqueaux et al., 2006). However, while *in vitro* both Neurexins and Neuroligins are synaptogenic (Graf et al., 2004; Scheiffele et al., 2000), Neuroligin knock-out mice appear to have morphologically intact synaptic connections, while synaptic transmission appears altered (Varoqueaux et al., 2006).

Retrograde modulation of presynaptic release might be mediated by PSD-95-Neuroligin signaling. Interestingly, PSD-95 has been shown to redistribute rapidly *in vivo* at the mouse neocortex, while retention times increased with increasing developmental age (Gray et al., 2006). Alongside with the Neurexin-Neuroligin pair, IgCAMs, and Nephrins (see 1.3.1), Ephrin ligand-Ephrin receptor interactions have been shown to regulate synapse formation via bidirectional signaling (Klein, 2009). Thus, Ephrin B reverse signaling is involved in maturation of synapses in a structural as well as in a functional manner.

1.5.2. Diffusible Retrograde Signals

Diffusible retrograde signals emanating from the postsynaptic compartment mark a further class of transsynaptic signals. For example, postsynaptically released nitric oxide has been proposed to regulate presynaptic endocytosis (Micheva et al., 2003).

Drosophila Synaptotagmin IV is crucial for Ca^{2+} triggered exocytosis of postsynaptic vesicles. Downstream signaling results in activation of the presynaptic cAMP-dependent protein kinase pathway (Yoshihara et al., 2005). Moreover, postsynapically released neurotrophic factors appear to modulate presynaptic transmission (Gottmann et al., 2009). However, further signals released from the presynaptic side can influence the postsynaptic compartment.

Thus, the synaptogenic morphogen Wnt has been shown to be transported transsynaptically in vesicles containing the protein Evi (Korkut et al., 2009).

1.5.3. The Postsynaptic Density

While signals released from the postsynaptic compartment can regulate presynaptic stability, presynaptic signals can regulate the integrity of the postsynaptic compartment. At synapses, the PSD is defined via its receptor composition as well as scaffolding proteins interlinking receptors and further postsynaptic proteins.

Excitatory synapses in the mammalian brain are predominantly glutamatergic (Seeburg, 1993). Apart from other excitatory neurotransmitter systems (e.g. acetylcholine), inhibitory synapses (e.g. GABAergic) play major roles in wiring the CNS in mammals. The following discussion will concentrate on glutamatergic synapses.

For mammalian glutamatergic synapses ionotropic receptors either belong to the NMDA-, AMPA- or kainate specific receptor complexes, which differ in several parameters, including their conductance, desensitization properties, or ion specificity (Nicoll and Schmitz, 2005). For example, NMDA receptors, in the open state, show high degrees of Ca^{2+} permeability. Ca^{2+} can signal via, amongst others, the CamKII (Mayford et al., 1997) pathway, playing a role in long-term potentiation of synapses (LTP). LTP, together with long-term depression, appears to be necessary for formation of memory and learning processes (Bliss and Lomo, 1973; Collingridge and Bliss, 1995). Thus, basal synaptic transmission can be mediated by AMPA receptors only, and synapses solely comprising NMDA receptors remain silent (Cingolani and Goda, 2008). These synapses can incorporate AMPA receptor complexes upon induction of LTP (Shi et al., 1999). Regulation of the receptor complex composition of PSDs hence defines the strength and properties of synapses. Receptors can hereby be recruited from diffuse pools in the plasma membrane by lateral diffusion (Frischknecht et al., 2009), or by transport from intracellular pools (Barry and Ziff, 2002).

At glutamatergic mammalian synapses, AMPA receptor complexes are recruited in a subunit-specific manner at Neurexin-Neuroligin contacts (Heine et al., 2008). On the other hand, the Ephrin B receptor appears to directly cluster

NMDA receptors (Dalva et al., 2000; Lim et al., 2008). Indeed Ephrins play a prime role in homeostatic signaling at the *Drosophila* NMJ (Frank et al., 2009a), linking DGluRIIA-dependent homeostasis to the Rho Cdc42 and presynaptic Ca^{2+} channels. Cdc42, in turn, might play a role in regulating Actin dynamics at the synapse (Cingolani and Goda, 2008).

1.6. Synapse Disassembly

During nervous system development, synaptic circuitry must be defined by forming synaptic connections with high spatio-temporal precision. While developmental synapse formation seems to proceed properly in the absence of neurotransmission, as for example seen in *Drosophila unc 13* mutants (Aravamudan et al., 1999), neuronal activity can trigger changes in the molecular composition and functional status of synapses. Early circuit formation comprises both the assembly and the disassembly of individual synapses. Here, transmembrane proteins might be involved in stabilizing synaptic contacts. Moreover, pioneering the field, Wiesel and Hubel found that stimuli were necessary to wire ocular dominance columns (Hubel and Wiesel, 1959). Thus, activity appears to be crucial for neural circuit development. Information might well be conferred via mechanisms, such as LTP or spontaneous activity (Katz and Shatz, 1996).

Dismantling of synapses can lead to *input elimination*, where a cell loses all connections to its target, or more subtle *synapse disassembly* comprising the removal of a certain population of synapses (Eaton et al., 2002; Goda and Davis, 2003). These processes may well be driven by synaptic activity.

At the vertebrate NMJ, synaptic activity seems to stabilize synaptic contacts (on molecular terms), as inferred from elevated acetylcholine receptor dynamics after blocking neurotransmission (Akaaboune et al., 1999). Similarly, at the *Drosophila* NMJ, receptor clustering appears dependent on presynaptic stimuli (Featherstone and Broadie, 2000). These appear to be activity dependent, yet not dependent on neurotransmitter release, as inferred from tetanus toxin (which abolishes neurotransmitter release) experiments (Featherstone and Broadie, 2000).

Interestingly, the protein Rsy-1 has been shown to locally regulate synapse disassembly in *C. elegans* (Patel and Shen, 2009). Whether this process is dependent on synaptic activity remains unanswered.

1.7. The *Drosophila* Neuromuscular Junction

Thomas Hunt Morgan introduced *Drosophila melanogaster* (the fruit fly) to modern genetic research at the beginning of the 20th century. Since then, this model system has proven valuable in cell and developmental biological research, as well as the neurosciences. Being confound to a relative simple genetic architecture comprising two (and a very small) autosomes, the euchromatic portion of the *Drosophila* genome comprises approximately 120 megabases, encoding for approximately 13,600 genes (Adams et al., 2000). Thus, although with comparable functional diversity, the *Drosophila* genome encodes for less genes than the nematode *C. elegans* (Adams et al., 2000). Genetic variants can be kept stable over generations by use of balancer chromosomes, which through inverted segments have made meiotic recombination (which only occurs in females) with "normally organized" chromosomes unlikely (Thompson, 1977).

P-element based genetics have made the fly widely accessible to transgenesis. Especially the use of the *Gal4*-UAS system has revolutionized the field making tissue and temporally specific expression feasible (Brand and Perrimon, 1993). Easy and cheap handling of *Drosophila*, along with its short generation time, have made this model prone to large scale forward genetic screens (Featherstone and Broadie, 2000).

The *Drosophila* NMJ synapses are glutamatergic and the synaptic cleft between presynapse and muscle does not exceed 20 nm. Therefore, *Drosophila* NMJ synapses rather seem to resemble mammalian central synapses [with e.g. similar modes of glutamate receptor regulations (Featherstone and Broadie, 2000)] than mammalian cholinergic NMJs in some aspects.

The embryonic development of the *Drosophila* NMJ comprises the fusion of multiple myoblasts to form a multinucleate fiber (Bate et al., 1993). Thereafter motoneuronal growth cones contact the muscles and appropriate attempts are stabilized by focal contacts (Rheuben et al., 1999; Ritzenthaler et al., 2000). Two motoneurons, with their axons emerging from the ventral nervous system, innervate the embryonic and larval NMJ of muscle 6 and 7 (for a schematic overview see Fig. 4A and B). This innervation can be subdivided into two types of bouton, those of small (Is) and those of large diameter [Ib, Fig. 4B, (Atwood et al., 1993; Feeney et al., 1998)]. The segmental organization of body wall muscles and innervations is highly stereotypical at this stage (Fig. 4C). Resembling “pearls on a string” (Fig. 5A), individual boutons comprising AZs are interconnected by axonal cytoplasm.

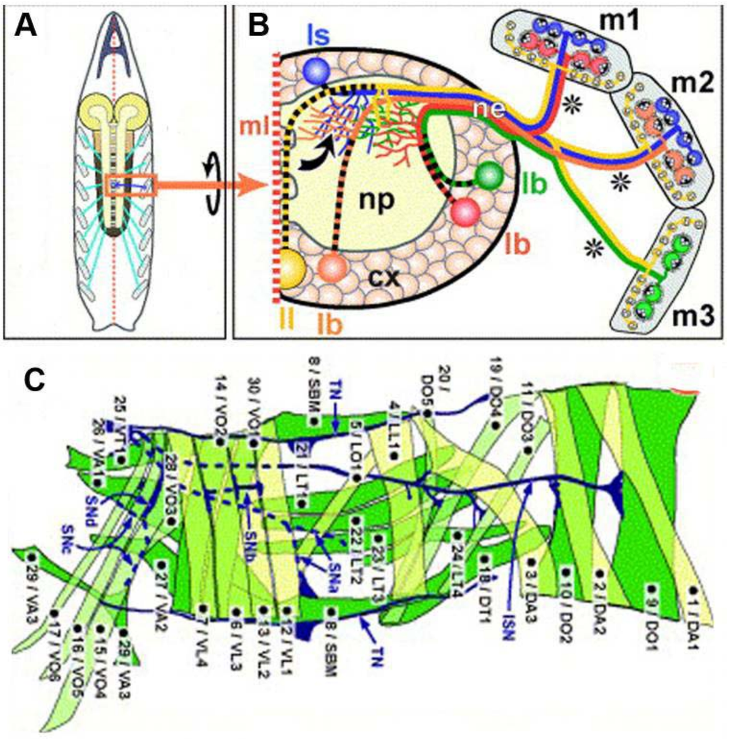
A
B
Is
m1
m2
m3
ml
ne
np
Ib
Ib
cx
II
Ib
C
25 / VT1
26 / VA1
SNd
SNc
29 / VA3
17 / VO6
16 / VO5
15 / VO4
29 / VA3
27 / VA2
28 / VO3
14 / VO2
30 / VO1
SNb
7 / VL4
6 / VL3
13 / VL2
12 / VL1
8 / SBM
TN
21 / LT1
SNa
22 / LT2
23 / LT3
5 / LO1
8 / SBM
TN
4 / LL1
20 / DO5
24 / LT4
18 / DT1
ISN
19 / DO4
11 / DO3
3 / DA3
10 / DO2
2 / DA2
9 / DO1
1 / DA1

Fig. 4 The larval nervous system **A**) The panel shows a scheme of a *Drosophila* larva. Nerves (blue) emanate from the brain (brown) in a segmental manner. **B**) Frontal view of one segment (as boxed in A) showing five efferent neurons innervating three muscles (m1–3). Cell bodies of efferent neurons lie in the cortex (cx), each of which send one neurite (black dashes) toward the neuropil (np), where they form dendrites exclusively in dorsal positions (curved arrow), and from where they project into the segmental nerve (ne) that splits into nerve branches (asterisks). Most type-Ib neurons (Ib) innervate only one muscle, forming terminals with large varicosities, whereas type-Is and type-II neurons innervate groups of muscles and develop smaller varicosities. **C**) Overview of an abdominal larval segment. Identified muscles are ordered stereotypically and innervated by nerves (blue). The studies presented in this thesis concentrate on muscles 6 and 7, 12 and 13, 26 and 27, as well as muscle 4. Modified from Prokop et al. (2006).

Importantly, *Drosophila* NMJs seem highly plastic. Temperature-induced high crawling activity results in the addition of synapses (Sigrist et al., 2003), and high AP firing rates lead to synaptic potentiation. Following synaptic potentiation, increased neurotransmission results in structural consolidation, including induction of subsynaptic protein synthesis (Sigrist et al., 2000) and addition of boutons (Schuster, 2006).

Larval development can be subdivided into three stages (first, second and third instar). Eventually, larvae pupate and eclose as adult flies. Locomotion, but also learning and memory tasks can be studied using this system (Heisenberg, 2003; Siddiqi and Benzer, 1976). Moreover, adult fly heads can easily be used for biochemical analyses.

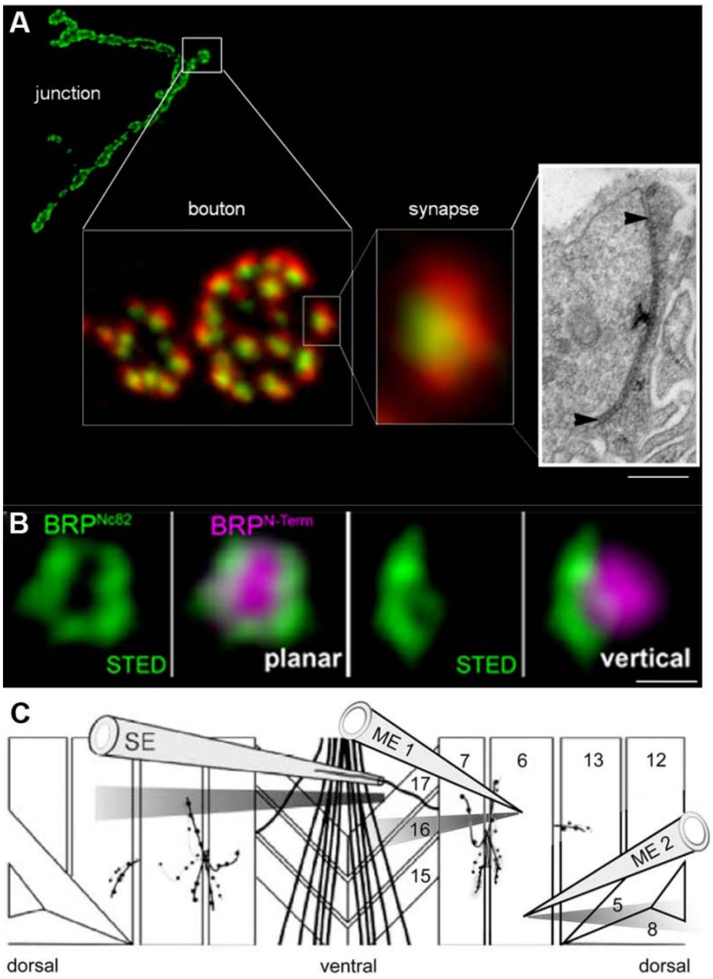

Fig. 5 The *Drosophila* NMJ
A) *In vivo* imaged NMJ expressing GFP-tagged glutamate receptors. On a bouton level pre- and postsynaptic compartments can readily be separated as seen from immunostainings for BRP (green) and postsynaptic glutamate receptors. BRP marks an individual AZ (ultramicrograph, arrows), centered by an electron dense projection (T bar). Scale bar: 5 μm, 1 μm, 200 nm, 100 nm. **B**) STED images of co-stained N-term and C-term of BRP: when viewed from a planar view the C-term of BRP forms a donut-like arrangement, while the N-term is situated at the center of the arrangement. A vertical view demonstrates that the C-term of BRP is localized towards the bouton interior, while the N-term is oriented towards the plasma membrane. Adapted from Fouquet et al. (2009). Scale bar: 100 nm **C**) Schematic overview of a two electrode voltage clamp arrangement. The severed nerve is stimulated via the suction electrode (SE). ME1 and ME2 represent sharp micro electrodes penetrating muscle 6. ME1 is current sensing, while ME2 clamps the muscle potential. Courtesy of Robert Kittel (Würzburg). Modified from Pawlu et al. (2004).

In order to assess protein dynamics, one would seek to do this in an intact animal. The *Drosophila* larva has a highly transparent cuticle making it prone to high-resolution imaging studies of fluorescently tagged proteins *in vivo* [(Fouquet et al., 2009; Rasse et al., 2005; Schmid et al., 2008), Fig. 5A]. Experiments can be carried out over extended periods in which larval NMJs grow substantially, allowing for *de novo* forming synapses to be monitored (Rasse et al., 2005).

Moreover, the system is accessible to high resolution light microscopy, such as Stimulated Emission Depletion microscopy [STED, Fig. 5B, and (Hell, 2007)]. Importantly, confocal sectioning of *Drosophila* NMJ boutons allows for a reliable definition of the orientation of synapses relative to the optical axis, since bouton surfaces are nearly spherical (Fig. 5A). Larval muscles are furthermore easily accessible to electrophysiological techniques, such as voltage clamping [Fig. 5C, (Kittel et al., 2006)].

On an ultrastructural level, AZs are marked by a characteristic CAZ (T bar, Fig. 5A). The T bar is localized towards the centre of two planar membranes apposing each other, and representing the AZ and the PSD. Typically, a halo of SVs can be found surrounding the T bar with few SVs docked to the plasma membrane. The bouton interior is largely devoid of SVs and an estimate comprises 300 quanta of the readily releasable pool (Delgado et al., 2000) of total 84,000 quanta per NMJ (Rizzoli and Betz, 2005) with up to 1,000 release sites, although this estimate seems debatable in the context of low frequency short-term depression (Wu et al., 2005).

Combining light microscopy, electron microscopy, biochemistry and electrophysiology with genetic approaches allows for in-depth functional analyses of synaptic proteins in this system.

1.8. The Scope of this Thesis

Genetic studies of both vertebrate and invertebrate model synapses have provided first insights into the regulation of AZ formation. Despite these recent successes, the dissection of synapse assembly processes has proven difficult due to genetic redundancies. This probably reflects a highly cooperative and regulated nature of synapse assembly, complicating the straightforward deduction of molecular models here. This study attempts to genetically define event hierarchies and assembly intermediates, complemented by biochemical, electrophysiological, ultrastructural and *in vivo* protein trafficking data.

BRP is shown to be a direct building block of the electron dense T bar (CAZ). Starting from a biochemical interaction screen for BRP, *Drosophila* Syd-1 is identified as an AZ-resident protein important for AZ assembly and the integrity of the CAZ. Processes of *in vivo* AZ assembly are dissected and shown to be reversible in early phases. Presynaptic DSyd-1 is furthermore found to regulate postsynaptic receptor field size and composition. Potential modes of transsynaptic regulation via the Neurexin-Neuroligin axis are characterized in this context. Finally, the GED of the GTPase Dynamin is shown to interact with a 30 aa motif towards the N-term of BRP *in vivo*, potentially linking the CAZ to the SV exo/endo-cycle.

2. Material and Methods

2.1. Co-Immunoprecipitations and Mass Spectrometry

BRP solubilization was optimized by testing a variety of combinations of salts and detergents at different pH (7-9). Optimal solubilization of BRP was reached when using 50 mM Tris/HCl pH 8, 1% NaDOC, 0.1% Triton X-100, 150 mM NaCl, and Roche complete protease inhibitor. Buffers were used to solubilize BRP and putative interaction partners from fly heads for subsequent immunoprecipitation, using the monoclonal antibody Nc82 (Wagh et al., 2006), polyclonal BRP$^{N\text{-}Term}$ (Fouquet et al., 2009) or BRP^{D2}, and polyclonal mouse or rabbit IgGs (Dianova) as controls.

Adult fly heads were obtained by vortexing anaesthetized flies on liquid nitrogen and sieving. Wild type adult fly heads (5 ml flies per immunoprecipitation) were mechanically homogenized in corresponding buffer followed by incubation at 36 °C for 30 min. A 1‰ volume of Triton-buffer was then added and the lysate was incubated at 4 °C for 30 min. Tissue debris were isolated from the supernatant by repeated centrifugation at 13,000 g. The supernatant was precleared with random IgGs coupled to Protein A-Sepharose beads and subsequently used in immunoprecipitations with the corresponding antibodies coupled to Protein A-Sepharose (Bio-Rad) beads. After incubation at RT for 30 min at slow rotation, the beads were washed five times in the solubilization buffer and proteins were eluted by boiling in SDS sample buffer. Samples were subjected to SDS-PAGE using NuPAGE 4-12% Gradient gels and subsequently stained with silver or Ruthenium (II) tris-bathophenanthroline disulfonate (Moebius et al., 2007). Identified bands were cut out from sample gels and corresponding controls. Samples were in-gel digested with trypsin, and peptides were subjected to nano-LC-MS/MS analysis (in collaboration with Albert Sickmann, Dortmund). MS data were searched against the flybase.org database using the software search algorithm MASCOT.

2.2. Antibody Production

A rabbit serum against the C-terminal DSyd-1 peptide SSGDSKNGSDEYDDIK was produced (Eurogentec). Serum was affinity purified with the same peptide. *Drosophila* fly head extracts (5 heads per lane) were probed with affinity-purified antibody.

For the DNlg1 antibody, a rabbit polyclonal serum was raised (Seqlab) against a synthetic peptide (C-QQFQPAPGRSITTNI) representing amino acids 1340-1354 of DNlg1. The specificity of the affinity-purified anti-DNlg1 antibody was confirmed by immunofluorescence analysis of larval muscle fillet preparations**.**

2.3. Western Blotting

For Western blot analysis protein samples were fractionated by standard SDS-PAGE and then transferred to a nitrocellulose membrane in prechilled western blot transfer buffer (25 mM Tris, pH 8.0, 150 mM glycine, 20% methanol) for 120 min at 100 V at 4°C. The membrane was blocked in 5% milk-powder in phosphate buffered saline (PBS) and blots were probed with the respective primary antibodies. Primary antibodies were used at the following dilutions: mouse monoclonal anti-BRP^{Nc82}, 1:100; rabbit polyclonal anti-Dynamin [(Estes et al., 1996), Mani Ramaswami, Dublin], 1:500; rabbit polyclonal anti-BRP^{D2}, 1:2000; rabbit polyclonal anti-DSyd-1, 1:500; rabbit polyclonal anti-GFP (A11122; Molecular Probes, Invitrogen), 1:500; mouse monoclonal anti-Myc (9E10, Santa Cruz Biotechnology) 1:500.

2.4. Molecular Cloning

All experiments were performed according to standard protocols (Sambrook et al., 1989). Enzymes, including T4 ligase and restriction enzymes, were purchased from Roche (Mannheim, Germany). All polymerase chain reactions (PCRs) for obtaining transgenic constructs were performed with either Elongase (Invitrogen) or Vent polymerase (New England Biolabs).

DSyd-1: As the partial clone LD28013 (DGRC, Indiana) was available, a full length *dsyd-1* cDNA was designed according to exon prediction of flybase.org. For this, the bps1183-2933 (not covered by LD28013) were amplified by elongase PCR from adult fly head cDNA using 5’-CCAGTGGGTCCCTCGAGAAGAATG-3’ and TCCAAATCAGCGCCGAAGAGC. The resulting fragment was *Stu*I digested and ligated with LD28013. This ligation was *Xho*I digested, ligated into pBluescript

KS (+) (Stratagene), *Xho*I-*Xba*I cut out and ligated into pUASt (pUASt/*dsyd-1* bp 1183-5537). Bps 1-1182 were amplified by elongation PCR from fly head genomic DNA using 5’-ATGACGGTGCAACCGGCTGAAATG-3’ and 5’-CGTTGACATTCTTCTCGAGGGA-3’. Fragments without introns were amplified via vent PCR (A: (A1) 5’-GAGCGCGGCCGCGATGACG-3’ and 5’-GAACTGATCTTCCATTTTCCGCCATTTCAGCCGGTTGCAC-3’; B: 5’-TGCAACCGGCTGAAATGGCGGAAAATGGAAGATCAG-3’ and (B2) 5’-CCGCAAGGATTTCGTCGCCCACCCGCAAGCAGCCG-3’; C: (C1) 5’-CAACAGCGGCTGCTTGCGGGTGGGCGACGAAATCCT-3’ and 5’-CCGTCATTTCGCGACCATCTCGTGATGAGCGCGGCCTC_3’; D: 5’-CCGAGGCCGCGCTCATCACGAGATGGTCGCGAAATGAC-3’ and (D2) 5’-TCCCGTTGACATTCTTCTCG-3’). Fragments A and B were linked via elongation PCR using A1 and B2, fragments C and D were linked using primers C1 and D2. Resulting fragments were linked using primers A1 and D2. Bps 1-1182 and pENTER were digested with *Not*I and *Xho*I and ligated. Bps 1183-5537 were amplified via PCR from pUASt/*dsyd-1* bps 1183-5537 using primers: 5’-GTCCGCCAGTGGGTC-3’ and 5’-GTCTATTCTAGACTTGATGTCATCGTACTCAT-3’. pENTER/*dsyd-1* (Wagh et al., 2006) bps 1-1182 and *dsyd-1* bps 1183-5537 were digested with *Xho*I and *Xba*I and ligated thereafter. All sequences were validated by double strand sequencing. pUASt/*dsyd-1* cDNA, pTGW/*dsyd-1*$^{\mathrm{cDNA}}$ (for N-terminal GFP-tag), and pTSW/*dsyd-1*$^{\mathrm{cDNA}}$ (for N-terminal mStrawberry-tag) constructs were obtained using the GATEWAY system (Invitrogen).

The *dynamin* cDNA (LD21622) was obtained from the DGRC. A first amplicate was produced using the primers A1 5’-GTCTATGTCGACATGGATAGTTTAATTACAA-3’ and A2 5’-GCTGTGCACATGCGCACGACCAC-3’ and joined to a second amplicate obtained using B1 5’-GTCTATGCGGCCGCGACTTGAATCGCGAACTGAAGGC-3’ and B2 5’-GTGGTCGTGCGCATGTGCACAG-3’ using A1 and B2. *Sal*I and *Not*I restriction sites were introduced. The cDNA was ligated to pENTR4 (Invitrogen).

Constructs for cell culture experiments were obtained using the GATEWAY system (cDNA was placed downstream of an ubiquitin promoter and tags were either GFP or Myc; vectors courtesy of Alf Herzig, Göttingen).

2.5. Pulldowns from *Drosophila* Schneider Cells

(together with Harald Depner, Berlin): *Drosophila* Schneider S2R+ cells were cultured at 25 °C in an ambient atmosphere in Schneider´s *Drosophila* medium (Biowest) supplemented with 10% fetal calf serum (FCS) + 2 mM L-glutamine, 100 U/mL penicillin and 100 µg/mL Streptomycin (Gibco, Invitrogen). Medium was exchanged every three to four days. To avoid outgrowth, cell cultures were split every 10 to 14 days. Cell co-transfection was conducted using the Effectene transfection reagent kit (Qiagen). Cell lysis was carried out with lysis buffer containing 25 mM Tris-HCl pH 7.5, 150 mM NaCl, 2 mM EDTA, 2 mM EGTA, 10% (V/V) Glycerol, 1% (V/V) NP-40 and Roche complete protease inhibitor for 45 min at 0 °C. Total protein concentrations were determined by BCA protein assay (Pierce, Thermo Scientific).

For co-immunoprecipitations, 350 µg total protein extract from whole-cell lysates was mixed with 20 µL of Protein A agarose bead suspension (Affi prep Protein A support; Bio-Rad) pre-coupled with either monoclonal mouse anti-Myc antibody (9E10, Santa Cruz Biotechnology), polyclonal rabbit anti-GFP (A11122; Molecular Probes, Invitrogen), polyclonal rabbit anti-BRP$^{\text{N-Term}}$ or the respective IgG control from mouse or rabbit (Dianova). Following incubation at RT, the coupled beads were thoroughly washed repeatedly and eluted by boiling in 40 µL sample buffer.

2.6. Yeast Two-Hybrid

Yeast two-hybrid (Y2H) constructs for DSyd-1 and Dynamin were obtained by PCR on the corresponding cDNA (pUASt/*dsyd1* cDNA or LD21622 (DGRC) respectively) and cloned into pGAD-T7-IIB (Clontech) using following primers and restriction enzymes:

DSyd-1$^{1\text{-}400}$:	**forward:**	**GTCTATATCGATACATGACGGTGCAACCGGCTGAA**
	reverse:	**GTCTATGGATCCCGTTGACATTCTTCTCG**
	digest:	***Cla*I, *Bam*HI**

DSyd-1$^{301-900}$:	forward:	GTCTATATCGATACTCTAGGCTAGGTCTGGGTCTTAA
	reverse:	GTCTATGGATCCATCCGTGTGCCGCATGCGAATGT
	digest:	*Cla*I, *Bam*HI
DSyd-1$^{801-1400}$:	forward:	GTCTATGAATTCACACAGGGCCAAACCAGAGA
	reverse:	GTCTATCTCGAGGGGAGTGTAGCTACTGTT
	digest:	*Eco*RI, *Xho*I
DSyd-1$^{1301-1844}$:	forward:	GTCTATATCGATACGTTAAGCAAGTCAAGATCGT
	reverse:	GTCTATCTCGAGCTTGATGTCATCGTACTCAT
	digest:	*Cla*I, *Xho*I
Dynamin$^{1-300}$:	forward:	GTCTATGAATTCATGGATAGTTTAATTACAA
	reverse:	GTCTATCCCGGGAGCATCGCCTGGCTGAA
	digest:	*Eco*RI, *Xma*I
Dynamin$^{270-580}$:	forward:	GTCTATGAATTCACTTTGGAGAAGGAGGTGGAG
	reverse:	GTCTATGGATCCCTCCAGTTGTTTGTAGTC
	digest:	*Eco*RI, *Bam*HI
Dynamin$^{569-877}$:	forward:	GTCTATGAATTCGATATTGAACAGGGATTTATG
	reverse:	GTCTATGGATCCCTTGAATCGCGAACTGAAGGC
	digest:	*Eco*RI, *Bam*HI
Dynamin$^{569-658}$:	forward:	GTCTATGAATTCATGGATAGTTTAATTACAA
	reverse:	GTCTATGGATCCAACCAGATTACGAATGG
	digest:	*Eco*RI, *Bam*HI
Dynamin$^{569-738}$	forward:	GTCTATGAATTCATGGATAGTTTAATTACAA
	reverse:	GTCTATGGATCCTGATACGTCACCTATTA
	digest:	*Eco*RI, *Bam*HI
Dynamin$^{569-828}$	forward:	GTCTATGAATTCATGGATAGTTTAATTACAA
	reverse:	GTCTATGGATCCTGGGGGAAGAGATCCTCCG
	digest:	*Eco*RI, *Bam*HI
Dynamin$^{643-738}$	forward:	GTCTATGAATTCGAGGAGAGTTCCAGCGATCC
	reverse:	GTCTATGGATCCTGATACGTCACCTATTA
	digest:	*Eco*RI, *Bam*HI
Dynamin$^{729-828}$	forward:	GTCTATGAATTCCGTGCTTGCAAGGATGC
	reverse:	GTCTATGGATCCTGGGGGAAGAGATCCTCCG
	digest:	*Eco*RI, *Bam*HI
Dynamin$^{819-877}$	forward:	GTCTATGAATTCGGCGGTCGTCCCGGAGG
	reverse:	GTCTATGGATCCCTTGAATCGCGAACTGAAGGC
	digest:	*Eco*RI, *Bam*HI

Y2H constructs for the N-term of BRP were obtained by PCR on the corresponding cDNA [(pGBK-T7/*brp* D1 (Fouquet et al., 2009)] and cloned into pGBK-T7 (Clontech) using following primers and restriction enzymes:

BRP$^{1-83}$:	**forward:**	**GTCTATCGGAATTCATGGGCAGTCCATACTAC**
	reverse:	**GGAATTCGTCGACGAGCTCGTCCTCTAGGTAC**
	digest:	***EcoR*I, *Sal*I**
BRP$^{84-210}$:	**forward:**	**GTCTATCGGAATTCTATGGCAGATCAGCGCGTC**
	reverse:	**GGAATTCGTCGACCTGCTGCCGCATCTCCAG**
	digest:	***EcoR*I, *Sal*I**
BRP$^{211-264}$:	**forward:**	**GTCTATCGGAATTCATGGAGGCGATCTACGCGGAG**
	reverse:	**GGAATTCGTCGACTCCCTTGGCCTGCAGCATTT**
	digest:	***EcoR*I, *Sal*I**
BRP$^{113-254}$:	**forward:**	**GGAATTCGTCGACTCCCTTGGCCTGCAGCATTT**
	reverse:	**GGAATTCGTCGACCTTGATACTCTCGTCGCGG**
	digest:	***EcoR*I, *Sal*I**

Other baits and preys for BRP were used as in (Fouquet et al., 2009). In principle all experiments were conducted according to the Y2H protocols of Clontech using the strain AH109. In brief, AH109 was co-transformed with the corresponding bait and prey constructs, grown on SD/-Leu/-Trp plates and at least ten clones each were analyzed on SD/-Ade/-His/-Leu/-Trp/X-α-gal plates to select for positive interaction. If > 90% of the clones plated on SD/-Ade/-His/-Leu/-Trp/X-α-gal grew, this was regarded as positive interaction. Negative controls consisted of Laminin as bait and the prey to be tested.

2.7. Genetics

Fly-strains were reared under standard laboratory conditions (Sigrist et al., 2003) at 25°C. Either w1 or w1118 strains were used as background for generation of transgenes (Bestgene Inc.).

2.7.1. Generation of dsyd-1 *Mutants*

dsyd-1 mutants (*dsyd-1*$^{\mathrm{ex3.4}}$, eliminating the complete *dsyd-1* and partially the 3’ *heph* locus and *dsyd-1*$^{\mathrm{ex1.2}}$ eliminating the complete *dsyd-1* locus and partially the 5` *ferrochelatase* locus) were constructed and validated by genomic PCR (Owald et al., 2010) according to (Parks et al., 2004).

2.7.2. Other Single and Double Mutants

For *dliprin-*α, *dliprin-*$\alpha^{\mathrm{EPexR60}}$/*dliprin-*$\alpha^{\mathrm{F3ex15}}$ (Kaufmann et al., 2002) was used. *dliprin-*$\alpha^{\mathrm{EPexR60}}$; *dsyd-1*$^{\mathrm{ex3.4}}$ and *dliprin-*α^{F3ex15}; *dsyd-1*$^{\mathrm{ex1.2}}$ were kept using the

T(2;3)CyOGFP-TM3GFP compound balancer (Eissenberg et al., 2005). For *brp*, *brp*^{69}/DfBSC29 (Kittel et al., 2006), *brp*^{c04298}/DfBSC29, *brp*$^{1.3}$/DfBSC29, *brp*$^{5.45}$/DfBSC29 were used. For *dnlg1*, *dnlg1*$^{ex1.9}$/*dnlg1*$^{ex2.3}$ and *dnlg1*^{I960}/*dnlg1*^{H324} were used (Banovic et al., 2010). For *dnrx*, *dnrx*^{241}/Df7670 (Li et al., 2007) were used.

2.7.3. Synthesis of Other Genetic Combinations

The presented combinations make use of the UAS *Gal4* system (Brand and Perrimon, 1993), allowing for tissue specific expression of the transgenes. Following *Gal4* lines were used: *ok6-Gal4* (Aberle et al., 2002) and *D42-Gal4* (Yeh et al., 1995) driving expression in all motoneurons; *ok319-Gal4* (Schmid et al., 2008) driving expression in a subset in motoneurons; *G14-Gal4* (Aberle et al., 2002) driving expression in muscle cells.

UAS-^{GFP}DLiprin-α, UAS-BRP-short^{mStraw}/*ok6-Gal4*.

ok6-Gal4, UAS-BRP-short^{mStraw}/+; UAS-DLiprin-α^{GFP}/+.

ok6-Gal4, UAS-BRP-short^{mStraw}/+; UAS-^{GFP}DSyd-1/+.

ok6-Gal4/+, UAS-DLiprin-α^{GFP}/UAS-^{mStrawberry}DSyd-1.

ok6-Gal4, UAS-^{GFP}DLiprin-α /+; UAS-^{mStrawberry}DSyd-1/+.

dliprin-α^{F3ex15}/*dliprin-*$\alpha^{EPexR60}$; UAS-BRP-short^{mCherry}, *D42-Gal4*/ UAS-^{GFP}DSyd-1.

UAS-^{GFP}DLiprin-α, UAS-BRP-short^{mStraw}/*ok6-Gal4*; *dsyd-1*$^{ex1.2}$/*dsyd-1*$^{ex3.4}$.

UAS-^{GFP}DLiprin-α, UAS-BRP-short^{mStraw}/*ok6-Gal4*; *dsyd-1*$^{ex1.2}$*,* UAS-DSyd-1/*dsyd-1*$^{ex3.4}$.

ok6-Gal4/+; *dsyd-1*$^{ex1.2}$*,* UAS-DSyd-1/*dsyd-1*$^{ex3.4}$.

D42-Gal4/+; *dsyd-1*$^{ex1.2}$*,* UAS-DSyd-1/*dsyd-1*$^{ex3.4}$.

exp228A22 (Petersen et al., 1997), *ok6-Gal4*, UAS- UAS-BRP-short^{mStraw}/ex (P228g9) (Petersen et al., 1997); UAS^{GFP}DSyd-1/+.

exp228A22, *ok6-Gal4*, UAS-BRP-short^{mStraw}/ ex (P228g9); UAS-^{GFP}DLiprin-α/+.

brp^{69}/DfBSC29, *ok6-Gal4*; UAS-^{GFP}DSyd-1/DGluRIIA^{mRFP}.

brp^{69}/DfBSC29, *ok6-Gal4*; UAS- ^{GFP}DLiprin-α/DGluRIIA^{mRFP}.

UAS-Mito^{GFP}/*ok6-Gal4.*

UAS-Mito^{GFP}/*ok6-Gal4*; *dsyd-1*$^{ex1.2}$/*dsyd-1*$^{ex3.4}$.

2.8. Image Acquisition

Confocal microscopy was performed using a Leica TCS SP5 setup (Leica 63x 1.4 N.A. oil immersion objective). STED microscopy was performed with the Leica TCS STED setup (Leica 100x 1.4 N.A. oil immersion objective). Images of fixed and live samples were acquired at room temperature. NMJ z-stacks had a step size of 0.5 μm between single optical slices. All images were acquired using the Leica LCS AF software. Images were acquired from larval NMJs of muscles 6 and 7 or 4. For embryos, NMJs on muscle 4, 12 and 13 as well as 6 and 7 were imaged.

2.9. Immunostainings of Larval and Embryonic NMJs

Dissections were performed in chilled HL3 (see 2.13.) by opening the larva/embryo dorsally along the midline. Intestines were removed and dissections were fixed with 4% paraformaldehyde in phosphate buffered saline (pH 7.2) for 10 min. After fixation the fillets were washed with 0.05% Triton-X 100 in PBS (PBT) and blocked for 30 min in 5% normal goat serum (NGS).

For the immunostainings the preparations were incubated with primary antibodies at 4 °C over night and subsequently washed in a 0.05% PBT solution for 4-12 h at room temperature. For the anti-DSyd-1 stainings the primary antibody was diluted in 0.3% instead of 0.05% PBT. Preparations were then incubated over night with secondary antibodies at 4 °C. Washing procedures were repeated as described above. Larvae were mounted either in Vectashield (Vector Laboratories) or Mowiol (Qin et al., 2005). Antibody dilutions: mouse anti-Nc82 1:100-1:200 (Erich Buchner, Würzburg); rabbit anti-DSyd-1 1:500; rabbit anti-BRP$^{N\text{-}Term}$ 1:250 (Fouquet et al., 2009); rabbit anti-DGluRIID 1:500 (Qin et al., 2005); guinea pig anti-DGluRIID 1:500; mouse anti-DGluRIIA 1:100 (Developmental Studies Hybridoma Bank, Iowa); rabbit anti-DGluRIIB 1:1000 [(Liebl et al., 2005; Marrus et al., 2004), David Featherstone, Chicago)]; mouse anti-GFP 1:500 (Invitrogen); rabbit anti-GFP 1:500 (Invitrogen); rabbit anti-DVGlut 1:500 (Hermann Aberle, Münster); rabbit anti-DNlg1 1:500; goat anti-HRP-Cy5 1:250 (Dianova). All confocal secondary antibodies (goat anti-mouse, goat anti-rabbit or goat anti-guinea pig) coupled to either Alexa 488, Cy3, Cy5 or Alexa 647 (Invitrogen, Dianova) were diluted 1:500. Secondary antibodies used for STED images (sheep anti-mouse-Atto647N and sheep anti-rabbit-Atto647N, Sigma) were diluted 1:100.

Embryos were staged temporally (22-24 h) and morphologically and stained as described above.

2.10. *In Vivo* Live Imaging of NMJs

(together with Wernher Fouquet, Berlin): Intact living *Drosophila* larvae were covered with Voltalef H10S oil (Atofina) and placed into an airtight imaging chamber. During image acquisition the larvae were briefly (10 to 20 min) anaesthetized by introducing a Desflurane (Baxter) air mixture into the imaging chamber. Selected NMJs were identified in abdominal segments A2 and A3 on muscles 26 and 27. Larvae were removed from the imaging chamber and reared at 25 °C between the two imaging time points (when imaging at 12 h intervals). Larvae imaged repetitively at 30 min intervals were maintained in the imaging chamber and wakened by applying brief air pulses.

2.11. Image Processing

In order to compare different time points in live imaging experiments, all images were normalized by adjusting the brightest pixel of the NMJ to 255 a.u.. Confocal stacks were processed with ImageJ software (http://rsbweb.nih.gov/ij/). Single slices and confocal stacks were deconvolved; ImageJ plugins: iterative deconvolution and iterative deconvolution 3D respectively (Bob Dougherty, OptiNav, Inc.).

STED images were processed using a linear deconvolution software integrated into the Imspector Software bundle (Max-Planck Innovations GmbH, Munich, Germany). For visualization, images for figures were enhanced using the brightness/contrast function of ImageJ and edited in Adobe Photoshop (Adobe Systems Inc.).

2.12. Quantifications of AZ/PSD Size and Intensity

Images to be quantified were acquired using the same microscope settings. Control and mutant dissections were stained in the same vial.

The original image stack was first scaled up two-fold. A Gaussian filter with a radius of two pixels was applied. The contrast of the maximum projection of an image stack was adjusted to an intensity maximum of the picture of 255 (min/max contrast function, ImageJ). Afterwards a threshold was set excluding all pixels with a value < 51. Synapses were segmented using the pencil tool (line thickness of 2 pixels). The processed picture was then transformed into a binary picture with all pixels with a value lower than 51 receiving the value “0” and all pixels with a value higher and equal to 51 being reassigned to a value of “255”. This binary mask was then projected onto the original unmodified image using the “min” operation from the ImageJ image calculator. For STED images no Gaussian blur was applied.

To define the DVGlut and Mito^{GFP} signal intensity of NMJs a ROI was applied by surrounding the Ib innervations (based on the HRP signal) and the mean pixel intensity was measured. In order to compare several experiments the mean signal was subsequently normalized to the corresponding HRP signal.

2.13. Two Electrode Voltage Clamp Recordings

brp mutants measured were: *brp*^{c04298}/DfBSC29 and w1118 as controls. *dnlg1* mutants measured were: CD8-GFP-Sh, *mef2-Gal4*, *dnlg1*^{H324}/CD8-GFP-Sh, *dnlg1*^{I960} and CD8-GFP-Sh/*mef2-Gal4*, CD8GFP-Sh as controls. *dsyd-1* (*ok6-Gal4*/+*; dsyd-1*), *dsyd-1* rescue (*ok6-Gal4*/+*; dsyd-1,* UAS-*dsyd-1*^{cDNA}*/dsyd-1*) and controls (*ok6-Gal4*/+) as well as *dliprin-*α and controls (w1118) were also measured. Recordings were acquired from muscle 6 of segments A2 and A3 of late third instar larvae (experimental groups consisted of either males or females only). Larval fillets were prepared in Ca^{2+}-free HL3 saline (mM): 70 NaCl, 5 KCl, 20 $MgCl_2$, 10 $NaHCO_3$, 5 trehalose, 115 sucrose, and 5 HEPES; pH adjusted to 7.2 at room temperature (Stewart et al., 1994). Dissections were carried out as described in (2.9.). The larval brain was carefully removed leaving the nerve innervating muscle 6 and 7 intact. The recording solution consisted of HL3 with either 1 or 0.5 mM $CaCl_2$. Cells were recorded at RT and had an input resistance $\geq$ 4 MΩ and an initial membrane potential of > 40 mV. Intracellular electrodes (borosilicate glass with filament, outer diameter 1.5 mm) were filled with 3 M KCl and resistances ranged from 10-25 MΩ. The cells were clamped to -60 mV (for mEJCs: -80 mV) and the clamp was tuned to 0.5 ms (for mEJCs: 1.5 ms) settling time when giving a step from -60 mV to -70mV. For stimulation, the nerve was pulled in by a fire polished suction electrode and 300 µs stimuli (npi stimulator) were passed at voltage steps recruiting both motoneurons (5-30 mV). For eEJC amplitudes, the nerve was stimulated at 0.2 Hz. Either 7-10 or 15-20 sweeps were averaged for mean values. Data analysis was performed using the pClamp software. Current rise times were measured between 10% and 90% of the peak amplitudes of averaged traces. Decay constants were fitted from 60% mean amplitude exponentially. Stimulation artifacts of eEJCs were removed for clarity. 10 Hz trains were evaluated in Excel. Paired pulse stimulation protocols were performed with paired pulse intervals of either 10 ms or 30 ms and experiments were performed in 0.5 mM extracellular [Ca^{2+}]. For determination of the second pulse's base line at 10 ms inter pulse interval, the decay of the first pulse was extrapolated. mEJCs were analyzed using pClamp. Mean amplitudes and frequencies were detected manually and decay constants were automatically detected by the software. For frequency distributions, the data was binned in GraphPad Prism.

Recordings were performed with an AxoClamp 2B amplifier in the TEVC mode. Data were sampled at 5 kHz and low-pass filtered at 1 kHz. Holding currents never exceeded ±10 nA.

2.14. Transmission Electron Microscopy

(together with Carolin Wichmann, Göttingen and Berlin): For high pressure freezing ~2-10 (22-24 h) staged *Drosophila* embryos were placed in an aluminium specimen carrier of 200 µm depth (type A; Bal-Tec), filled with yeast paste and covered with a lid. The samples were frozen immediately in a Bal-Tec HPM010 and rapidly transferred to liquid nitrogen for storage.

Freeze-substitution and embedding were performed in acetone in an EM AFS (Leica Microsystems). In brief, freeze-substitution was performed in acetone with 0.1% tannic acid at -90 °C for 4 days, followed by acetone with 2% osmium during the last 7 h. The samples were warmed (5 °C/h) to -20 °C and incubated for

16 additional hours before being warmed (10 °C/h) to 4 °C. At 4 °C, the samples were washed in acetone and warmed to room temperature. They were then embedded in Epon [see (Rostaing et al., 2006; Siksou et al., 2007)].

Subsequently, 55-65 nm (grey-silver) sections were cut using an EM Ultracut 6 (Leica Microsystems). Sections were collected on formvar-coated 100 mesh grids. Sections were dried and post-stained with uranyl acetate and lead. Micrographs were taken with a 1024 × 1024 CCD detector (Proscan CCD HSS 512/1024; Proscan Electronic Systems) in an EM 902A (Zeiss), operated in bright field mode.

For conventional room temperature, embedding images were obtained from dissected preparations of third instar larvae (NMJ 6 and 7, segments A2/A3). Dissected larvae were fixed in 4% paraformaldehyde and 0.5% glutaraldehyde in 0.1 M PBS (pH 7.2) for 10 min and then for 60 min in 2% glutaraldehyde in 0.1 M sodium cacodylate buffer (pH 7.2), washed three times for 5 min in sodium cacodylate buffer and postfixed on ice for 1 h with 1% osmium tetroxide (in 0.8% KFeCn in 0.1 M sodium cacodylate buffer). This was followed by washing in sodium cacodylate buffer for 1 h and subsequent rinsing in distilled water. The samples were stained *en bloc* with 1% uranyl acetate for 1 h on ice. Samples were dehydrated (Wagh et al., 2006). After infiltration in Epon resin, muscles were cut out (6 animals for each genotype) and embedded in a single block. Sections were stained in uranyl acetate (4%).

Quantifications: The number of vesicles at the AZ were evaluated within three shells (each shell of 50 nm thickness) surrounding the T bar (n w1: 26; n *dsyd-1*: 26 AZs). For the vesicle diameter all vesicles in a radius of 150 nm surrounding the T bar were taken and the diameter measured with the ImageJ software. *Reconstructions:* For 3D-reconstructions of larval T bars (w1 vs. *dsyd-1*), three to five serial 60 nm sections were reconstructed with the free software (Fiala, 2005) Reconstruct (Owald et al., 2010).

2.15. Behavioral Analysis

Female animals were tested within 48 hours after eclosure and at least one night at 18°C. Prior to testing, flies were anesthetized on ice and wings were clipped. Experiments were carried out under red light and animals were allowed to adapt to darkness for at least one hour before testing. To test the walking ability, flies were placed on a flat surface with a 2 x 2 cm grid and allowed to walk freely for 10 seconds. The number of lines crossed was counted. Negative geotaxis was measured with flies placed on the bottom of an empty, scaled food vial and the maximum height (max = 9 cm) reached within 30 s was recorded (Owald et al., 2010).

2.16. Statistics

Data was analyzed with Prism (GraphPad Software). Asterisks are used to indicate statistical significance of the results (* = $p < 0.05$; ** = $p < 0.01$; *** = $p < 0.005$; ns = $p > 0.05$).

3. Results

BRP is needed for the formation of the electron dense T bar and is responsible for Ca^{2+} channel clustering at the AZ. Moreover, a mutant for *brp (brp*^{69}*)* showed inefficient neurotransmitter release and changes in synaptic short-term plasticity (Kittel et al., 2006; Wagh et al., 2006). So far, the analysis of BRP function was based on the *brp*^{69} deletion allele, where most of the protein coding sequence (corresponding to aa 283 to 1744) is removed (Fig. 6). It, however, remained unclear whether BRP is a direct building block of the T bar or merely is involved in signaling needed for T bar formation. To answer this, further genetic analysis including the identification of additional *brp* alleles was performed.

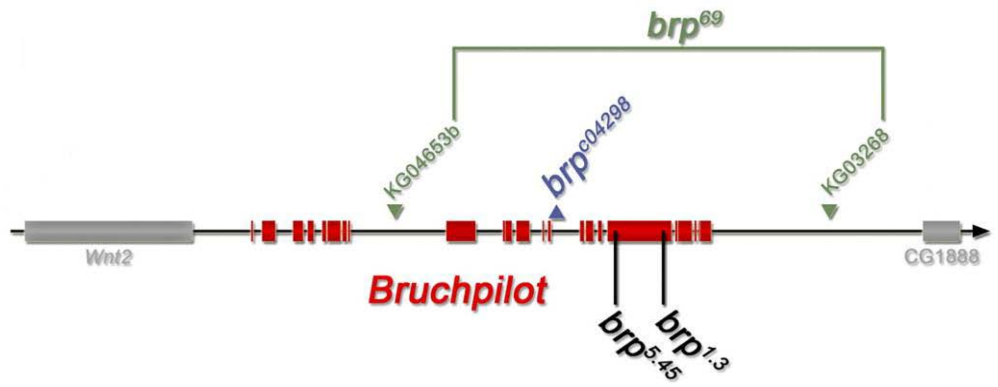

Fig. 6 Genomic analysis of the *brp* locus
The deletion mutant (*brp*^{69}) and the parental transposon-insert lines are shown in green, the pBac transposon insert (Bellen et al., 2004) allele is highlighted in blue. Position of EMS induced stop-codons of the *brp*$^{1.3}$ and *brp*$^{5.45}$ alleles are shown in black. Modified from Fouquet et al. (2009).

3.1. BRP is an Integral Element of the Electron Dense Body

As previously reported (Kittel et al., 2006), *brp*^{69} deficient AZs completely lack T bars (compare Fig. 7A and B). In order to further validate these defects, a piggybac-transposon insert (*brp*^{c04298}) located towards the middle of the *brp* locus was characterized (Fig. 6). For this, immunostainings using the antibodies BRP^{Nc82} [labels the C-term of BRP (Hofbauer et al., 2009; Wagh et al., 2006)] and BRP$^{N\text{-}Term}$ [labels the protein's N-term (Fouquet et al., 2009)] were performed. In *brp*^{69}

animals, both the BRP^{Nc82} label (compare Kittel et al., 2006) and the BRP$^{N\text{-}Term}$ label were completely absent (Fig. 7B). This indicates that the predicted residual protein (corresponding to aa 1 to 282) is unstable, or at least does not localize to the NMJ.

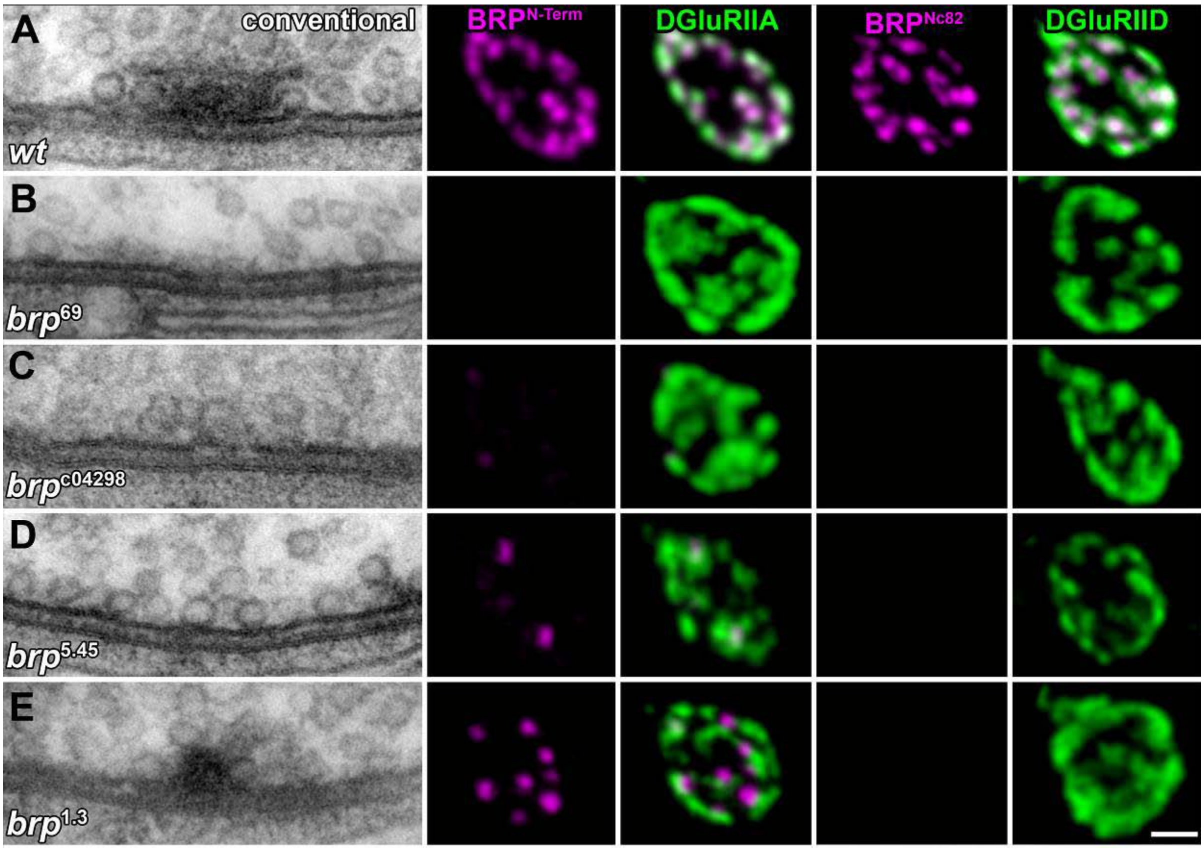

Fig. 7 AZ organization of different *brp* alleles
A-E) Left panel: ultrastructure of *Drosophila* NMJ AZs. The following genotypes are depicted: A) wild type (*wt*), B) *brp*^{69}, C) *brp*^{c04298}, D) *brp*$^{5.45}$, and E) *brp*$^{1.3}$ (left panel). Right panels: Corresponding confocal images of boutons co-stained for either BRP$^{N\text{-}Term}$ or BRP^{Nc82} (magenta) and DGluRIIA or DGluRIID (green). Modified from Fouquet et al. (2009).

At *brp*^{c04298} NMJs the BRP^{Nc82} label was absent, while the BRP$^{N\text{-}Term}$ label was dramatically reduced (Fig. 7C). Comparable to observations for *brp*^{69} (Kittel et al., 2006), EM analysis of *brp*^{c04298} showed a complete lack of T bars (Fig. 7C, together with Carolin Wichmann), and only traces of electron dense material remained at AZ membranes. Thus, as this allele is a site-specific insertion but not a deletion (which in principle might eliminate control elements of genes other than *brp*), it provides further proof that BRP is essential for T bar assembly. As the molecular alterations of *brp*^{c04298} cannot be predicted easily, amino acid point mutations in *brp* were analyzed. To do so, a chemical mutagenesis screen (EMS, ethyl methyl sulfonate; together with Sara Mertel, Berlin) selecting for reduced viability over *brp* null (e.g. *brp*^{69}) alleles was performed (Fouquet et al., 2009).

3.1.1. Truncated BRP gives Truncated T bars

The *brp*$^{5.45}$ allele is characterized by a stop codon at amino acid position 867 (corresponding to about 50% of the 1744 aa protein), which leads to overall pupal lethality over *brp* null, with weak escapers hatching (Fig. 6). As expected, the BRP^{Nc82} label was absent from *brp*$^{5.45}$ NMJs. While the number of BRP$^{N\text{-}Term}$ clusters was reduced over the whole NMJ, those remaining in *brp*$^{5.45}$ were slightly smaller, though of comparable intensity as in controls (Fig. 7D, for quantifications see Fouquet et al., 2009). Despite extensive analysis, T bars were not detected at *brp*$^{5.45}$ NMJs [Fig. 7D, (Fouquet et al., 2009)].

The EMS allele *brp*$^{1.3}$ comprised a premature stop codon at amino acid position 1390 (generating a protein 523 aa longer than predicted for *brp*$^{5.45}$, Fig. 6) and delivered paralyzed adult escapers over *brp* null. While the number of BRP$^{N\text{-}Term}$ clusters was reduced to about 40%, the cluster size and intensity was comparable to controls (for quantifications see Fouquet et al., 2009). At the same time, the BRP^{Nc82} label was absent (Fig. 7E). Importantly, T bar-like structures were observed at *brp*$^{1.3}$ NMJs (Fig. 7E), though at lower frequency than in controls. Upon closer inspection, the T bar-like structures typically appeared truncated [Fig. 7E, (Fouquet et al., 2009)].

As truncating BRP directly leads to a truncated CAZ, this data indicates that BRP is indeed an integral part of the electron dense T bar.

3.1.2. Functional Analysis of a New Severe *brp* Allele

In order to test for the severe electrophysiological defects observed in *brp*^{69}, two electrode voltage clamp recordings of *brp*^{c04298} were acquired at 1 mM extracellular [Ca^{2+}]. All tested features, including the alterations of short-term plasticity, were similar to those observed in *brp*^{69}, and confirmed previous results (Kittel et al., 2006). Thus, evoked excitatory junctional current (eEJC) amplitudes were reduced to approximately 30% of control values when stimulating at low frequencies (0.2 Hz, Fig. 8A). Furthermore, the eEJC rise time was largely delayed (Fig. 8C), which indicated a direct link to Ca^{2+} channel coupling, as seen previously (Kittel et al., 2006). In addition, high frequency trains (10 Hz) showed initial facilitation as opposed to control animals (Fig. 8B), which again suggested a change in Ca^{2+} dependent release probability.

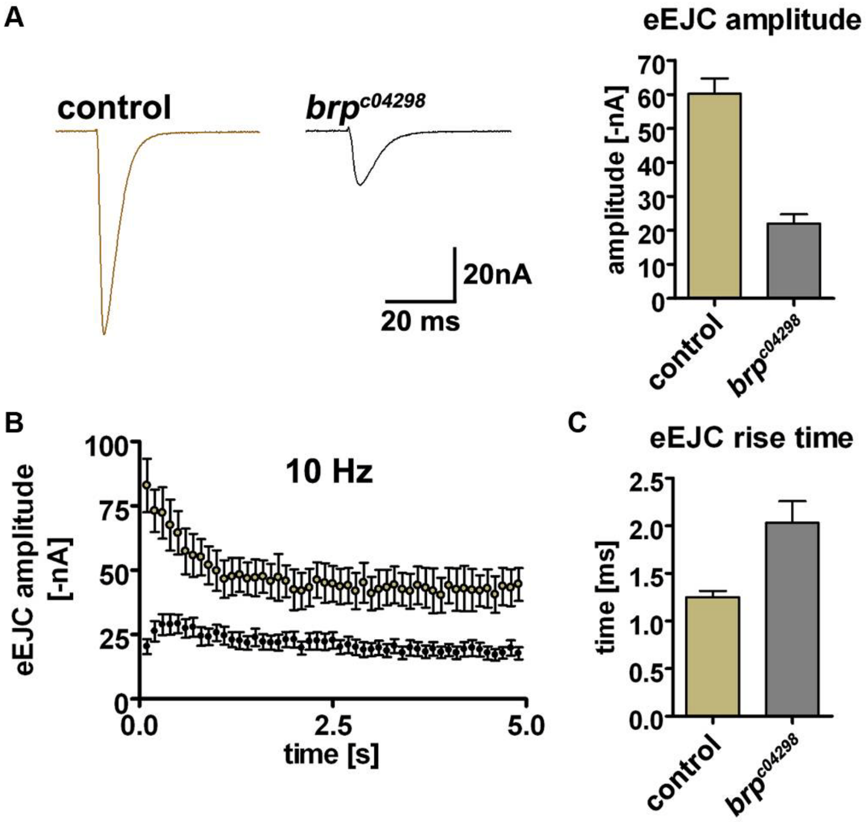

Fig. 8 ***brp*^{c04298} physiology**
A) eEJC sample traces for control and *brp*^{c04298} recorded from muscle 6. eEJC amplitudes are significantly reduced in *brp*^{c04298} animals (right upper panel, control: 60.2 ± 4.5 nA, n = 6; *brp*^{c04298}: 22.0 ± 2.7 nA; n = 12; p < 0.005, Mann-Whitney test). **B**) 10 Hz stimulation shows initial facilitation in *brp*^{c04298}, but depression in control animals. **C**) eEJC rise time is significantly prolonged (control: 1.3 ± 0.1 nA, n = 6; *brp*^{c04298}: 2.0 ± 0.2 nA; n = 12; p = 0.01, Mann-Whitney test) in *brp*^{c04298} animals compared to controls. Modified from Fouquet et al. (2009).

Taken together, the lack of T bars results in synaptic transmission defects as observed for *brp* alleles. Moreover, truncated BRP results in truncated T bars. This finding strongly indicates that BRP is the primary component of the T bar, and thus shapes the CAZ.

3.2. DSyd-1 Regulates Initial Active Zone Formation

Knowing that BRP appears to be a direct component of the T bar, the protein was used as a starting point for an unbiased proteomics screen for novel *Drosophila* CAZ-associated proteins. Indeed, BRP is an elongated protein (Fouquet et al., 2009) that comprises several coiled coil domains and might therefore serve as a protein-protein interaction platform.

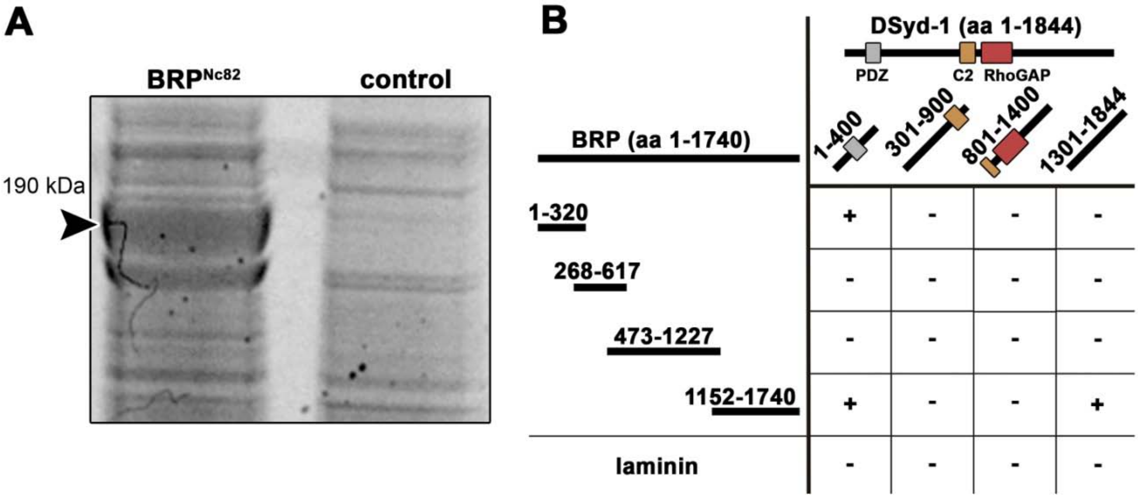

BRP (aa 1-1740)	1-400	301-900	801-1400	1301-1844
1-320	+	-	-	-
268-617	-	-	-	-
473-1227	-	-	-	-
1152-1740	+	-	-	+
laminin	-	-	-	-

Fig. 9 Identification of *Drosophila* Syd-1 as an interactor of BRP
A) BRP^{Nc82} efficiently precipitates BRP (arrow head), as seen in this SYPRO Red stained SDS-gel. Amongst others, DSyd-1 was found to co-precipitate with BRP, as confirmed by MS/MS analysis [performed by Manuela Schmidt (2006)]. **B**) The matrix shows the yeast two-hybrid assay results, confirming a direct physical interaction between BRP and DSyd-1. A C-terminal domain of BRP (aa 1152-1740) showed positive for interaction with a C-terminal region of DSyd-1 (aa 1301-1844). Moreover, an N-terminal DSyd-1 (aa 1-400) fragment as bait interacted with both the N-terminal fragment of BRP (aa 1-320) and the very C-terminal BRP fragment (aa 1152-1740). Modified from Owald et al. (2010).

3.2.1. *Drosophila* Syd-1 is a BRP-associated Protein

Using the monoclonal antibody Nc82 (BRP^{Nc82}), BRP was immunoprecipitated from adult fly head extracts. While BRP was strongly enriched in Nc82-precipitates, it was not detected in control eluates, as visualized by staining SDS-PAA gels (Fig. 9A, arrow head) and as confirmed by tandem mass spectrometry (MS/MS) using two independent protocols [performed by Manuela Schmidt (Owald et al., 2010; Schmidt, 2006)]. Next, bands of co-immunoprecipitating proteins were subjected to MS/MS analysis (performed by

Manuela Schmidt). Several peptides were found to correspond to a conceptual protein annotated at www.flybase.org as CG1976-PA or RhoGAP100F. Hereupon, the protein is referred to as DSyd-1 because of its striking similarity to *C. elegans* Syd-1. Together with Syd-2/Liprin-α, *C. elegans* Syd-1 has been implicated in AZ assembly (Dai et al., 2006; Hallam et al., 2002; Patel et al., 2006). In addition, *C. elegans* Syd-1 was shown to physically interact with the BRP homologue ELKS (Patel and Shen, 2009).

In order to elucidate whether *Drosophila* Syd-1 can bind to BRP directly, subregions of each protein were tested for interaction in a yeast two-hybrid (Y2H) assay. Several interaction sites between both proteins were found (Fig. 9B). Thus, the physical interaction between BRP/ELKS and DSyd-1/Syd-1 seems to be evolutionarily conserved.

Following the peptide sequence and an existing partial cDNA clone, a full-length cDNA was cloned, encoding for a protein of 195 kDa. The protein is predicted to comprise a Ca^{2+}-sensing/lipid and/or protein binding C2 domain, a PDZ protein-protein interaction domain, a putative RhoGAP domain and a serine-rich repeat towards the C-term [Fig. 10, (Owald et al., 2010)].

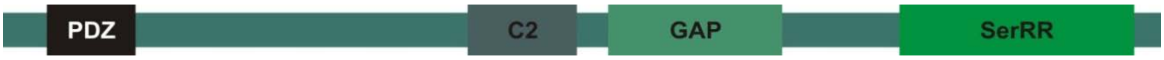

Fig. 10 The DSyd-1 protein
Schematic overview of the DSyd-1 protein. The 195 kDa protein comprises a PDZ protein-protein interaction domain, a Ca^{2+}/lipid-binding C2 domain, a putative RhoGAP domain and a serine rich stretch (SerRR).

3.2.2. Reduced Lifespan and Impaired Behavior of *dsyd-1* Deficient Flies

Next, *dsyd-1* deficient animals were constructed using Flippase-mediated trans-deletion of FRT-site containing transposon lines (Parks et al., 2004) flanking the *dsyd-1* locus (Fig. 11A). Two *dsyd-1* deficient lines (*dsyd-1*$^{ex1.2}$ and *dsyd-1*$^{ex3.4}$) were isolated, and deletions were confirmed by genomic PCR (Parks et al., 2004). A combination of both lines results in flies specifically deficient for *dsyd-1* (Fig. 11A). While *dsyd-1* adults appeared morphologically normal and, under optimal culturing conditions, eclosed at rates close to the Mendelian ratio, they rarely survived longer than a week (> 80% died within one week, n = 36). In contrast, more than 80% of control flies (n = 159) lived for at least two weeks, and typically longer.

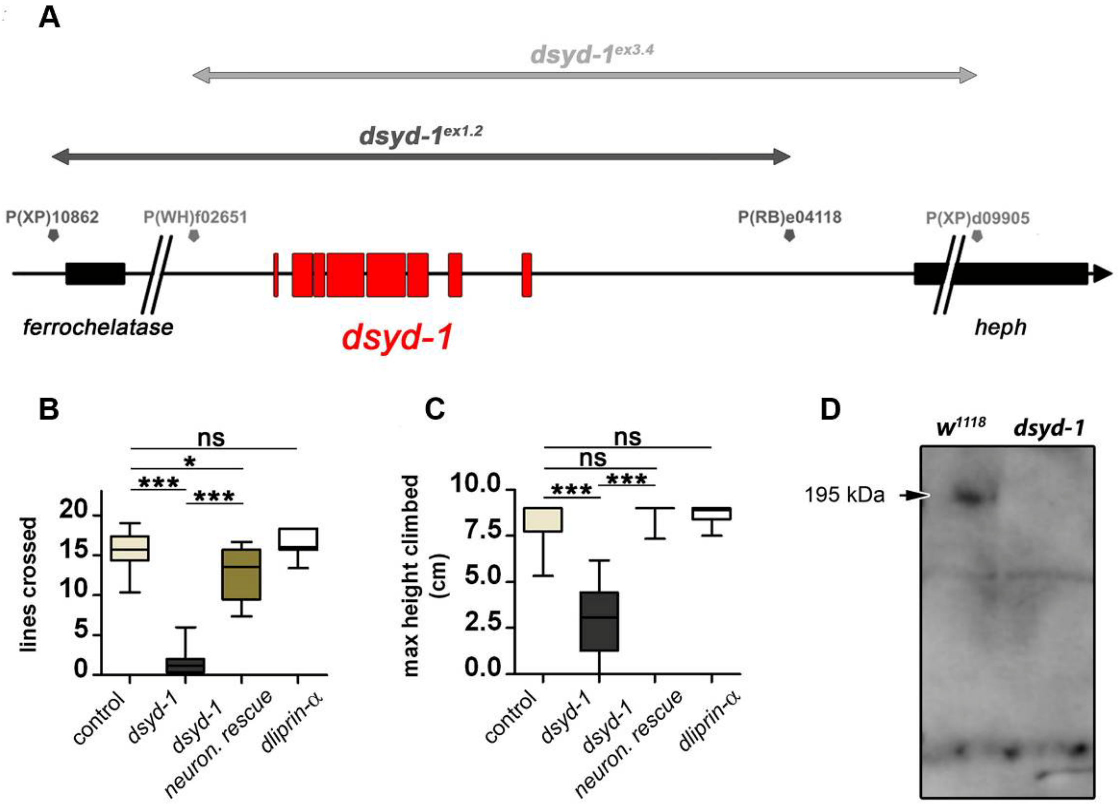

Fig. 11 *dsyd-1* deficient flies
A) Genomic location of *dsyd-1* on chromosome arm 3R at 100D2-100D3. *dsyd-1* deficient animals were constructed using *Drosophila* lines carrying transposon mediated FRT sites (Parks et al., 2004) that neighbored the *dsyd-1* locus (for *dsyd-1*$^{ex1.2}$ depicted in black and for *dsyd-1*$^{ex3.4}$ in grey). Two deficiencies were obtained and confirmed by genomic PCR. In both cases, the entire *dsyd-1* locus (red) was excised. In one case (*dsyd-1*$^{ex1.2}$, black line) the 5' *ferrochelatase* and in the other case the 3' *heph* (*dsyd-1*$^{ex3.4}$, grey line) locus were affected. Taking these deficiencies in trans eliminates both copies of *dsyd-1*, yet leaves one intact copy of both *heph* and *ferrochelatase*. **B-C**) Behavioral tests demonstrate a requirement for DSyd-1, and less so for DLiprin-α, in the adult CNS. Impaired locomotive behavior in *dsyd-1* flies is rescued by pan-neural (*elav-Gal4*) re-expression of the *dsyd-1* cDNA. B) Walking ability (control: 15.69 ± 0.57 lines, n = 15; *dsyd-1*: 1.62 ± 0.69 lines, n = 8; *dsyd-1*^{rescue}: 12.86 ± 0.99 lines, n = 10; *dliprin-α*: 16.19 ± 0.65 lines, n = 7; control x *dsyd-1*: p = 0.0001; control x *dsyd-1*^{rescue}: p = 0.02; control x *dliprin-α*: p = 0.67; *dsyd-1* x *dsyd-1*^{rescue}: $p < 0.0001$ according to Mann-Whitney test), C) Negative geotaxis (control: 8.32 ± 0.37 cm; *dsyd-1*: 2.92 ± 0.60 cm; *dsyd-1*^{rescue}: 8.833 ± 0.17 cm; *dliprin-α*: 8.67 ± 0.15 cm; all: n = 10; control x *dsyd-1*: $p < 0.0001$; control x *dsyd-1*^{rescue}: p = 0.32; control x *dliprin-α*: p = 0.91; *dsyd-1* x *dsyd-1*^{rescue}: $p < 0.0001$ according to Mann-Whitney test). **D**) A polyclonal anti-DSyd-1 AB recognizes a band at the predicted molecular weight of 195 kDa on immunoblots of w1118 control fly head lysate (arrow). This band is missing in *dsyd-1* head extracts. Unspecific bands are regarded as loading control. Modified from Owald et al. (2010).

The early adult lethality was completely overcome by *elav-Gal4* driven pan-neuronal expression of the composite full-length cDNA (UAS-*dsyd-1*$^{\mathrm{cDNA}}$) in the mutant background (n = 42). In fact, *dsyd-1* mutant animals showed impaired locomotive behavior (as revealed by two independent experimental settings), which was rescued by pan-neuronal expression of UAS-*dsyd-1*$^{\mathrm{cDNA}}$ (Fig. 11B and C).

For further assessment of DSyd-1 at the protein level, a polyclonal antibody against a C-terminal peptide of DSyd-1 (DSyd-1 AB) was raised. The DSyd-1 AB identified a band of predicted size (195 kDa) in wild type adult head extracts that was missing in extracts of *dsyd-1* mutants [Fig. 11D, (Owald et al., 2010)].

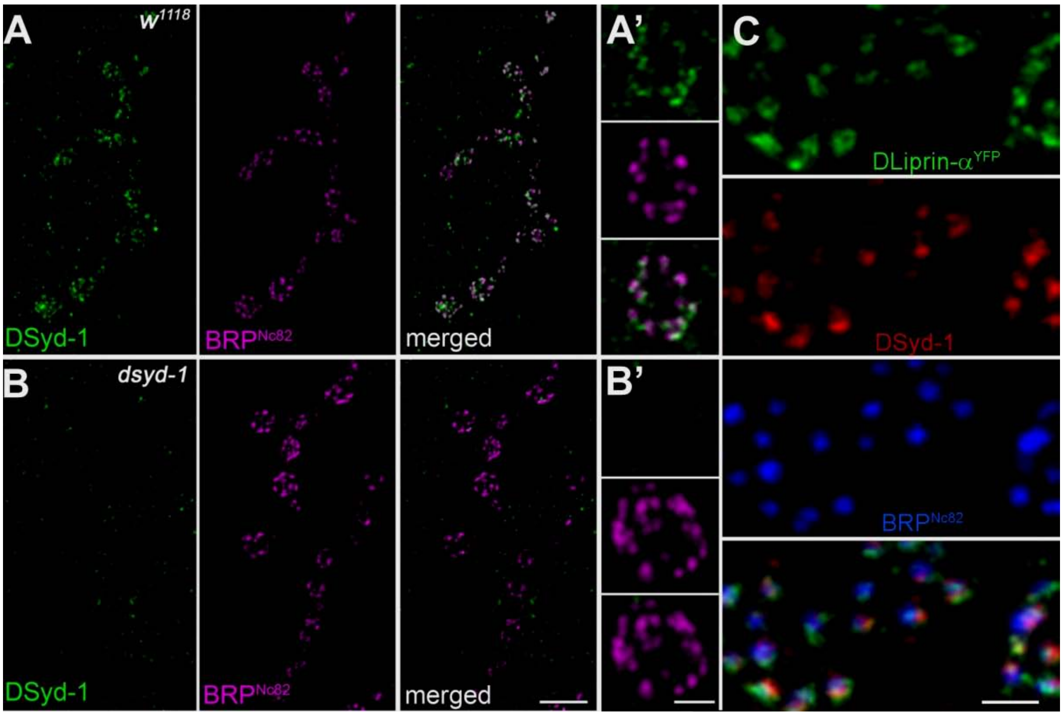

Fig. 12 DSyd-1 localizes to AZs
A) Boutons of larval NMJ innervating muscles 6 and 7. Anti-DSyd-1 label is tightly correlated with AZs (BRP$^{\mathrm{Nc82}}$). Most DSyd-1 protein clusters are found associated with BRP$^{\mathrm{Nc82}}$ label, as seen in high magnification images (**A'**). **B-B'**) There is no DSyd-1 AB immunoreactivity detected at *dsyd-1* deficient NMJs. A) and B): Scale bar: 2 µm. A') and B'): Scale bar: 500 nm. **C**) Triple label for DLiprin-α^{YFP} (green), DSyd-1 (red) and BRP (blue). Scale bar: 500 nm. Modified from Owald et al. (2010).

3.2.3. DSyd-1 Localizes to Active Zones

Protein-protein interactions can take place at multiple locations, e.g. during transport, or at the proteins' site of action. The question arose whether endogenous DSyd-1, similar to BRP, might localize to AZs.

The expression pattern of DSyd-1 was analyzed using the DSyd-1 AB. Co-labeling at the larval NMJ revealed a strong overlap with BRP signals, which suggested that DSyd-1 is an AZ protein (Fig. 12A and A'). This staining was not detected in *dsyd-1* deficient animals (Fig. 12B and B').

DLiprin-α (Fig. 12C) localizes towards the edge of AZs (Fouquet et al., 2009). Co-stainings of DSyd-1 and DLiprin-α indicated that the same might hold true for DSyd-1. While DLiprin-α roughly co-localized with BRP ($R_{BRP::DLiprin\text{-}\alpha} = 0.66 \pm 0.01$, $n = 12$), DLiprin-α and DSyd-1 co-localized even closer ($R_{DSyd\text{-}1::DLiprin\text{-}\alpha} = 0.81 \pm 0.01$, $p < 0.0001$, $n = 12$ each; together with Wernher Fouquet). Indeed, DSyd-1 surrounds the AZ core (marked by BRP) in single quantal compartments, as revealed by STED microscopy (see Owald et al., 2010).

The DSyd-1 specific staining was strongest in young first instar larvae (L1) and declined in later larval stages (L3). This might indicate a specific requirement for the protein during early NMJ development (Fig. 13).

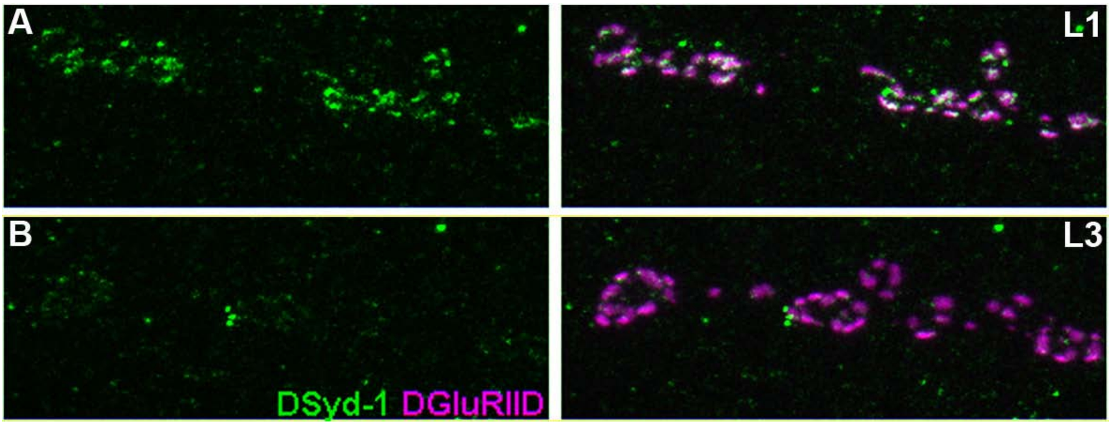

Fig. 13 High DSyd-1 levels in young larvae
A-B) Co-staining for DSyd-1 and DGluRIID in young first instar larvae (L1, A) and late third instar larvae (L3, B). DSyd-1 levels detected by the DSyd-1 AB are higher in L1 than in L3 larvae. Scale bar: 2 μm.

3.2.4. Reduced Evoked Current Amplitudes at *dsyd-1* Mutant NMJs

To explore whether DSyd-1 is needed for proper synaptic neurotransmitter release at AZs, two electrode voltage clamp recordings of larval NMJs were acquired.

Compared to controls, eEJC amplitudes were reduced in *dsyd-1* mutant larvae (Fig. 14A). These were rescued by presynaptic expression of UAS-*dsyd-1*$^{\mathrm{cDNA}}$ using the motoneuronal driver *ok6-Gal4* (Fig. 14A). For comparison, recordings from mutants of the AZ organizing protein *dliprin-*α were performed [Fig. 14A, compare (Kaufmann et al., 2002)]. Interestingly, eEJC amplitudes were decreased to a comparable level in both *dsyd-1* and *dliprin-*α. Spontaneous mini current amplitudes (mEJCs), in turn, were on average not changed between *dsyd-1* and controls (Fig. 14B, but see 3.4.1.).

Neurotransmitter release deficits at *dsyd-1* mutant NMJs might be explained by a drop in release probability of SVs, e.g. by a reduction of Ca^{2+} sensitivity of the SVs that are to be released. In this case, a change in short-term plasticity (tested for using the paired pulse paradigm), or an altered sensitivity towards different extracellular Ca^{2+} concentrations, might be expected. However, when comparing evoked release at two different Ca^{2+} concentrations, the ratio between *dsyd-1* mutants and controls was unchanged (Fig. 14C), which argues against a change in Ca^{2+} sensitivity here. Moreover, despite a tendency towards a slight paired pulse facilitation at 10 ms inter pulse interval, no significant alteration was observed in *dsyd-1* animals (Fig. 14D).

Collectively, these data imply that the characteristics of SV release tested for here are only moderately altered after loss of DSyd-1. As a result, the question arose as to whether the number of release sites (i.e. an individual PSD with an adjunct AZ) that formed at *dsyd-1* mutant NMJs and/or the number of releasable SVs was reduced (Owald et al., 2010).

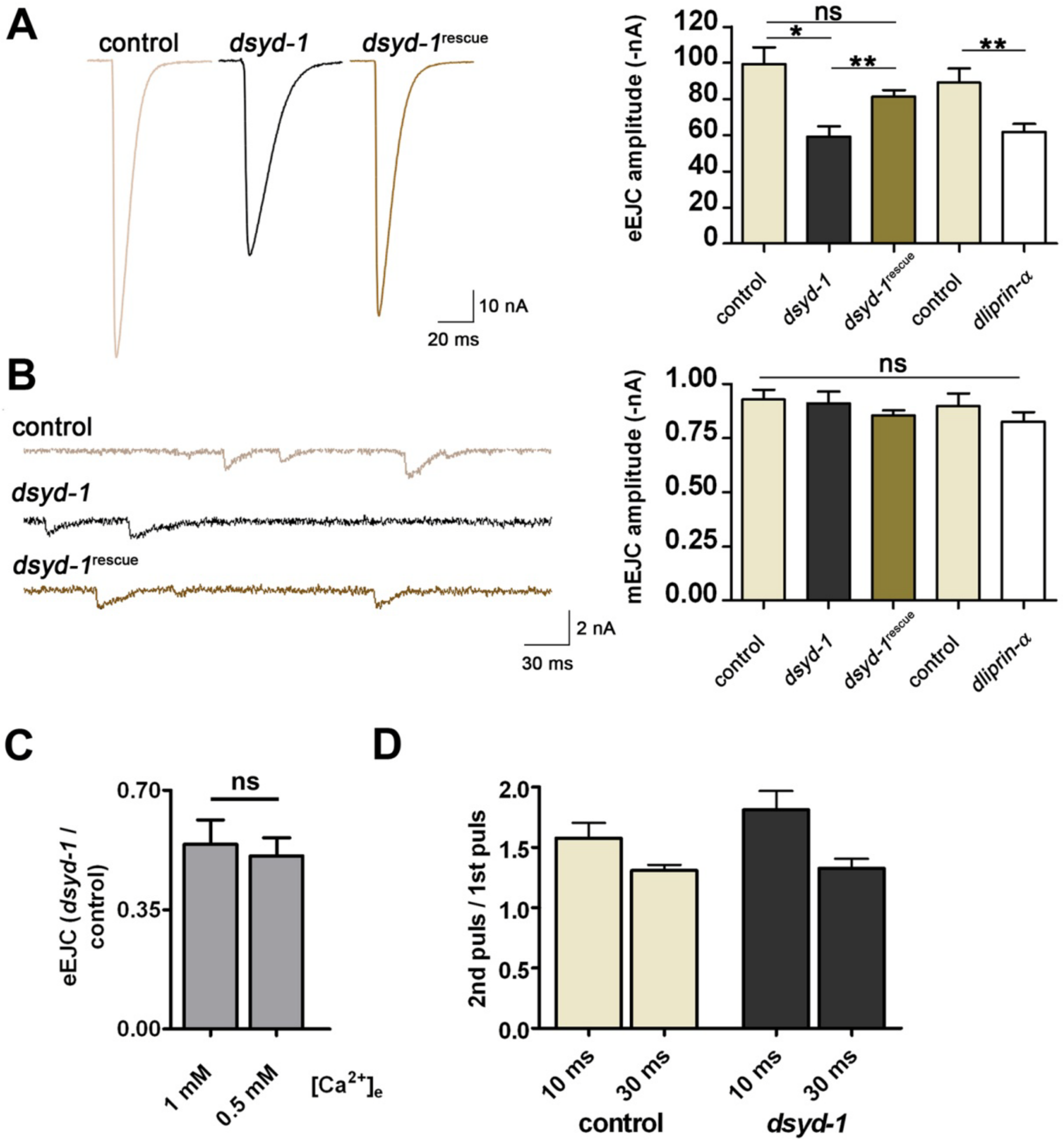

Fig. 14 Physiological analysis of *dsyd-1* and *dliprin-α* mutant NMJs

A) Average traces (left) of eEJCs at 0.2 Hz nerve stimulation recorded from the larval NMJ at 1 mM extracellular $[Ca^{2+}]$ for controls, *dsyd-1* and *dsyd-1*^{rescue}. Average eEJC amplitudes (right) for controls, *dsyd-1* (control: 99.3 nA ± 9.6 nA; *dsyd-1*: 59.2 nA ± 5.9 nA; both n = 9; p = 0.01, Mann-Whitney test), *dsyd-1*^{rescue} (81.4 nA ± 4.5 nA; n = 9; p = 0.003 to *dsyd-1* and p = 0.162 to control, Mann-Whitney test), as well as *dliprin-α* and controls (control: -89.4 ± 7.7 nA; *dliprin-α*: -62.0 ± 4.3 nA; both n = 7; p = 0.007, Mann-Whitney test). Both *dliprin-α* and *dsyd-1* show reduced amplitudes compared to controls. This defect is significantly rescued by re-expressing *dsyd-1* cDNA in *dsyd-1* deficient animals using a motoneuron specific driver (*ok6-Gal4*). **B**) Sample traces of mEJCs (left) for controls, *dsyd-1* and *dsyd-1*^{rescue} animals. Average mEJC amplitudes (right) for controls (0.93 ± 0.05 nA; n = 7), *dsyd-1* (0.91 ± 0.05; n = 8), *dsyd-1*^{rescue} (0.86 ± 0.02; n = 9) as well as *dliprin-α* (0.83 ± 0.05; n = 7) and control (0.90 ± 0.06; n = 7) are comparable (*dsyd-1* x control: p = 0.86; *dsyd-1* x *dsyd-1*^{rescue}: p = 0.54; control x *dsyd-1*^{rescue}: p = 0.14; control x *dliprin-α*: p = 0.46; all Mann-Whitney test). **C**) *dsyd-1* eEJC amplitudes normalized against the mean control eEJC amplitude recorded at 1 mM (0.54 ± 0.07, n = 11) or 0.5 mM (0.51 ± 0.05, n = 8; p = 0.48, Mann-Whitney test) extracellular $[Ca^{2+}]$ respectively. **D**) Paired pulse experiments with 10 ms (control: 1.58 ± 0.13, n = 11; *dsyd-1*: 1.81 ± 0.16, n = 13; p = 0.25, Mann-Whitney test) or 30 ms (control: 1.31 ± 0.05, n = 12; *dsyd-1*: 1.33 ± 0.08, n = 12; p = 0.98, Mann-Whitney test) paired-pulse interval recorded at 0.5 mM extracellular $[Ca^{2+}]$. Modified from Owald et al. (2010).

3.2.5. Reduced Numbers of Synaptic Release Sites at *dsyd-1* Mutant NMJs

In order to get a rough estimate of the number of SVs, *dsyd-1* mutant terminals were stained for the SV marker DVGlut [*Drosophila* vesicular glutamate transporter, (Daniels et al., 2004; Mahr and Aberle, 2006), Fig. 15A]. Overall, both *dsyd-1* and control NMJs showed comparable immunoreactivity (Fig. 15B), which indicated that the absolute number of SVs per terminal was not changed dramatically.

However, the SV signal appeared uneven between individual boutons at *dsyd-1* NMJs when compared to controls (Fig. 15A). In order to investigate whether this distribution could account for the observed reduced eEJC amplitudes at low frequency stimulation (Fig. 14A), SV distribution closely surrounding the electron dense projection at AZs was evaluated in electron-micrographs (Fig. 15C-D). Here, the SV size (Fig. 15E) as well as the number of SVs surrounding the AZs (Fig. 15D and E) was comparable between controls and *dsyd-1* mutant animals (together with Carolin Wichmann). Thus, the SV distribution appears normal at *dsyd-1* AZs, and therefore should not account for the reduced eEJC amplitudes observed after low frequency stimulation (Fig. 14A).

To address axonal transport in *dsyd-1* mutant animals, the distribution of mitochondria at *dsyd-1* NMJ terminals was studied using the transgenic mitochondrial marker Mito^{GFP} [(Pilling et al., 2006), Fig. 15F]. Here, the mean NMJ signal did not differ significantly between controls and mutants (Fig. 15F). As mitochondria are transported to the presynaptic terminals, loss of DSyd-1 does not seem to result in a generalized defect in axonal transport.

In order to test whether reduced eEJC amplitudes might partially be accounted for by altered NMJ morphology, NMJ size and release site numbers were quantified. Indeed, *dsyd-1* mutant NMJs were significantly reduced in size compared to controls (Fig. 15G). NMJ size was reduced to a similar extent in *dliprin-*α mutants (Fig. 15G).

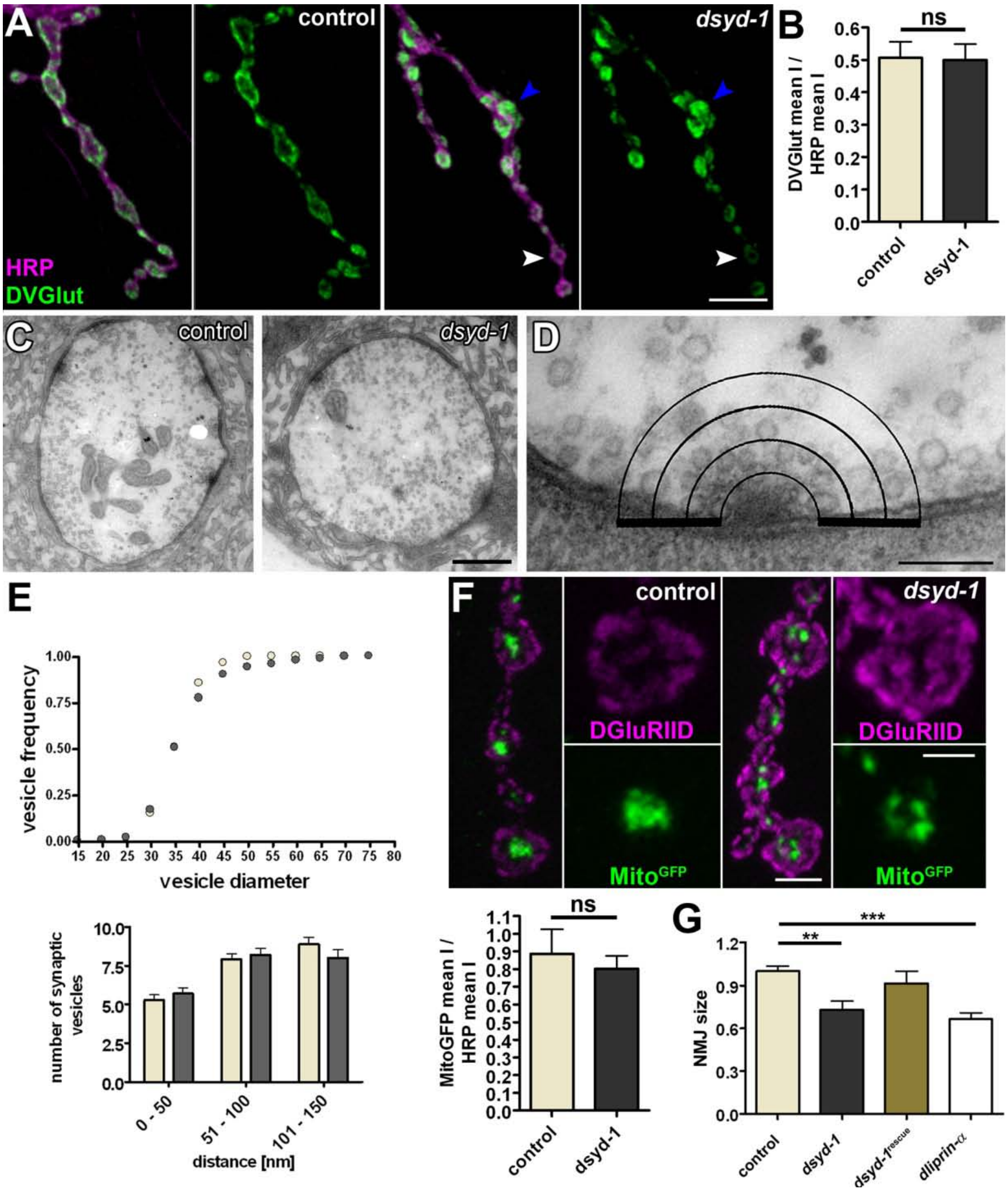
A
control
dsyd-1
HRP
DVGlut
B
ns
DVGlut mean I / HRP mean I
0.0
0.1
0.2
0.3
0.4
0.5
0.6
control
dsyd-1
C
control
dsyd-1
D
E
vesicle frequency
0.00
0.25
0.50
0.75
1.00
15 20 25 30 35 40 45 50 55 60 65 70 75 80
vesicle diameter
number of synaptic vesicles
0.0
2.5
5.0
7.5
10.0
0 - 50
51 - 100
101 - 150
distance [nm]
F
control
dsyd-1
DGluRIID
DGluRIID
MitoGFP
MitoGFP
ns
MitoGFP mean I / HRP mean I
0.0 0.1 0.2 0.3 0.4 0.5 0.6 0.7 0.8 0.9 1.0 1.1
control
dsyd-1
G
**
***
NMJ size
0.0
0.3
0.6
0.9
1.2
control
dsyd-1
dsyd-1rescue
dliprin-α

Fig. 15 SV distribution and size is mildly affected, while NMJ size is reduced in *dsyd-1*
A) HRP (anti-horseradish peroxidase, recognizes nerval membranes) and DVGlut co-staining of control and *dsyd-1* NMJs. The DVGlut distribution seems to be inhomogeneous in *dsyd-1* mutants (blue arrow head indicates bouton with strong reactivity, white arrow head indicates bouton with weak reactivity). Scale bar 5 µm. **B**) The mean DVGlut intensity is comparable between mutant and control (control: 0.51 ± 0.05, n = 7; *dsyd-1*: 0.50 ± 0.05, p = 0.88 according to Mann-Whitney test). **C-E**) illustrates the ultrastructural analysis. C) Bouton overview. Scale bars: 700 nm. The relative cumulative frequency of SV diameters in *dsyd-1* mutants and controls is comparable (D and E, upper panel), as is the SV distribution surrounding the T bar at AZs (D and E, lower panel). D) Scale bar: 150 nm. **F**) Co-labeling for Mito^{GFP} and DGluRIID. Scale bars: 1 µm and 500 nm (upper panel). Mean intensity of Mito^{GFP} is not altered significantly (control: 0.89 ± 0.14, n = 7; *dsyd-1*: 0.80 ± 0.08, p = 0.97 according to Mann-Whitney test, lower panel). **G**) *dliprin-*α and *dsyd-1* mutants showed a reduction in NMJ size, as judged from a comparison of HRP stainings between mutants and controls; the latter was rescued by motoneuron-specific re-expression of *dsyd-1*^{cDNA} (control: 1.0 ± 0.04, n = 30; *dsyd-1*: 0.73 ± 0.06, n = 14; *dsyd-1*^{rescue}: 0.91 ± 0.08, n = 8; *dliprin-*α: 0.66 ± 0.04, n = 14; control x *dsyd-1*: p < 0.01; control x *dsyd-1*^{rescue}: p > 0.05; control x *dliprin-*α: p < 0.001; *dsyd-1* x *dsyd-1*^{rescue}: p > 0.05; *dsyd-1* x *dliprin-*α: p > 0.05; *dsyd-1*^{rescue} x *dliprin-*α: p > 0.05 according to one way ANOVA). Modified from Owald et al. (2010).

Moreover, a significant reduction of AZs was observed in *dsyd-1* (a reduction by 28% compared to controls, n = 14 each, p = 0.02) mutants. This reduction was even more pronounced in *dliprin-α* (65% reduction, n = 8, p = 0.0002) mutant larvae (Owald et al., 2010). Thus, presynaptic DSyd-1 is needed for developing NMJs to reach full morphological size and a corresponding number of release sites. Consistent with previous reports, release site numbers are also reduced (Kaufmann et al., 2002) at *dliprin-α* mutant NMJs.

Taken together, eEJC amplitude reduction was comparable between *dsyd-1* and *dliprin-α* mutants, while both *dsyd-1* and *dliprin-α* mutants formed less synapses. As the reduction in synapse numbers was more pronounced in *dliprin-α* than in *dsyd-1* mutants, this reduction might only partially account for the observed decrease in eEJC amplitudes (Owald et al., 2010).

3.2.6. Defective Active Zone Assembly and Ectopic BRP Accumulations at *dsyd-1* Mutant Terminals

BRP signals appeared atypically large at *dsyd-1* mutant NMJs. In order to analyze *dsyd-1* mutant AZ morphology more accurately, STED microscopy was used for further analyses. STED allows for detailed assessment of AZ substructures, which are hard to resolve with classical light microscopy (Owald and Sigrist, 2009).

At wild type AZs, the N-term of BRP localizes close to Ca^{2+} channels at the AZ membrane, while the C-term of BRP (recognized by the antibody BRP^{Nc82}) reaches towards the bouton interior. Moreover, the epitope of BRP^{Nc82} defines the edge of the distal T bar platform, which results in a typical donut-shaped appearance in STED images [Fig. 5B, 16A and A', arrow head]. This donut-type morphology was clearly compromised at *dsyd-1* mutant AZs (Fig. 16B and B', arrow head). As shown in figure 16B, BRP organization often appeared enlarged and misshapen at individual sites (Fig. 16B and B', arrow heads, Fig. 16D). Wild type BRP morphology was, however, partially restored by re-expression of UAS-*dsyd-1*^{cDNA} (Fig. 16C and C').

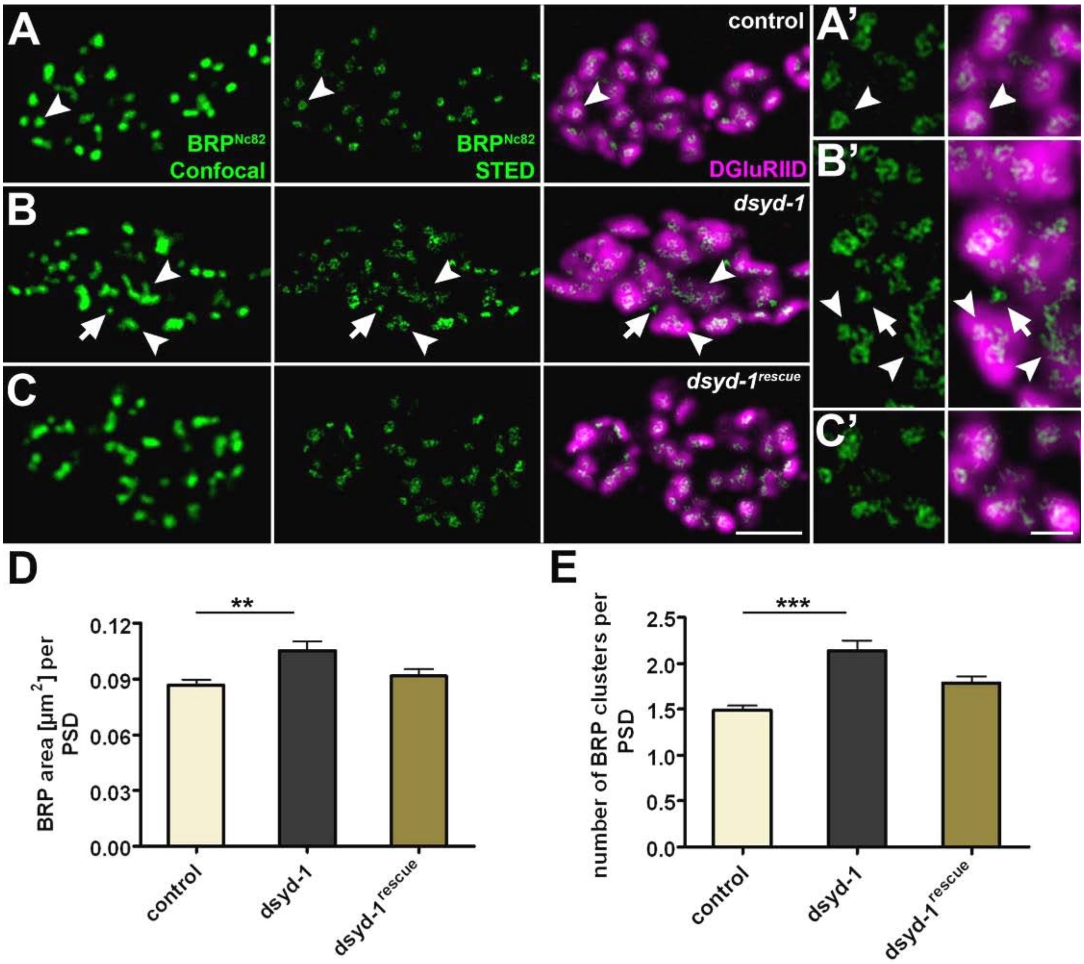
A
BRP^Nc82 Confocal
BRP^Nc82 STED
control
DGluRIID
A'
B
dsyd-1
B'
C
dsyd-1^rescue
C'
D
**
BRP area [µm²] per PSD
0.12
0.09
0.06
0.03
0.00
control
dsyd-1
dsyd-1^rescue
E
***
number of BRP clusters per PSD
2.5
2.0
1.5
1.0
0.5
0.0
control
dsyd-1
dsyd-1^rescue

Fig. 16 Abnormal BRP clusters at *dsyd-1* mutant NMJs
A-C) show BRP spots (confocal, left panel), BRP donuts (STED, middle panel) and an overlay of DGluRIID with BRP donuts (right panel). A) A control BRP donut is indicated by the arrow head. B) AZ size (arrow heads) is affected in *dsyd-1.* BRP donuts lacking postsynaptic DGluRIID receptors are observed (arrow). BRP donuts are frequently interconnected and abnormally shaped (arrow heads). This is rescued by re-expression of UAS-*dsyd-1*$^{\mathrm{cDNA}}$ (C). Scale bar: 1 µm. **A'-C'**) show magnifications of A-C). Scale bar: 250 nm. **D**) Quantification shows elevated areas of individual BRP$^{\mathrm{Nc82}}$ clusters (control: 0.087 ± 0.002 µm^2, n = 298; *dsyd-1*: 0.105 ± 0.005 µm^2, n = 265; *dsyd-1*^{rescue}: 0.091 ± 0.004, n = 207; control x *dsyd-1*: $p < 0.01$; control x *dsyd-1*^{rescue}: $p > 0.05$; *dsyd-1* x *dsyd-1*^{rescue}: $p > 0.05$ according to one way ANOVA). **E**) Individual BRP clusters per single PSD (control: 1.49 ± 0.05, n = 297; *dsyd-1*: 2.14 ± 0.12, n = 265; *dsyd-1*^{rescue}: 1.79 ± 0.08, n = 207; control x *dsyd-1*: $p < 0.001$; control x *dsyd-1*^{rescue}: $p > 0.05$; *dsyd-1* x *dsyd-1*^{rescue}: $p > 0.05$ according to one way ANOVA). Taken from Owald et al. (2010).

Individual synaptic entities (as defined by presynaptic BRP in conjunction with opposing PSDs) showed further abnormalities in *dsyd-1* mutants. While the size of individual PSDs was enlarged (see 3.4.1.), individual release sites (defined by their postsynaptic PSDs) often comprised several BRP clusters (Fig. 16E). Furthermore, the spacing between AZs appeared irregular. At the same time, small BRP assemblies lacking adjacent receptor fields were observed (Fig. 16B and B’, arrow). These assemblies might represent a population of AZs that fails to reach a mature size due to a lack of sufficient BRP accumulation at newly forming AZs (in the following referred to as “nucleation”).

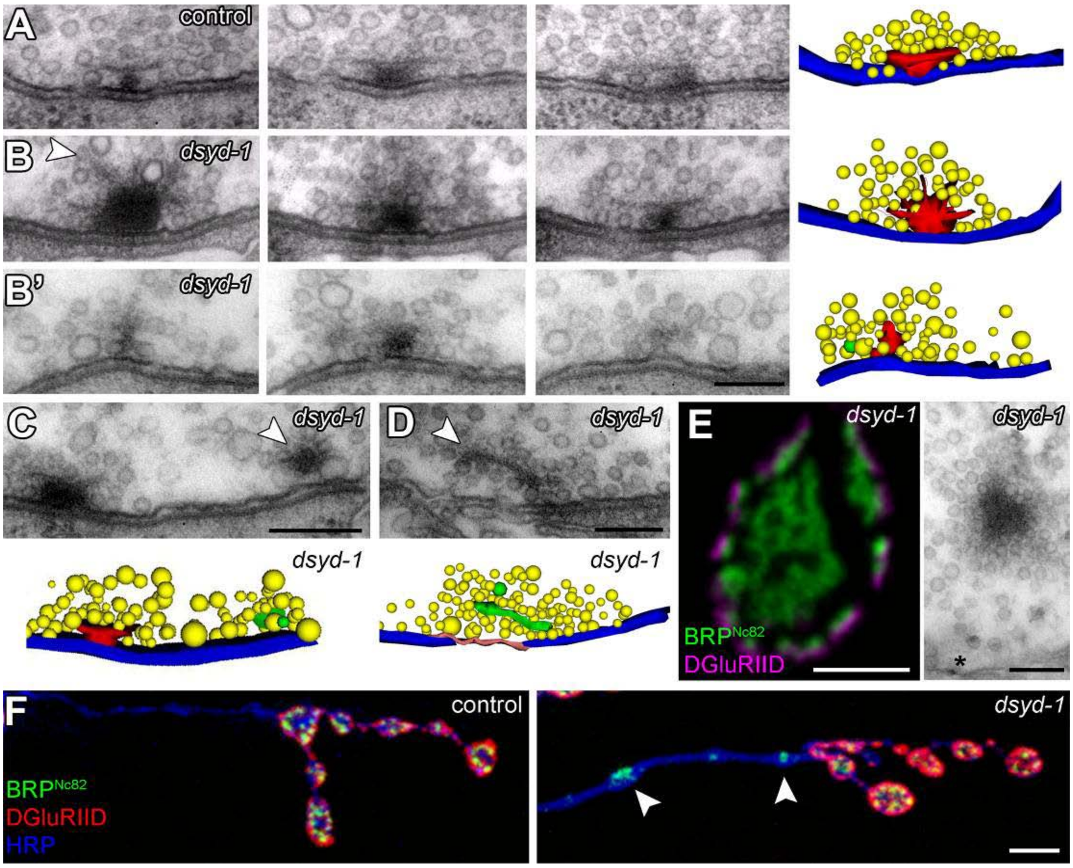

Fig. 17 Abnormal organization of T bar and electron dense material in *dsyd-1* mutant animals

A-B’) Serial sections of misshapen T bar at a *dsyd-1* deficient AZ (B and B’) compared to a control T bar (A). Scale bar: 100 nm. The arrow head indicates filaments emerging from an overgrown T bar in *dsyd-1* (B). B’) Immature small T bar in *dsyd-1*. A-D) Reconstructions: T bar material is depicted in red, SVs are illustrated in yellow and the AZ membrane is shown in blue. **C**) Non-anchored electron dense material can be found at AZs (arrow head, green in reconstruction) and electron dense material associated with SVs is found proximal to AZs (**D**, scale bar 150 nm). **E**) Detached BRP (confocal image, left, green) is found at the bouton center in *dsyd-1* mutants. Consistent with this, electron dense material is found throughout the bouton on an ultrastructural level (right). Scale bars: 1 µm and 100 nm. Floating electron dense material (not shown) and BRP immunoreactivity (**F,** arrow heads, scale bar: 1 µm) is also found in axonal stretches. Taken from Owald et al. (2010).

3.2.7. Dense Body Morphology at *dsyd-1* Mutant AZs

In order to address T bar morphology at *dsyd-1* mutant AZs, ultrastructural studies were conducted (together with Carolin Wichmann, Fig. 17A) and combined with 3D reconstruction of serial sections. As expected from the aberrant BRP morphology (Fig. 16B and B'), T bars often appeared irregular in shape (Fig. 17B) in *dsyd-1* mutants. A population of T bars showed large pedestals, which were characterized by multiple, atypically prominent filamentous projections at their distal ends (Fig. 17B, arrow head, also see reconstruction). Such misshapen T bars (as in Fig. 17B) were never observed in controls (Fig. 17A). Moreover, atypically small T bar-like assemblies could be observed as well in these animals (Fig. 17B'). These might well correspond to the small BRP clusters observed in STED images (Fig. 16B and B', arrow).

At control NMJs, electron dense material is absolutely restricted to the T bar assembly, which centers the AZ (here an AZ is defined by a planar apposition between the pre- and postsynaptic membrane). Interestingly, ectopic electron dense material was observed at *dsyd-1* mutant NMJ terminals. Such material frequently appeared at the edge of AZs (Fig. 17C), and seemed only loosely (Fig. 17D, arrow head), or not at all (Fig. 17E) associated with the presynaptic plasma membrane. Moreover, floating electron dense material, highly decorated with SVs, was present in the bouton interior as well (Fig. 17E). As BRP seems to be the principal component of the electron dense T bar (Fig. 7), these ectopic electron dense assemblies in *dsyd-1* mutants should contain BRP.

Consistent with this, ectopic BRP reactivity was detected at the bouton center and throughout the axon (Fig. 17E and F) in *dsyd-1* mutants. Moreover, axonal BRP accumulations co-localized with the SV marker DVGlut [(Daniels et al., 2004; Mahr and Aberle, 2006), Fig. 18], indicating that ectopic BRP/electron dense material might be capable of clustering SVs.

Taken together, less mature-sized AZs formed in *dsyd-1* mutants. Likely, some AZs do not progress in maturation and remain small. A second population of AZs incorporates excessive amounts of BRP, while additional electron dense material "precipitates" ectopically. Thus, DSyd-1 appears necessary for an adequate distribution of AZ material between individual AZs and to promote the assembly of newly forming sites.

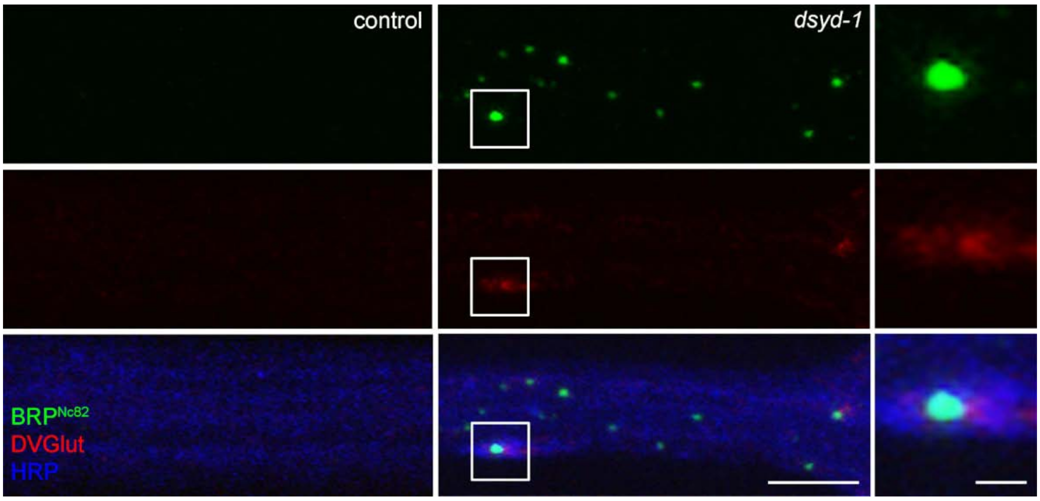

Fig. 18 Ectopic BRP and DVGlut co-localize in *dsyd-1* mutant axons
Some axonal BRP positive spots are also positive for the SV marker DVGlut. Scale bars: 3 µm and 500 nm. Taken from Owald et al. (2010).

3.2.8. DSyd-1 Regulates AZ Morphology Dependent on DLiprin-α

Behavioral analysis indicated that DSyd-1 shares functions with DLiprin-α, but that DSyd-1 also executes DLiprin-α-independent functions (Fig. 11B and C).

If both proteins solely acted in the same pathway, double mutant combinations should show similar phenotypes to single mutants. In order to test this, *dliprin-α; dsyd-1* double mutants were established. While *dsyd-1* and *dliprin-α* single mutants survived to adulthood, double mutants were embryonic lethal, again indicating that the functions of both proteins do *not* fully overlap.

The embryonic lethality of *dsyd-1; dliprin-α* might be due to an inability to form AZs and synapses altogether. To test this, ultrastructural analysis of high pressure frozen/freeze substituted (HPF/FS, together with Carolin Wichmann) embryos was performed. T bars as well as planar synaptic membrane contacts were observable in *dsyd-1* and *dliprin-α* single mutants. However, they were also found in *dliprin-α*; *dsyd-1* double mutant embryos (Fig. 19A). Hence, synapse formation as well as T bar assembly can, in principle, proceed in the absence of both proteins. DSyd-1 and DLiprin-α do not seem to be essential for, but rather to promote AZ formation (Fig. 19A).

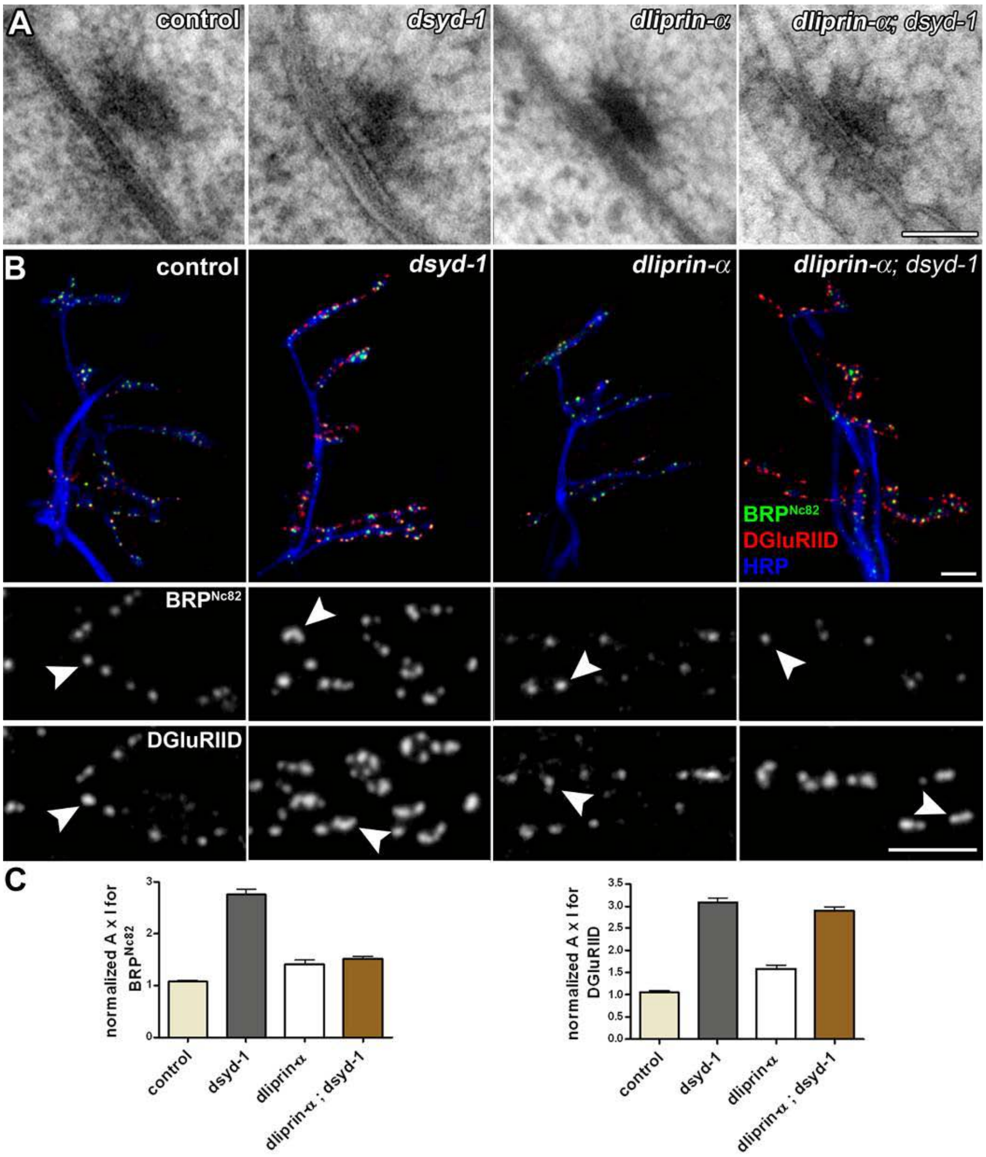
A
control
dsyd-1
dliprin-α
dliprin-α; dsyd-1
B
control
dsyd-1
dliprin-α
dliprin-α; dsyd-1
BRP^Nc82
DGluRIID
HRP
BRP^Nc82
DGluRIID
C
normalized A x I for BRP^Nc82
0
1
2
3
control
dsyd-1
dliprin-α
dliprin-α ; dsyd-1
normalized A x I for DGluRIID
0.0
0.5
1.0
1.5
2.0
2.5
3.0
3.5
control
dsyd-1
dliprin-α
dliprin-α ; dsyd-1

Fig. 19 DSyd-1 regulates AZ size dependent on, and PSD size independent of DLiprin-α

A) HPF/FS prepared NMJ synapse of (1) control, (2) *dsyd-1*, (3) *dliprin-α* and (4) *dliprin-α*; *dsyd-1* double mutant embryos. All genotypes form electron dense projections at the AZ. Scale bar: 70 nm. **B**) The immunostainings shows NMJs of muscles 6/7, 12/13 and 4 in late embryos: (1) control, (2) *dsyd-1*, (3) *dliprin-α* and (4) *dliprin-α; dsyd-1*; all are stained for HRP (nerve, blue), BRP (green) and DGluRIID (red). Scale bar: 2 µm. Below: magnifications show single synapses with arrow heads marking BRP (middle panels) and DGluRIID (lower panels) spots in the indicated mutants. Scale bar: 1 µm. **C**) Quantification of the BRP and the DGluRIID signal at embryonic synapses. The BRP signal is significantly increased in *dsyd-1* single mutants compared to (1) control, (2) *dliprin-α*, and (3) *dliprin-α*; *dsyd-1* double mutants. The DGluRIID signal is increased to a similar extent in (1) *dsyd-1*, and (2) *dliprin-α; dsyd-1* double mutants compared to (1) control and (2) *dliprin-α* mutant animals (for BRP: control: 1.07 ± 0.027, n = 735; *dsyd-1*: 2.75 ± 0.11, n = 457; *dliprin-α*: 1.41 ± 0.079, n = 183; *dliprin-α; dsyd-1*: 1.51 ± 0.054, n = 446; control x *dsyd-1*: $p < 0.001$; control x *dliprin-α*: $p < 0.05$; control x *dliprin-α; dsyd-1*: $p < 0.001$; *dsyd-1* x *dliprin-α*: $p < 0.001$; *dsyd-1* x *dliprin-α; dsyd-1*: $p < 0.001$; *dliprin-α* x *dliprin-α; dsyd-1*: $p > 0.05$ according to one-way ANOVA test; for DGluRIID: control: 1.06 ± 0.029, n = 765; *dsyd-1*: 3.08 ± 0.10, n = 541; *dliprin-α*: 1.59 ± 0.080, n = 218; *dliprin-α; dsyd-1*: 2.90 ± 0.088, n = 612; control x *dsyd-1*: $p < 0.001$; control x *dliprin-α*: $p < 0.001$; control x *dliprin-α; dsyd-1*: $p < 0.001$; *dsyd-1* x *dliprin-α*: $p < 0.001$; *dsyd-1* x *dliprin-α; dsyd-1*: $p > 0.05$; *dliprin-α* x *dliprin-α, dsyd-1*: $p < 0.001$ according to one-way ANOVA test). Taken from Owald et al. (2010).

Using BRP as a presynaptic and DGluRIID as a postsynaptic marker, embryonic synapse morphology was analyzed in the single and double mutant animals (Fig. 19B and C). Compared to controls, BRP reactivity was clearly elevated at *dsyd-1*, but only very mildly at *dliprin-α* mutant NMJs (Fig. 19B). More so, BRP levels at *dliprin-α; dsyd-1* double mutant NMJs were comparable to those at *dliprin-α* - rather than to those at *dsyd-1* mutant NMJs (Fig. 19B). Thus, increased BRP recruitment to *dsyd-1* mutant AZs is dependent on the presence of DLiprin-α.

Levels of DGluRIID were also drastically increased at *dsyd-1* and equally at *dsyd-1*; *dliprin-α* double mutant NMJs, but only mildly elevated at *dliprin-α* deficient synapses (Fig. 19B and C). Thus, DSyd-1 is involved in the regulation of glutamate receptor field size (at least largely) independently of DLiprin-α (see 3.4.1.).

3.3. DSyd-1 in the Assembly of Nascent Active Zones

3.3.1. DSyd-1 and DLiprin-α Arrive Early at Nascent Active Zones

So far, DSyd-1 and DLiprin-α were shown to co-operate in AZ assembly, while DSyd-1 has phenotypic consequences not seen after deletion of DLiprin-α (see 3.2.).

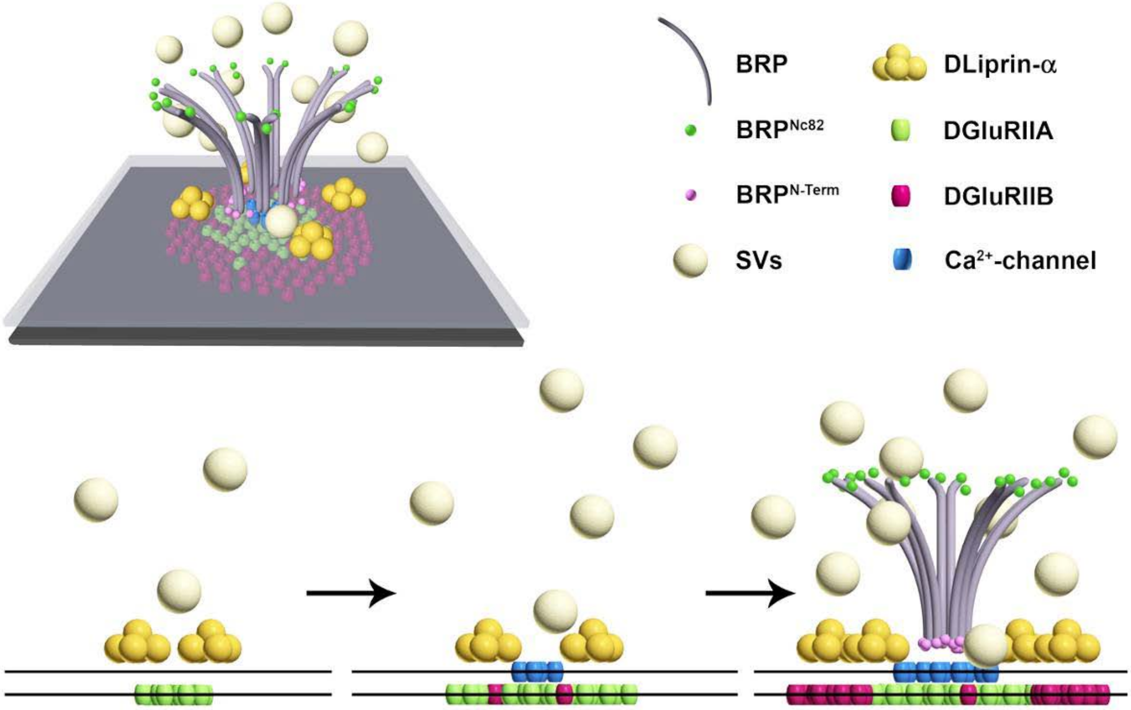

Fig. 20 Temporal model of DLiprin-α, BRP and glutamate receptor assembly at *Drosophila* NMJs
This scheme illustrates the protracted synapse assembly process, as known for the *Drosophila* NMJ. Presynaptic DLiprin-α precedes the postsynaptic accumulation of glutamate receptors. BRP arrives late during synapse assembly, yet is typically preceded by Ca^{2+} channels. Modified from Fouquet et al. (2009).

To get an impression of the spatio-temporal profile of DSyd-1 accumulation throughout AZ assembly, protocols for monitoring protein traffic over extended periods in intact living larvae were used (Fuger et al., 2007; Rasse et al., 2005; Schmid et al., 2008). Larvae co-expressing two fluorescently tagged synaptic proteins were imaged and quantitative data were obtained to analyze the temporal sequence of protein arrival at developing AZs. For a given larval NMJ, two *in vivo* images were acquired with a time interval of 12 hours. Sites were regarded as new synapses if protein-labels exceeded the average background by a factor of 2.5 at the second (t = 12 h) but not at the first time point (t = 0 h). Using this approach, we demonstrated that DLiprin-α precedes the accumulation of the postsynaptic glutamate receptor subunit IIA, as well as - by hours - the arrival of presynaptic BRP [for a schematic overview see Fig. 20, (Fouquet et al., 2009)].

To image DSyd-1 *in vivo*, ^{GFP}DSyd-1 (which when pan-neuronally-expressed rescues the sluggish behavior of *dsyd-1* mutant adults) and BRP-short^{mStraw} were co-expressed in motoneurons. ^{GFP}DSyd-1 specifically labeled AZs (Fig. 21A and B), as was to be expected from immunostainings of endogenous DSyd-1 (Fig. 12). Individual NMJs re-imaged after 12 hours, showed substantial growth of the NMJ along with the addition of new AZs (Fig. 21A). Strikingly, DSyd-1 clearly and invariably preceded BRP at newly forming sites [Fig. 21A, arrow heads, together with Wernher Fouquet (Owald et al., 2010)].

Next, DLiprin-α^{GFP} and ^{mStraw}DSyd-1 were co-expressed in motoneurons. Small, newly formed AZs (“nascent sites”) were usually decorated with both DLiprin-α^{GFP} and ^{mStraw}DSyd-1. This suggests that both proteins arrived at synaptic sites in very close temporal proximity [Fig. 21B, arrows and arrow heads, together with Wernher Fouquet, (Fouquet et al., 2009; Owald et al., 2010)].

3.3.2. Dynamic, Often Reversible Assembly of DLiprin-α and DSyd-1 during Initial Active Zone Assembly

To investigate the time course of early AZ assembly in more detail, DSyd-1 and DLiprin-α clusters were imaged at shorter time-intervals (t = 0, 30 and 60 min, Fig. 22, together with Wernher Fouquet). It became obvious, that the exact distribution of both proteins changed dynamically at mature, BRP positive AZs (Fig. 22A). At the same time, the intensity and distribution of BRP appeared rather static at these sites (Fig. 22A and D).

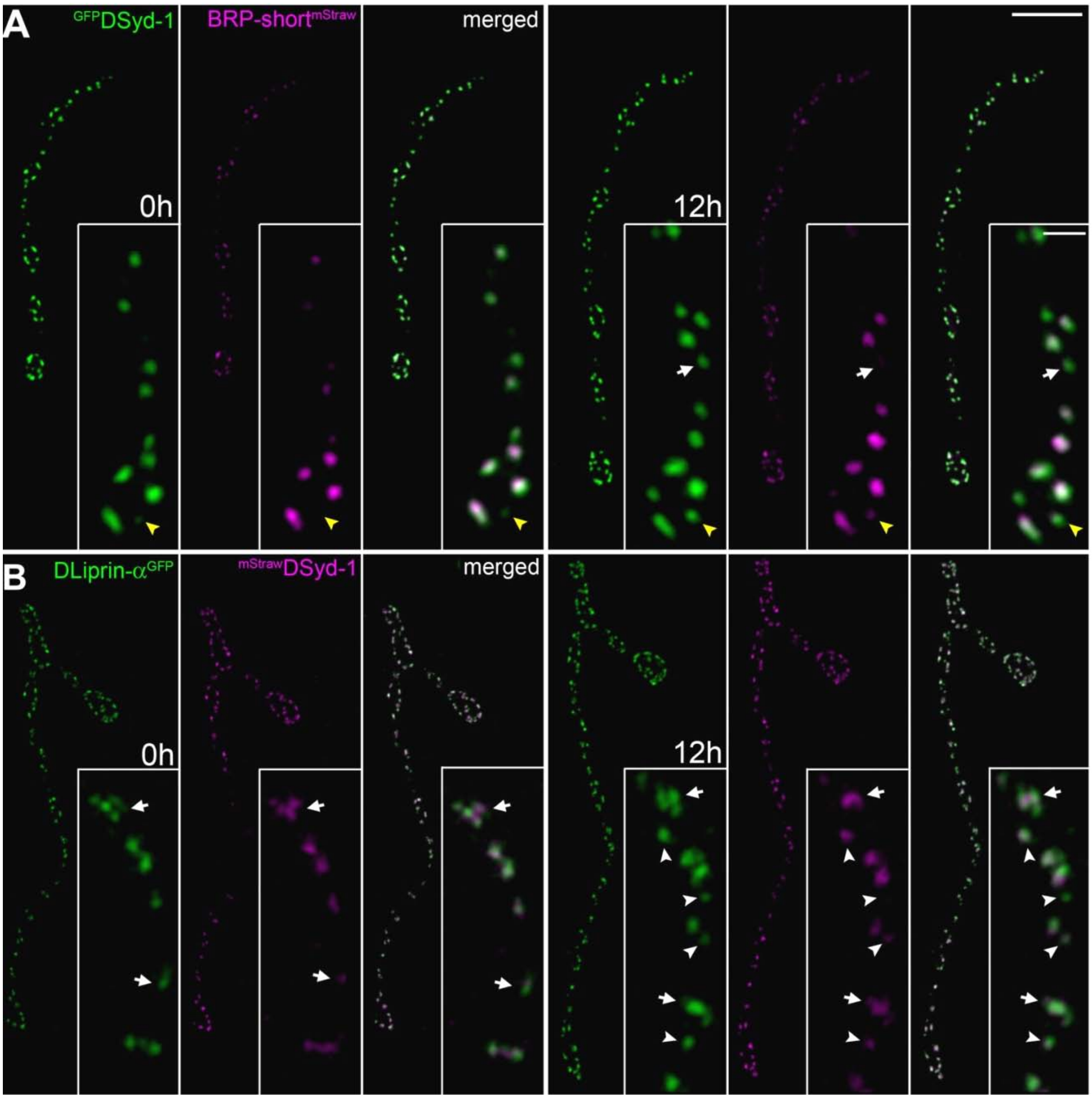

Fig. 21 DSyd-1 accumulates early during AZ formation
Confocal stacks of sequentially *in vivo* imaged NMJs (muscle 26), Δt = 12 h. NMJs co-expressing (**A**) ^{GFP}DSyd-1 and BRP-short^{mStraw} and (**B**) DLiprin-α^{GFP} and ^{mStraw}DSyd-1. The images in (A) illustrate that DSyd-1 precedes BRP (DSyd-1 precedes BRP: 65%; BRP precedes DSyd-1: 0%; not resolved: 35%; n = 37). The images in (B) show that DLiprin-α and DSyd-1 accumulate in close temporal proximity (DLiprin-α precedes DSyd-1: 26%; DSyd-1 precedes DLiprin-α: 6%; not resolved: 68%; n = 35). The arrows in (A) indicate a nascent AZ, where DSyd-1 precedes BRP accumulation. Scale bar: 4 µm, Inlet scale bar: 500 nm. The arrows in (B) mark AZs, where DSyd-1 and DLiprin-α accumulate in close temporal proximity. Together with Wernher Fouquet. Taken from Owald et al. (2010).

Moreover, at nascent sites (not positive for BRP, but for DLiprin-α and/or DSyd-1), small-to-medium-sized DLiprin-α and DSyd-1 positive clusters often dissolved over the time period of these 60 min experiments (Fig. 22A, C and D blue arrow heads).

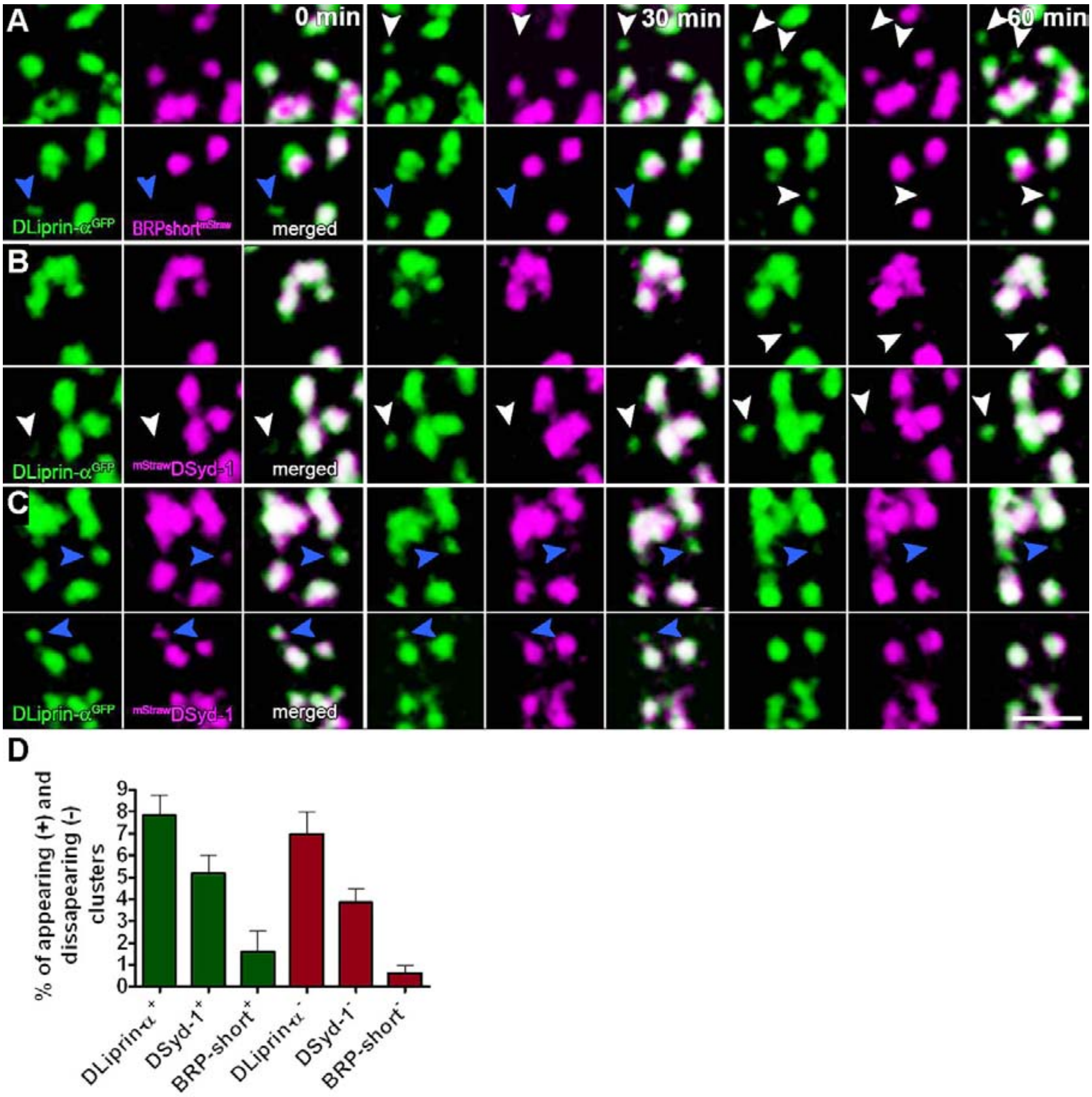
A
0 min
30 min
60 min
DLiprin-α^GFP
BRPshort^mStraw
merged
B
DLiprin-α^GFP
^mStraw DSyd-1
merged
C
DLiprin-α^GFP
^mStraw DSyd-1
merged
D
% of appearing (+) and dissapearing (-) clusters
0
1
2
3
4
5
6
7
8
9
DLiprin-α+
DSyd-1+
BRP-short+
DLiprin-α-
DSyd-1-
BRP-short-

Fig. 22 Reversible assembly of nascent AZs

Confocal stacks of sequentially *in vivo* imaged NMJ synapses (muscle 26), Δt = 30 min and 60 min. **A**) A subset of AZs of a NMJ co-expressing DLiprin-α^{GFP} and BRP-short^{mStraw}. The white arrow heads indicate newly forming DLiprin-α spots lacking BRP. The blue arrow heads indicate a DLiprin-α cluster that disappears at t = 60 min. **B-C**) A subset of AZs of a NMJ co-expressing DLiprin-α^{GFP} and ^{mStraw}DSyd-1. B) Upper panels: the arrow heads indicate a newly forming site at t = 60 min. The site is positive for both DLiprin-α and DSyd-1. Lower panels: a nascent presynaptic site positive for DLiprin-α but negative for DSyd-1 at t = 0 min and t = 30 min. This site is positive for both proteins at t = 60 min (arrow head). C) Upper panel: a nascent site positive for both DLiprin-α and DSyd-1 at t = 0 min and t = 30 min. This site is positive for DLiprin-α but negative for DSyd-1 at t = 60 min. Lower panel: A nascent site positive for both DLiprin-α and DSyd-1 at t = 0 min and for DLiprin-α only at t = 30 min. Both labels have disappeared at t = 60 min. Scale bar: 500 nm. **D**) Quantification of protein mobility with DLiprin-α showing the highest mobility, while BRP appears rather static (for appearing clusters (+): DLiprin-α: 7.82 ± 0.91, n = 13; DSyd-1: 5.13 ± 0.87, n = 13; BRP-short: 1.60 ± 0.93, n = 4; DLiprin-α x DSyd-1: p = 0.018; DLiprin-α x BRP-short: p = 0.008; DSyd-1 x BRP-short: p = 0.048, according to Mann-Whitney test; for disappearing clusters (-): DLiprin-α: 6.95 ± 1.01, n = 13; DSyd-1: 3.83 ± 0.61, n = 13; BRP-short: 0.62 ± 0.36, n = 4; DLiprin-α x DSyd-1: p = 0.024; DLiprin-α x BRP-short: p = 0.004; DSyd-1 x BRP-short: p = 0.011, according to Mann-Whitney test). Together with Wernher Fouquet.

Both DSyd-1 and DLiprin-α therefore appeared mobile (also referred to as “dynamic”). Thus, while DLiprin-α and DSyd-1 clusters seem obligatory in the assembly of stable AZs [Fig. 21, 22 and (Fouquet et al., 2009)], not all such clusters develop in the direction of mature AZs. Moreover, synaptic proteins that assemble temporally downstream of DLiprin-α and DSyd-1 appear rather static. This indicates that early processes in AZ assembly are still reversible (Fig. 22). In contrast, later steps of synapse assembly typically appear to be largely irreversible.

Interestingly, DLiprin-α sometimes preceded DSyd-1 during assembly (Fig. 22B, lower panel, arrow heads). At disassembling sites, however, DSyd-1 had the tendency to disappear prior to the retraction of DLiprin-α clusters (Fig. 22C, lower panel, blue arrow heads). While DLiprin-α showed highest mobility, DSyd-1 was somewhat more static. Indeed quantification of (+) appearing and (-) disappearing clusters (Fig. 22D) supported this impression.

3.3.3. DSyd-1 is Needed for Proper Active Zone Localization of DLiprin-α - but Not *Vice Versa*

Genetic analysis in *C. elegans* has placed the putative RhoGAP DSyd-1 upstream of Syd-2/Liprin-α in the assembly hierarchy (Dai et al., 2006; Patel et al., 2006). Would both factors reciprocally influence their distribution and AZ localization (Fig. 23A-E)?

At control NMJs (Fig. 23A), DLiprin-α and BRP co-labeled individual AZs in a regular pattern (23A, arrow heads). However, DLiprin-α distribution appeared irregular at *dsyd-1* mutant terminals (Fig. 23B), and many AZs (identified via BRP) lacked adequate DLiprin-α label (arrow heads). At the same time, large ectopic DLiprin-α spots appeared distant from BRP puncta (Fig. 23B, arrows). In turn, most AZs showed restored DLiprin-α label (Fig. 23C, arrow heads) after re-expression of UAS-*dsyd-1*^{cDNA}.

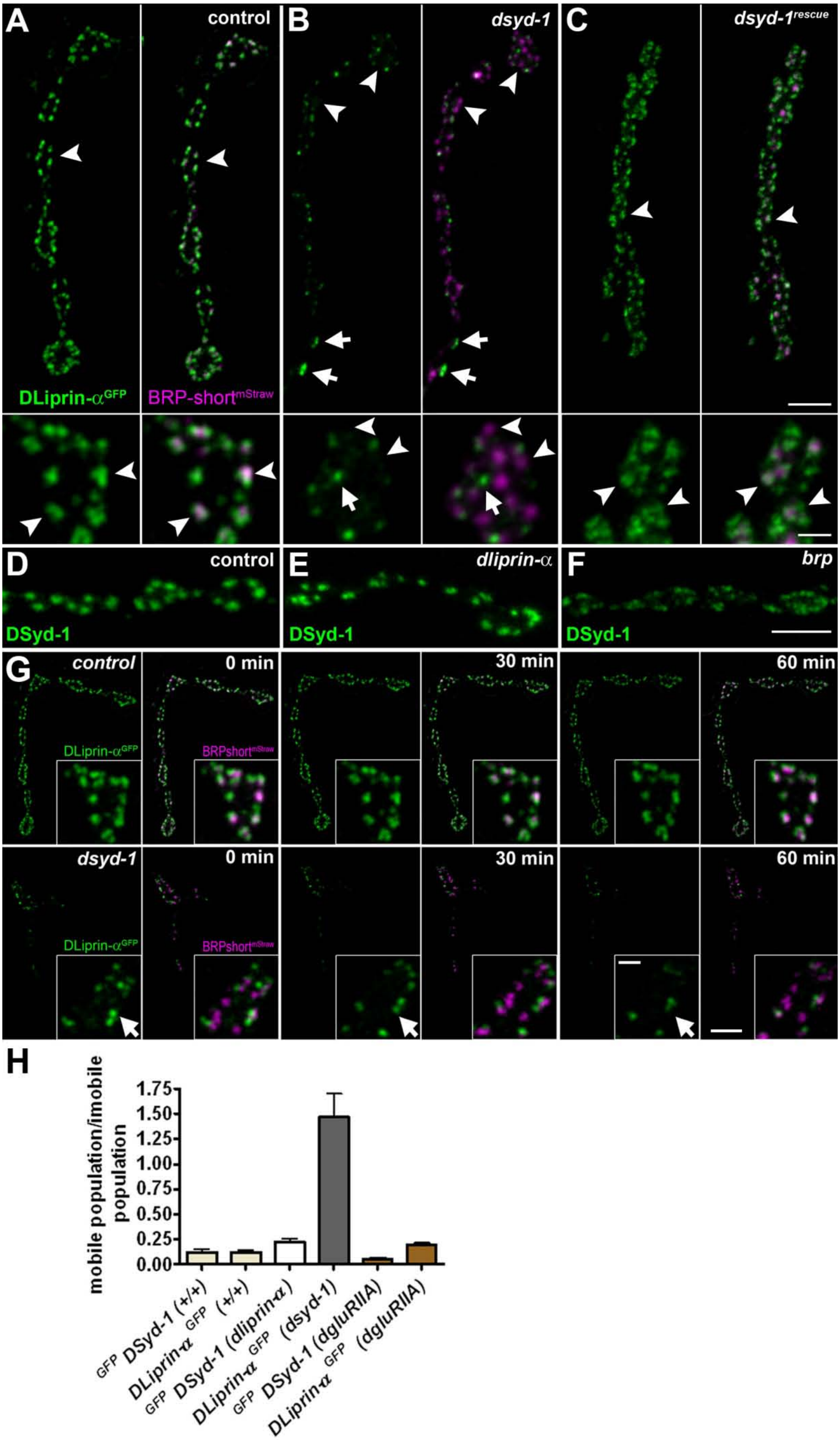
A
control
B
dsyd-1
C
dsyd-1^rescue
DLiprin-α^GFP
BRP-short^mStraw
D
control
DSyd-1
E
dliprin-α
DSyd-1
F
brp
DSyd-1
G
control
0 min
30 min
60 min
DLiprin-α^GFP
BRPshort^mStraw
dsyd-1
0 min
30 min
60 min
DLiprin-α^GFP
BRPshort^mStraw
H
mobile population/imobile population
1.75
1.50
1.25
1.00
0.75
0.50
0.25
0.00
GFP DSyd-1 (+/+)
DLiprin-α GFP (+/+)
GFP DSyd-1 (dliprin-α)
DLiprin-α GFP (dsyd-1)
GFP DSyd-1 (dgluRIIA)
DLiprin-α GFP (dgluRIIA)

Fig. 23 DLiprin-α is highly mobile in *dsyd-1* mutants
A-C) DLiprin-α^{GFP}/BRP-short^{mStraw} images of control (A), *dsyd-1* (B), and *dsyd-1*^{rescue} (C) NMJs are shown. The localization of DLiprin-α is changed in *dsyd-1* deficient animals compared to controls. The localization is rescued by re-expression of UAS-*dsyd-1*^{cDNA} in motoneurons. The arrow heads indicate AZs that are marked by BRP; the arrows indicate ectopic DLiprin-α in *dsyd-1* mutants**.** Scale bar: 2 µm and 500 nm. **D-F**) DSyd-1 localizes to AZs in control (D), *dliprin-α* (E), and *brp* (F) animals. A-F) Taken from Owald et al. (2010). **G**) A DLiprin-α^{GFP}/BRP-short^{mStraw} co-label from control (as shown in A), as well as from *dsyd-1* mutant boutons. The NMJs were reimaged with a Δt of 30 minutes. Arrow: DLiprin-α is highly mobile in *dsyd-1* mutants. Scale bar: 5 µm, Inlet scale bar: 500 nm. **H**) A quantification of nascent AZ marker dynamics in different mutant backgrounds. DLiprin-α dynamics are largely elevated in the *dsyd-1* deficient background (^{GFP}DSyd-1 (+/+): 0.123 ± 0.029; DLiprin-α^{GFP} (+/+): 0.122 ± 0.018; ^{GFP}DSyd-1 (*dliprin-α*): 0.23 ± 0.035; DLiprin-α^{GFP} (*dsyd-1*): 1.47 ± 0.233; ^{GFP}DSyd-1 (*dgluRIIA*) 0.056 ± 0.016; DLiprin-α^{GFP} (*dgluRIIA*): 0.196 ± 0.019; all: n = 4 NMJs; ^{GFP}DSyd-1 (+/+) x ^{GFP}DSyd-1 (*dliprin-α*): p = 0.057; ^{GFP}DSyd-1 (+/+) x ^{GFP}DSyd-1 (*dgluRIIA*): p = 0.114; DLiprin-α^{GFP} (+/+) x DLiprin-α^{GFP} (*dsyd-1*): p = 0.029; DLiprin-α^{GFP} (+/+) x DLiprin-α^{GFP} (*dgluRIIA*): p = 0.114, according to Mann-Whitney test).

In contrast, DSyd-1 targeted normally to AZs in *dliprin-α* mutants (compare Fig. 23D and E). Thus, presynaptic DSyd-1 is needed to properly localize DLiprin-α to AZs, but DLiprin-α is apparently not needed to target DSyd-1.

Would DSyd-1 also localize to *brp* mutant terminals? BRP arrives late during synapse assembly and is needed for proper maturation of release sites, as shown for the distribution of Ca^{2+} channels (Fouquet et al., 2009). Although DSyd-1 targeted to AZs (Fig. 23F), the distribution of the protein appeared “smeared”. This suggests that BRP is needed for the proper spacing of DSyd-1 at mature AZs.

3.3.4. DSyd-1 Stalls DLiprin-α at Nascent Synaptic Sites

As shown above (Fig. 23A-C), the distribution of DLiprin-α appears highly disorganized in the *dsyd-1* mutant background. In order to get an impression of whether DSyd-1 might regulate DLiprin-α cluster mobility, *dsyd-1* NMJs co-expressing DLiprin-α and BRP-short were re-imaged with a Δt of 30 minutes (Fig. 23G and H). Indeed, the distribution of DLiprin-α clusters changed rapidly in *dsyd-1* mutants (Fig. 23G arrow, and H), strikingly exceeding the already high DLiprin-α mobility in control situations. Thus, in agreement with the phenotypic analysis performed in embryos and larvae, DSyd-1 seems important to stall DLiprin-α at

AZs. In contrast, the mobility of DSyd-1 clusters remained unchanged in *dliprin-α* mutants when compared to controls (Fig. 23H).

It could be argued that a deficit in synapse formation *per se* might provoke deficits in protein accumulation and elevated protein mobility at AZs. While this would not explain the observed asymmetry between DSyd-1 and DLiprin-α, the mobility of both proteins was nonetheless checked for in an independent mutant (*dgluRIIA*) with reduced synapse formation (Sigrist et al., 2002). For both DLiprin-α and DSyd-1, distribution and mobility was comparable to controls in these settings (Fig. 23H).

The absence of DGluRIIA triggers a homeostatic mechanism, which leads to an increase of AZs that display a T bar (Frank et al., 2006; Schmid et al., 2006). If the presence of DSyd-1 stabilized DLiprin-α and BRP at AZs, mobility of DSyd-1 and DLiprin-α might be reduced compared to controls. Although DSyd-1 shows a slight tendency towards reduced mobility, overall results indicate that DGluRIIA mediated homeostasis is, at least largely, downstream of DSyd-1 and DLiprin-α based initial assembly processes (Fig. 23H).

Taken together, DLiprin-α and DSyd-1 appear to form mobile clusters at the plasma membrane. Some of these clusters increase in size, and once BRP (Fig. 21 and 22) and DGluRIIA (not shown) become visible at synaptic sites, they are destined to enter into a mature, stable state. Moreover, DLiprin-α and DSyd-1 localization is reversible at nascent AZs, while DSyd-1 appears to stall DLiprin-α clusters at synaptic sites.

3.4. Presynaptic DSyd-1 Controls the Composition of Postsynaptic Glutamate Receptor Fields

At the *Drosophila* NMJ, AMPA/Kainate-type receptors (assembled as heteromeric tetramers by selecting four from five subunits) mediate the postsynaptic response to glutamate. Three subunits, DGluRIIC, IID and IIE are essential for receptor formation and function and appear to be contained within all glutamate receptor complexes (Marrus et al., 2004; Petersen et al., 1997; Qin et al., 2005; Schmid et al., 2008). In order to assess PSDs in *dsyd-1* mutants, the distribution and signal intensity for different glutamate receptor subunits was studied (Fig. 24A-F).

3.4.1. Shifted Glutamate Receptor Composition in *dsyd-1* Mutants

Individual glutamate receptor fields were dramatically enlarged at *dsyd-1* mutant NMJs as seen in DGluRIID stainings (Fig. 16A and B, 24A-C, arrow heads). This enlargement was rescued after presynaptic (using the motoneuron driver *ok6-Gal4*, Fig. 24C and G), but not postsynaptic (using the muscle driver *G14-Gal4*, Fig. 24G) expression of UAS-*dsyd-1*$^{\mathrm{cDNA}}$ (DSyd-1 fails to localize to NMJs when expressed in muscles, not shown). Thus, presynaptic DSyd-1 has a role in defining the size of the postsynaptic glutamate receptor fields.

Each receptor also includes either DGluRIIA or DGluRIIB as a fourth subunit (Marrus et al., 2004; Petersen et al., 1997; Qin et al., 2005; Sigrist et al., 2002). On a genetic level, DGluRIIA complexes promote and DGluRIIB complexes limit the number of synapses, while on a physiological level DGluRIIA elicits slow desensitization and IIB desensitizes rapidly (Schmid et al., 2008).

DGluRIIA levels were dramatically increased at *dsyd-1* mutant NMJs, but restored to normal after presynaptic expression of UAS-*dsyd-1*$^{\mathrm{cDNA}}$ (Fig. 24D-F and H). However, the levels of DGluRIIB were specifically reduced at *dsyd-1* mutant NMJs (Fig. 24D-F and I), which shifted the ratio between the two glutamate receptor types (Fig. 24J).

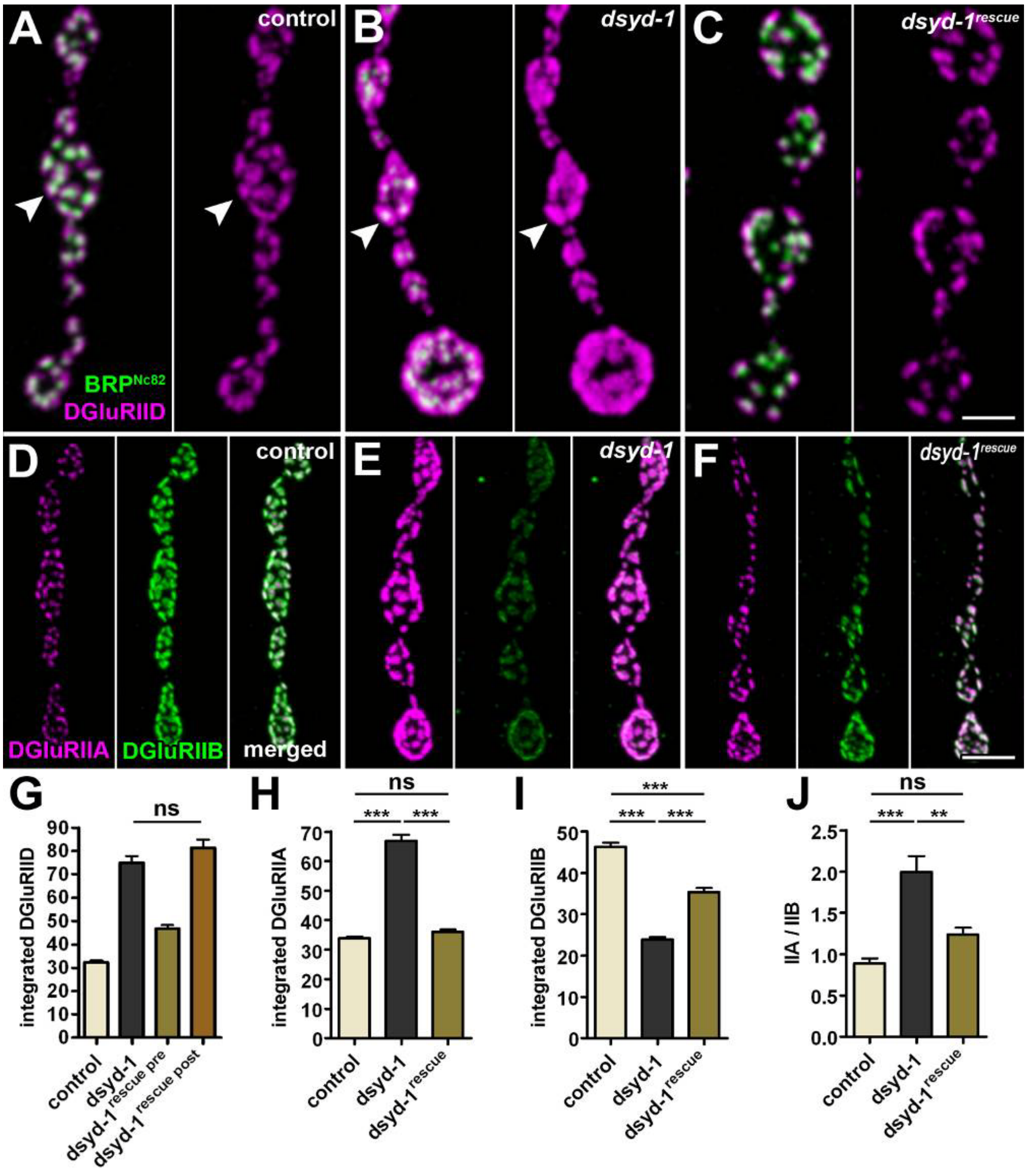
A
control
B
dsyd-1
C
dsyd-1rescue
BRPNc82
DGluRIID
D
control
E
dsyd-1
F
dsyd-1rescue
DGluRIIA
DGluRIIB
merged
G
ns
integrated DGluRIID
90
80
70
60
50
40
30
20
10
0
control
dsyd-1
dsyd-1rescue pre
dsyd-1rescue post
H
ns
***
***
integrated DGluRIIA
70
60
50
40
30
20
10
0
control
dsyd-1
dsyd-1rescue
I
***
***
***
integrated DGluRIIB
50
40
30
20
10
0
control
dsyd-1
dsyd-1rescue
J
ns
***
**
IIA / IIB
2.5
2.0
1.5
1.0
0.5
0.0
control
dsyd-1
dsyd-1rescue

Fig. 24 DSyd-1 controls postsynaptic glutamate receptor field size and composition
A-C) DGluRIID and BRP^{Nc82} co-stainings for control (A), *dsyd-1* mutant (B), and presynaptically rescued (by reexpression of UAS-*dsyd-1*^{cDNA}) *dsyd-1* mutant (C) NMJs. Individual PSDs are indicated by arrow heads. Scale bar: 1 µm. **D-F**) DGluRIIA and DGluRIIB co-staining for control (D), *dsyd-1* mutant (E) and presynaptically rescued *dsyd-1* (F) NMJs. Scale bar: 2 µm. **G**) The integrated DGluRIID signal in *dsyd-1* mutants (control: 32.25 ± 0.67 a.u., n = 1314; *dsyd-1*: 74.86 ± 2.98 a.u., n = 335; *dsyd-1*$^{\mathit{rescue\ pre}}$: 46.71 ± 1.60 a.u., n = 515; *dsyd-1*$^{\mathit{rescue\ post}}$: 81.25 ± 3.54 a.u., n = 344. control x *dsyd-1*: $p < 0.001$; control x *dsyd-1*$^{\mathit{rescue\ pre}}$: $p < 0.001$; control x *dsyd-1*$^{\mathit{rescue\ post}}$: $p < 0.001$; *dsyd-1* x *dsyd-1*$^{\mathit{rescue\ pre}}$: $p < 0.001$; *dsyd-1* x *dsyd-1*$^{\mathit{rescue\ post}}$: $p > 0.05$; *dsyd-1*$^{\mathit{rescue\ pre}}$ x *dsyd-1*$^{\mathit{rescue\ post}}$: $p < 0.001$ according to one way ANOVA). **H**) The integrated DGluRIIA signal in *dsyd-1* mutants (control: 33.88 ± 0.66 a.u., n = 1064; *dsyd-1*: 66.85 ± 2.09 a.u., n = 667; *dsyd-1*$^{\mathit{rescue}}$: 36.31 ± 0.87 a.u., n = 830. control x *dsyd-1*: $p < 0.001$; control x *dsyd-1*$^{\mathit{rescue}}$: $p > 0.05$; *dsyd-1* x *dsyd-1*$^{\mathit{rescue}}$: $p < 0.001$ according to one way ANOVA). **I**) The integrated DGluRIIB signal in *dsyd-1* mutants (control: 46.40 ± 0.99 a.u., n = 934; *dsyd-1*: 23.85 ± 0.60 a.u., n = 783; *dsyd-1*$^{\mathit{rescue}}$: 35.46 ± 0.89 a.u., n = 770. control x *dsyd-1*: $p < 0.001$; control x *dsyd-1*$^{\mathit{rescue}}$: $p < 0.001$; *dsyd-1* x *dsyd-1*$^{\mathit{rescue}}$: $p < 0.001$ according to one way ANOVA). **J**) The receptor field composition in *dsyd-1* mutants (control: 0.89 ± 0.06 a.u., n = 7; *dsyd-1*: 1.99 ± 0.19 a.u., n = 8; *dsyd-1*$^{\mathit{rescue}}$: 1.24 ± 0.08 a.u., n = 6. control x *dsyd-1*: $p < 0.001$; control x *dsyd-1*$^{\mathit{rescue}}$: $p > 0.05$; *dsyd-1* x *dsyd-1*$^{\mathit{rescue}}$: $p < 0.01$ according to one way ANOVA). Taken from Owald et al. (2010).

As DGluRIIA complexes exhibit slower desensitization kinetics than DGluRIIB complexes (Schmid et al. 2008), one might expect enlarged mEJCs at *dsyd-1* NMJs. Figure 14B shows that the mean mEJC amplitudes are not changed between *dsyd-1* mutants and controls. However, when analyzing the data more carefully (Fig. 25), a moderate tendency towards elevated frequencies of large mEJCs was observable for *dsyd-1* mutants in histogram plots (Fig. 25A).

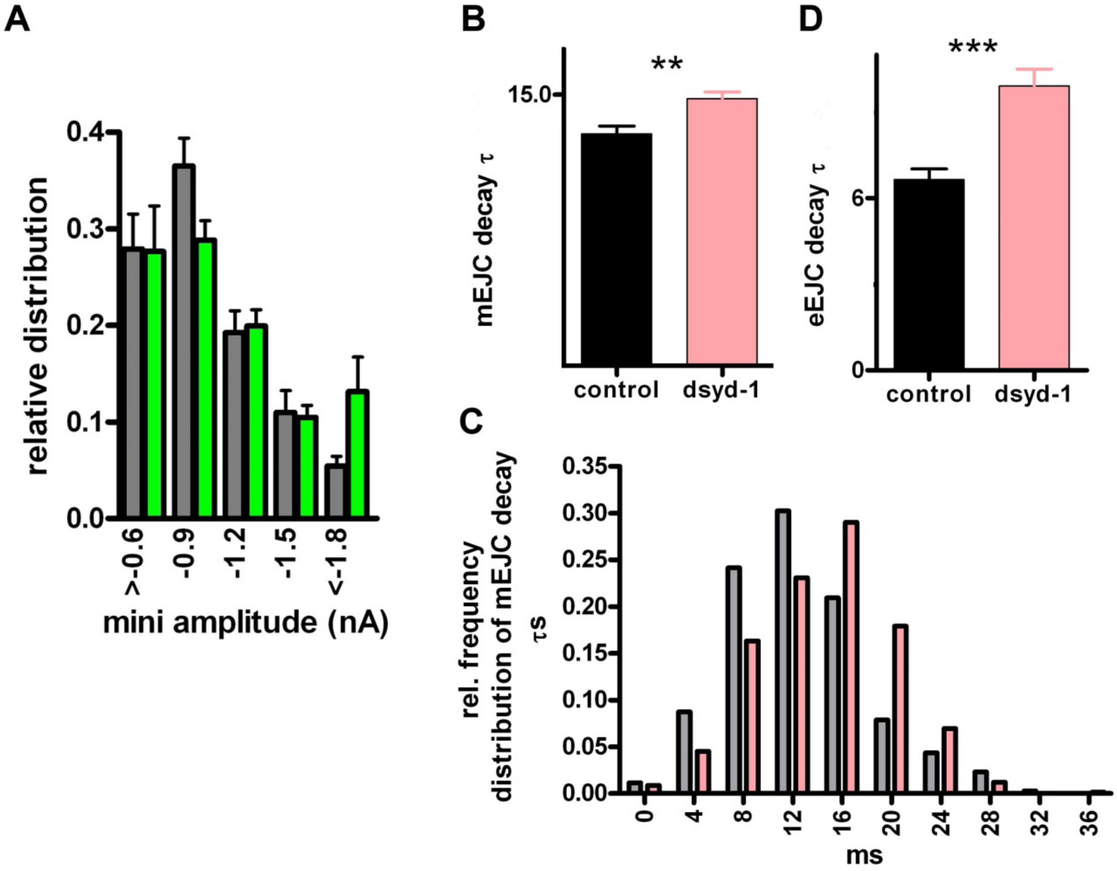

Fig. 25 The evoked junctional current decay constants in *dsyd-1* animals resemble those of DGluRIIA-dominated NMJs
A) The relative frequency distribution of mEJC amplitudes in controls (grey) and *dsyd-1* (green) mutants. Although not significantly different, there is a tendency towards an increased abundance of mEJCs amplitudes < -1.8 nA. **B**) The mean mEJC decay constants (n = 9 each). **C**) The relative frequency distribution of mEJC decay constants illustrates the tendency towards larger decay constants in *dsyd-1* (red) compared to controls (grey). **D**) The mean eEJC decay constants (n = 9 each) are elevated in *dsyd-1* mutants.

EJCs acquired from DGluRIIA-dominated NMJs also show slow decay kinetics (Schmid et al., 2008). Indeed, the decay τ of mEJCs recorded from *dsyd-1* mutant muscle cells was increased by approximately 12% compared to controls

(Fig. 25B and C, n = 9 cells each, p = 0.006, Mann-Whitney test). More so, the eEJCs decay τ was approximately 48% larger (Fig. 25D, n = 9 cells each, p = 0.008, Mann-Whitney test, compare Fig. 14A).

Collectively, parallel to its function of blocking overgrowth of presynaptic AZs, DSyd-1 has a specific function in restricting the size and defining the composition of postsynaptic glutamate receptor fields.

3.4.2. Presynaptically Differentiated Boutons Lacking Postsynaptic Glutamate Receptors in *dsyd-1* Mutants

Differentiated boutons are characterized by presynaptic BRP label that is closely aligned with postsynaptic glutamate receptor fields (Fig. 26). Boutons positive for the neuropil marker HRP, but lacking pre- or postsynaptic specializations, occur when interfering with Wnt signaling (Ataman et al., 2008; Packard et al., 2003). On the other hand, postsynaptic receptor footprints, where accumulated glutamate receptors miss presynaptic boutons, are signs of presynaptic retraction (Eaton and Davis, 2003).

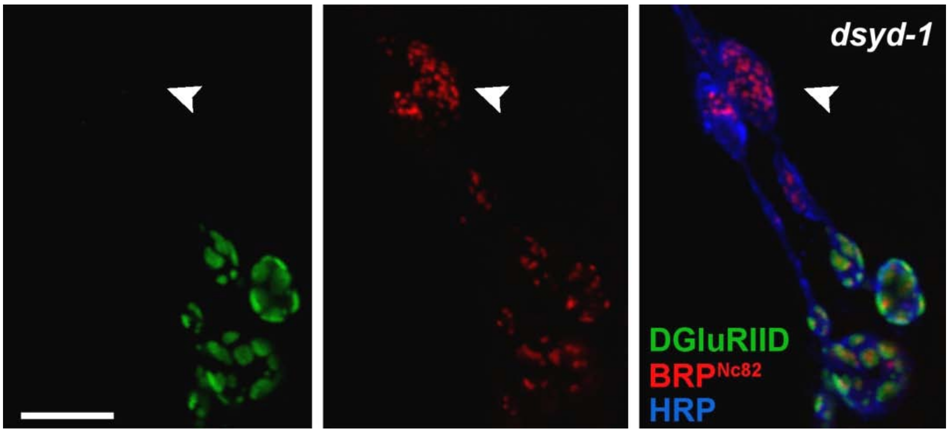

Fig. 26 Individual boutons lack postsynaptic receptor fields in *dsyd-1* mutants
A mature-sized bouton (arrow head), as judged from the HRP signal (blue), that is positive for BRP, but not for DGluRIID. Boutons that lack post-, but not presynaptic specialization are not observed in controls. Scale bar: 3 μm.

Along with overgrown glutamate receptors found at most boutons, *dsyd-1* mutant NMJs occasionally comprised boutons that completely missed postsynaptic glutamate receptor fields (in the following referred to as “orphan” boutons, Fig. 26). “Orphan” boutons were identified via the neuropil marker HRP (Fig. 26) and characterized by BRP assemblies displaying morphological aberrations as are typical for *dsyd-1* mutant terminals (Fig. 16, see 3.2.6.). Thus, along with constricting glutamate receptor field size, DSyd-1 appears to regulate postsynaptic differentiation *per se*.

As indicated above (see 3.2.3.), expression of DSyd-1 seems to be restricted to the presynaptic compartment, where it regulates AZ morphology via DLiprin-α. It hence appears intriguing that a further presynaptic substrate of DSyd-1 might regulate transsynaptic signaling in order to control postsynaptic receptor composition.

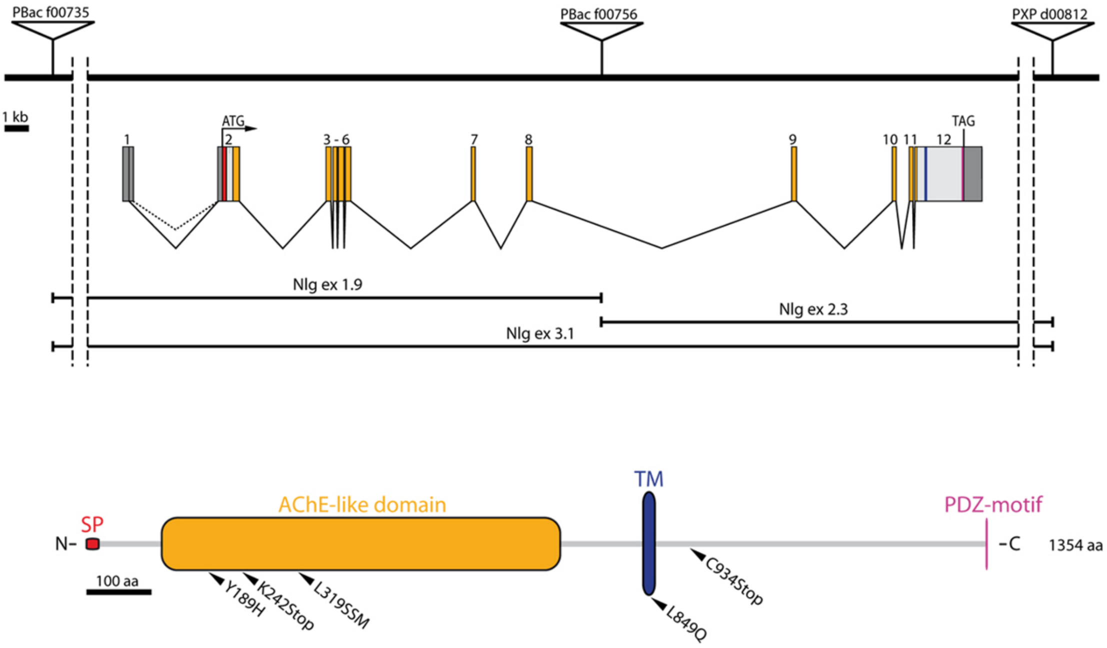
PBac f00735
PBac f00756
PXP d00812
1 kb
ATG
TAG
1
2
3 - 6
7
8
9
10
11
12
Nlg ex 1.9
Nlg ex 2.3
Nlg ex 3.1
TM
AChE-like domain
PDZ-motif
SP
N-
-C
1354 aa
100 aa
Y189H
K242Stop
L319SSM
L849Q
C934Stop

Fig. 27 *Drosophila* Neuroligin 1
A) Genomic locus of *dnlg1* (CG31146). The locus spans 12 exons which are color coded according to the protein domains they encode. The positions of three insertion elements, and the dimensions of the resulting excisions are indicated. Combining excisions *dnlg1*$^{ex2.3}$ and *dnlg1*$^{ex3.1}$ specifically removes only *dnlg1*. The *dnlg1* locus encodes a 1354 aa protein comprising a signal peptide (SP), an acetylcholine esterase-like domain (AChE), a transmembrane domain (TMD) and a C-terminal PDZ domain-binding motif. The EMS-induced point mutations in the respective *dnlg1* alleles are indicated. Courtesy of Daniel Banovic and Hermann Aberle.

3.4.3. *Drosophila* Nlg1 localizes adjacent to glutamate receptor fields

Presynaptically expressed transmembrane proteins might be prime candidates to mediate DSyd-1 controlled transsynaptic signaling.

Drosophila Neurexin (DNrx) was recently shown to localize close to AZs, while *dnrx* mutant NMJs show elevated glutamate receptor levels (Li et al., 2007), similar to what is observed at *dsyd-1* deficient NMJs (Fig. 24). Moreover, besides DSyd-1, DNrx co-immunoprecipitated with BRP [Fig. 9A, (Schmidt, 2006)], indicating that the three proteins may form a common complex.

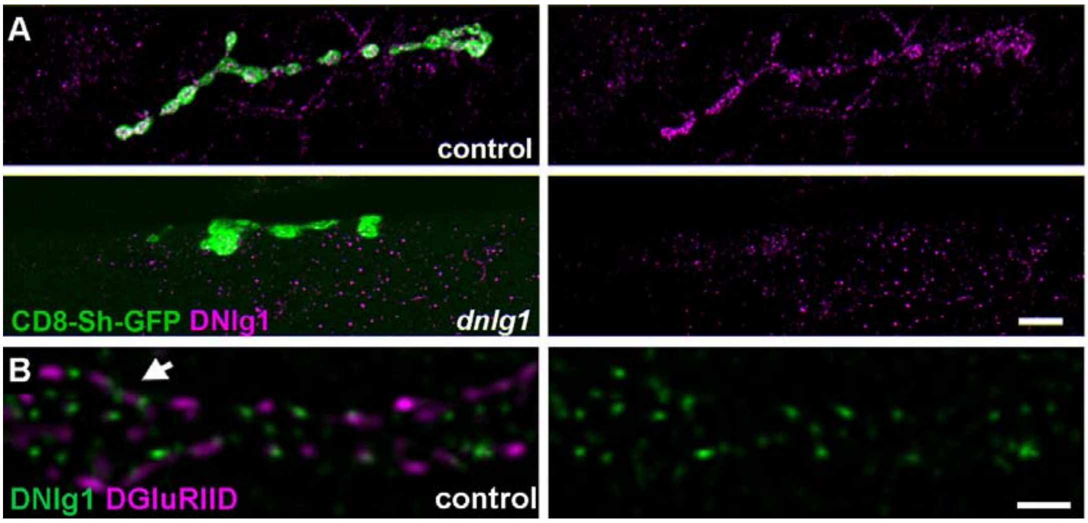

Fig. 28 DNlg1 localizes adjacent to postsynaptic glutamate receptor fields
A) Control and *dnlg-1* mutant NMJs labeled with CD8-GFP-Sh(aker) (Zito et al., 1999), which specifically labels the postsynaptic membrane, and the anti-DNlg1 AB. The polyclonal ABs recognize a punctuate pattern at control NMJs that partially overlaps with CD8-GFP-Sh. This staining is absent in *dnlg1* mutants. Scale bar: 5 µm. Modified from Banovic et al. (2010). **B**) A co-staining of DNlg1 and the glutamate receptor subunit IID (marking the PSD). DNlg1 appears to localize adjacent to, yet not fully overlapping with, individual PSDs (arrow). Scale bar: 700 nm.

Mammalian Nrx, in turn, is known to interact with postsynaptic Neuroligin [Nlg, (Sudhof, 2008; Varoqueaux et al., 2006)].

If *Drosophila* Nlgs were involved in the regulation of the composition of PSDs, similar phenotypes to those of *dsyd-1* and *dnrx* mutants might be expected.

Of four *Drosophila neuroligin* genes (CG13772, CG34127, CG34139, CG31146), only CG31146 (*Drosophila nlg1*, Fig. 27) appears to be specifically expressed in muscle tissue as judged from *in situ* hybridizations (Hermann Aberle, personal communication). In order to assess the localization of DNlg1 (Fig. 27), an antibody was raised against the C-term of the protein. DNlg1 immunoreactivity appeared close to PSDs (Fig. 28A). Moreover, DNlg1 was found to localize towards the edge of postsynaptic receptor fields (Fig. 28B). Specific staining was, however, absent in *dnlg-1* mutants (Fig. 28A). *dnlg-1* alleles either comprised chemically induced premature stop codons (EMS mutants were isolated by Daniel Banovic and Hermann Aberle, Fig. 27), or full deletions removing the entire, or most of the *dnlg1* locus (created by Rui Tian, Würzburg, see Fig. 27 for scheme).

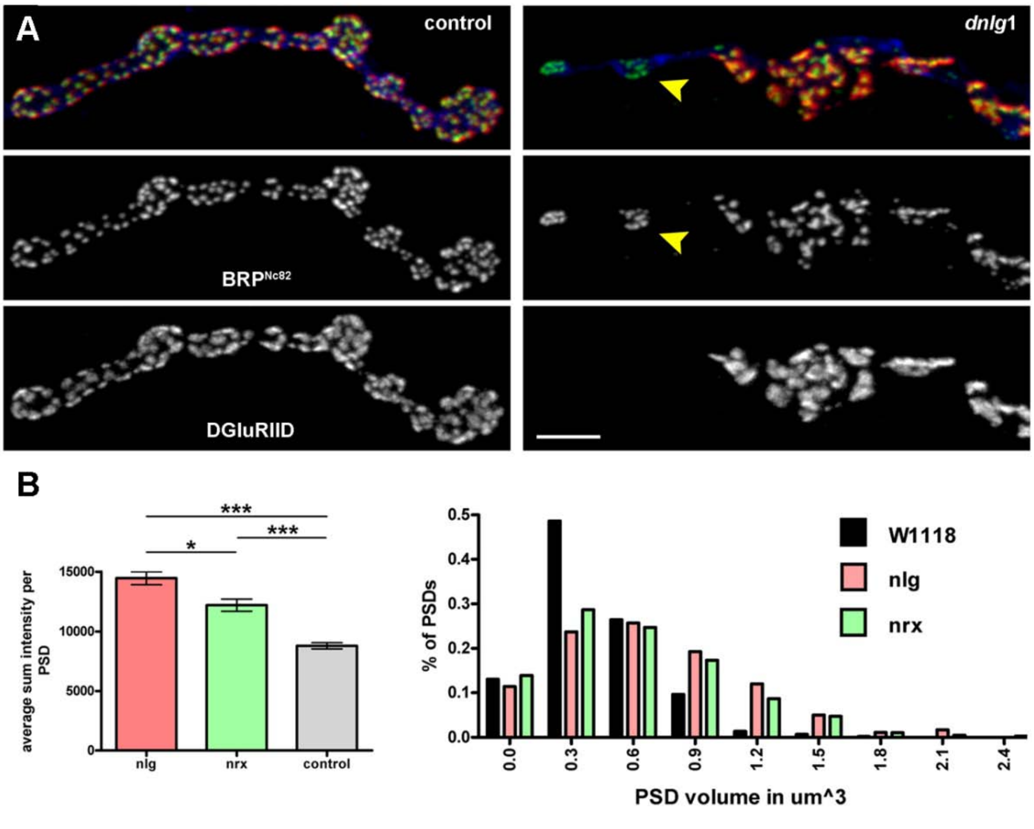
A
control
*dnlg*1
BRP^Nc82
DGluRIID
B
***
***
*
average sum intensity per PSD
15000
10000
5000
0
nlg
nrx
control
% of PSDs
0.5
0.4
0.3
0.2
0.1
0.0
0.0
0.3
0.6
0.9
1.2
1.5
1.8
2.1
2.4
PSD volume in um^3
W1118
nlg
nrx

Fig. 29 *dnlg1* and *dnrx* mutans show elevated levels of postsynaptic glutamate receptors
A) Images of control and *dnlg1*$^{ex1.9}$/*dnlg1*$^{ex2.3}$ mutant NMJs co-stained with BRP and DGluRIID. A subset of presynaptic AZs is not opposed by postsynaptic receptor fields (arrows) in *dnlg1* mutant boutons, and the remaining receptor fields appear enlarged. Scale bar: 5 µm. **B**) The average DGluRIID signal sum intensity measured per PSD (*dnlg1*: n = 463 synapses; *dnrx*: n = 428 synapses; control: n = 590 synapses; *dnlg1* x *dnrx*: p = 0.0014; *dnrx* x control: p < 0.0001; *dnlg1* x control: p < 0.0001). The relative frequency of large PSDs is increased in *dnlg1* and *dnrx* mutants, and PSDs with volumes larger than 1.5 µm^3 were measured in mutant boutons only. Together with Omid Khorramshahi. Modified from Banovic et al. (2010).

3.4.4. Mutants for *Drosophila* Neuroligin1 Show Presynaptically Differentiated Boutons Lacking Postsynaptic Differentiation

For comparison with *dsyd-1* mutants, NMJ morphology of *dnlg1* mutants was analyzed (Fig. 29, together with Omid Khorramshahi, Berlin). Similar to *dsyd-1* and *dnrx* (Fig. 29B) mutants, *dnlg1* deficient animals showed overgrown glutamate receptor fields (Fig. 29B, also see histogram). At the same time, boutons that were positive for presynaptic markers (such as BRP, Fig. 29A) frequently lacked postsynaptic receptor fields [Fig. 29A, (Banovic et al., 2010)].

Thus, *dnlg1* mutants display elevated glutamate receptor fields, as well as presynaptically differentiated (orphan) boutons that lack postsynaptic receptor fields, similar to what is observed in *dsyd-1* mutants. However, the overall frequency at which orphan boutons occurred in *dnlg1* mutants appeared higher than observed for *dsyd-1* mutants (not shown).

3.4.5. eEJC Amplitudes are Reduced in *dnlg1* Mutants

To address functional implications of *dnlg1*, TEVC recordings were performed. eEJC amplitudes (Fig. 30A) were reduced to approximately 50% of control levels at both 1 and 0.5 mM extracellular [Ca^{2+}] (Fig. 30A and B). Moreover, in an interesting parallel to *dsyd-1* mutants (Fig. 25D), eEJC decay kinetics were also prolonged in *dnlg1* mutants (Fig. 30B). This might be in agreement with enlarged postsynaptic receptor fields (Fig. 29). Overall amplitudes and frequencies of mEJCs were, however, not altered significantly from controls (Fig. 30C).

Taken together, eEJC amplitudes are drastically reduced in *dnlg1* mutants, which in a first approximation, is likely a result of less AZs forming (Omid Khorramshahi and Stephan Sigrist, personal communication). Further functional implications of the loss of *dnlg1* will need to be analyzed in the future.

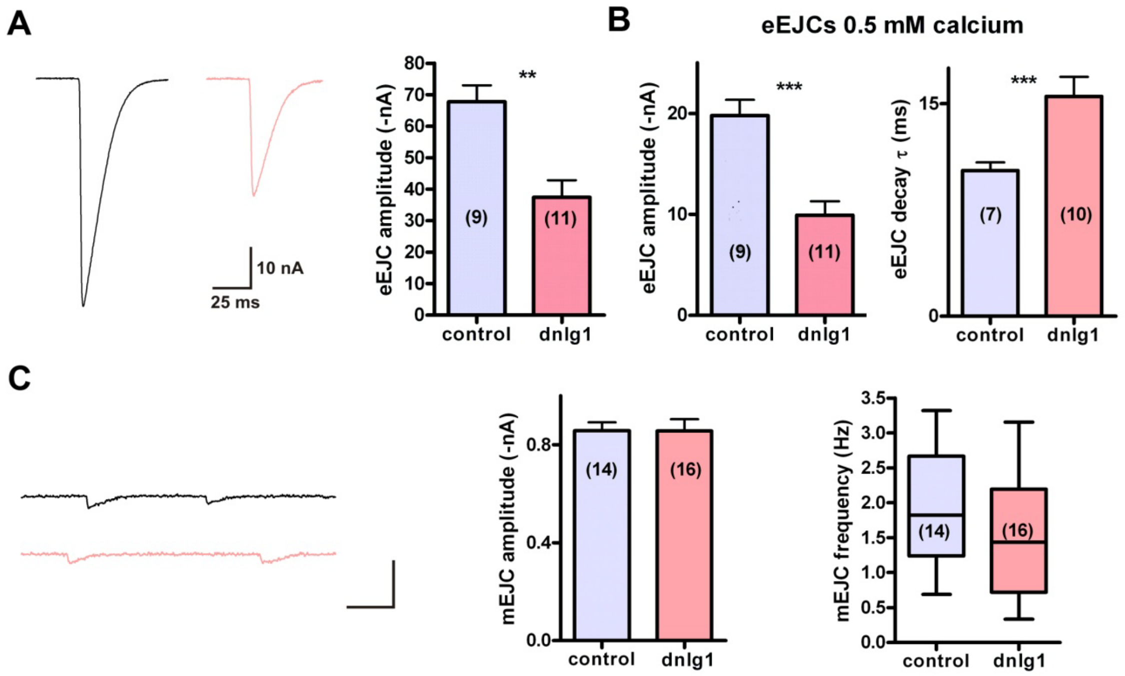

Fig. 30 Impaired neurotransmission in *dnlg1* mutants
A TEVC analysis of control (grey) and *dnlg1* mutant (red) NMJs. **A**) The left panel shows representative eEJC traces acquired from control and *dnlg1* mutant NMJs. The right panel shows the mean eEJC amplitudes (at 1 mM extracellular [Ca^{2+}]). **B**) The left panel shows the mean eEJC amplitude measured at 0.5 mM extracellular [Ca^{2+}]. The right graph shows the eEJC decay constants from traces acquired at 0.5 mM extracellular [Ca^{2+}]. **C**) The left panel shows representative mEJC traces. The middle panel shows the average mEJC amplitudes. The left panel shows the mEJC frequency. The number of cells measured is indicated in brackets. controls: CD8-GFP-Sh/*mef2-Gal4*, CD8-GFP-Sh; mutants: CD8-GFPSh, *mef2-Gal4*, *dnlg1*$^{\mathrm{H324}}$/CD8-GFP-Sh, *dnlg1*$^{\mathrm{I960}}$. Modified from Banovic et al. (2010).

3.4.6. DNlg1 Localization is Affected in *dsyd-1* Mutants

In order to directly test whether *dsyd-1* and *dnlg1* might share a common pathway, distribution of DNlg1 was looked into in *dsyd-1* mutants. Indeed the overall intensity of the DNlg1 signal was drastically reduced in *dsyd-1* mutants (Fig. 31). Thus, postsynaptic DNlg1 localization appears dependent on DSyd-1.

All in all, presynaptic DSyd-1 regulates the composition of postsynaptic glutamate receptor fields. Strikingly, apart from boutons with elevated levels of the glutamate receptor subunit IIA, *dsyd-1* NMJs display orphan boutons, which are positive for the presynaptic marker BRP, however lack postsynaptic glutamate receptors. Moreover, DNlg1 is found to localize to the edge of PSDs, while *dnlg1* mutants show enlarged glutamate receptor fields (as do mutants for presynaptic *dnrx*), as well as orphan boutons and impaired neurotransmitter release. Potentially "bridging the gap", DNlg1 localization is found to be impaired in *dsyd-1* mutants. In other words, presynaptic DSyd-1 appears to be required for proper localization of postsynaptic DNlg1.

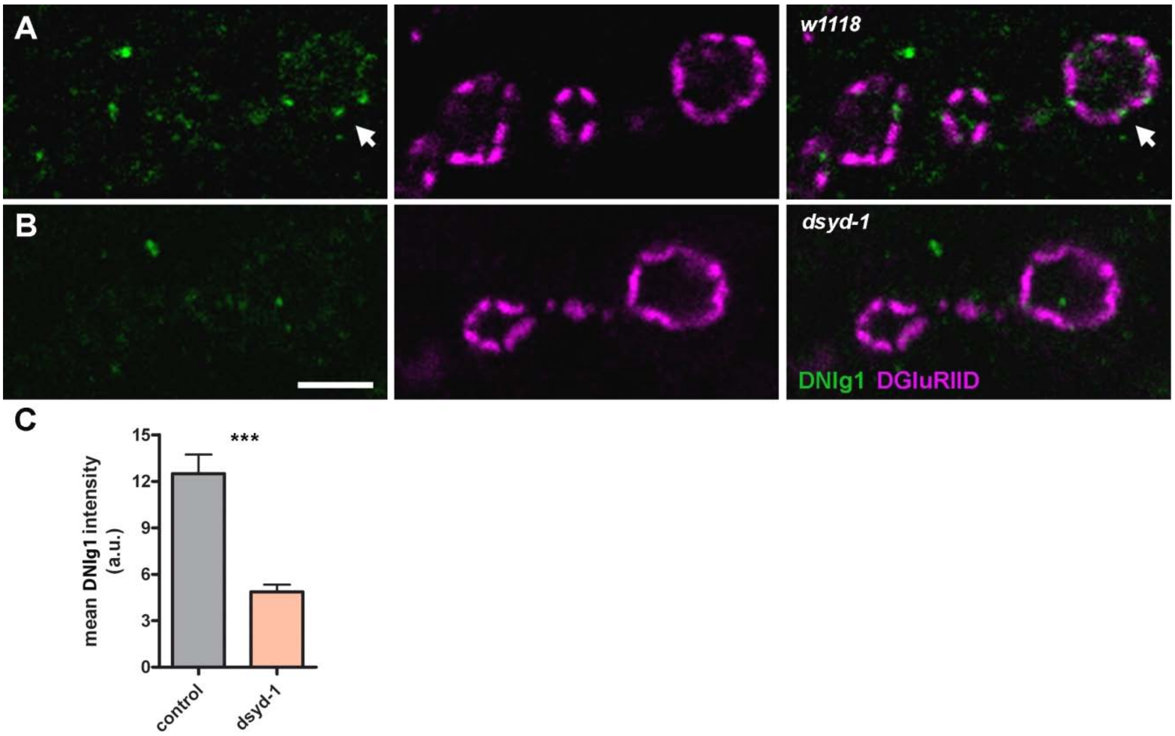
A
w1118
B
dsyd-1
DNlg1 DGluRIID
C
mean DNlg1 intensity (a.u.)
15
12
9
6
3
0
***
control
dsyd-1

Fig. 31 DNlg1 immunoreactivity is reduced in *dsyd-1* animals
A co-staining of DNlg1 (indicated by arrow) and DGluRIID at control (*w1118*) and *dsyd-1* mutant NMJs. The DNlg1 immunoreactivity is substantially reduced at *dsyd-1* mutant NMJs (control: 12.5 ± 1.2 a.u, n = 10; *dsyd-1*: 4.9 ± 0.5 a.u., n = 11; p = 0.0001, according to Mann-Whitney test). Scale bar: 1.5 μm.

3.5. Components of the Exo/Endo-Machinery Interact with BRP

The previously found interactors of BRP (see 3.2.1.) were extracted from adult fly heads at a pH of 9. Using these conditions, proteomics apparently primarily recovered proteins involved in synapse assembly or morphology (Fig. 9A). However, it seems likely that components of the exo/endo-machinery would also interact with the T bar. Clearly, certain protein-protein interactions have a (not to be neglected) dependence on both pH and salt concentration (Phillips et al., 2001). Thus, and in order to uncover further interactors, optimal solubilization of BRP was tested for, varying different buffer parameters (pH, detergents and salts, see Fig. 32). As to be expected for a putative membrane associated large coiled coil protein, rather high concentrations of detergent were needed for efficient BRP yield (1% Deoxycholate, DOC), along with 150 mM NaCl at a pH of 8.

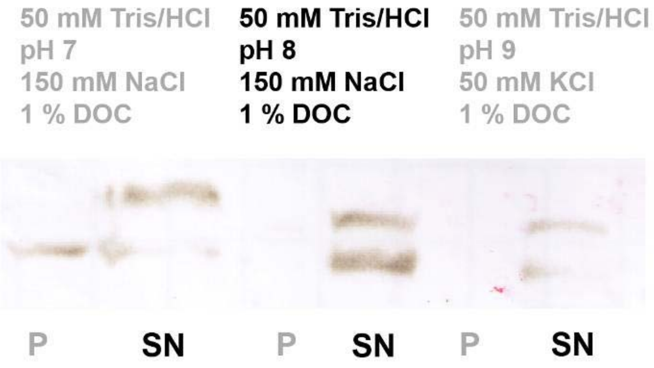

Fig. 32 Optimization of BRP solubilization
A western blot of fly head extracts. The buffers used for solubilization are indicated. Membranes were probed with the monoclonal antibody Nc82 that recognizes a band at 190 kDa and a band at 170 kDa (P = pellet; SN = supernatant fraction).

In order to cover for all three known isoforms of the BRP locus (190, 170 and 85 kDa, Sara Mertel and Stephan Sigrist, personal communication, see Fig. 33A), and to account for potential “epitope shielding”, co-immunoprecipitations were performed using three different BRP antibodies (epitopes are indicated in Fig. 33A). Bands uncovered in silver stained SDS-PAA gels and specific to BRP-immunoprecipitations were excised and subjected to MS/MS analysis (Fig. 33B, in collaboration with Albert Sickmann).

3.5.1. BRP and Dynamin Physically Interact

Amongst other candidates that are involved in the exo/endo-cycle (not shown), both BRP$^{N\text{-}Term}$- and BRP^{D2}-mediated co-immunoprecipitations recovered Dynamin as putative interactor of BRP (Fig. 33B and C). Immunoblots of BRP^{D2} and control co-immunoprecipitations were probed with Dynamin and BRP^{D2} antibodies subsequently (Fig. 34A). Both proteins were identified in the eluates supporting the MS/MS data.

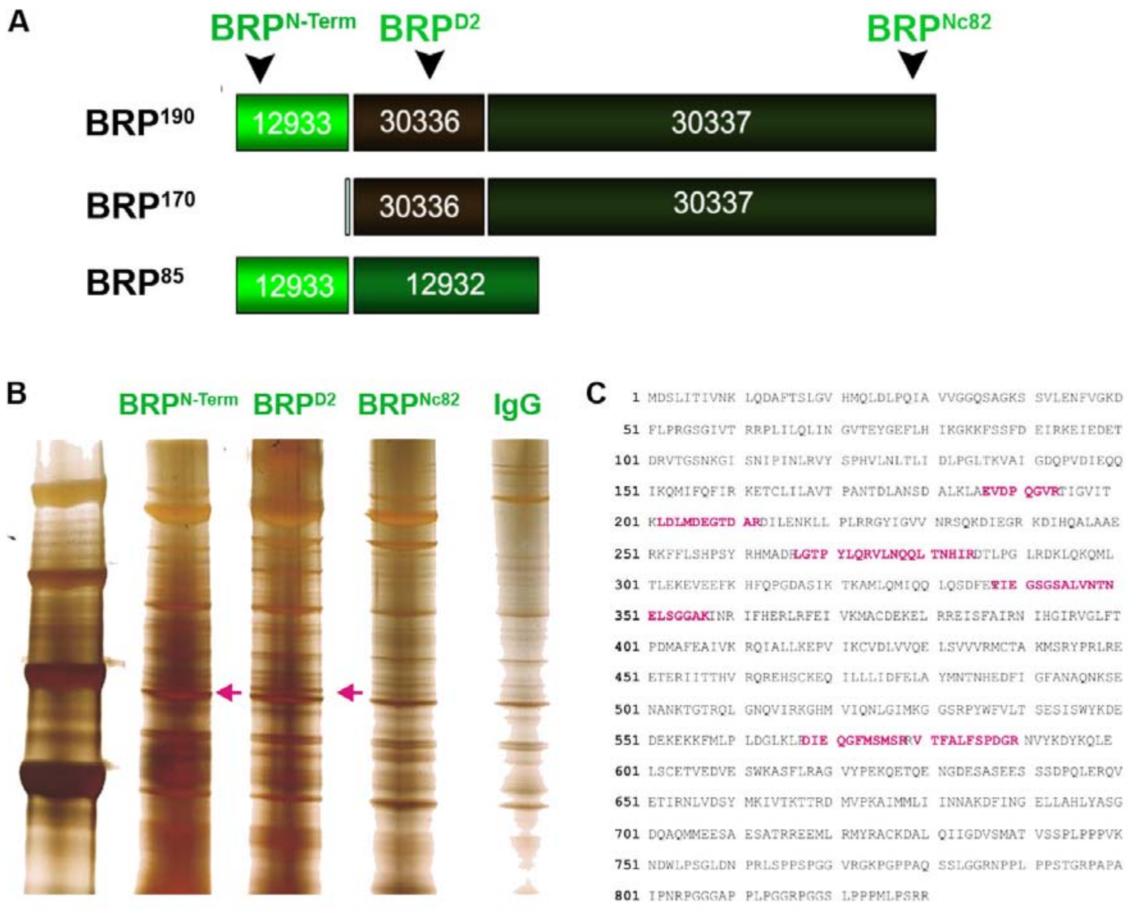
A
BRPN-Term
BRPD2
BRPNc82
BRP190
12933
30336
30337
BRP170
30336
30337
BRP85
12933
12932
B
BRPN-Term
BRPD2
BRPNc82
IgG
C
1 MDSLITIVNK LQDAFTSLGV HMQLDLPQIA VVGGQSAGKS SVLENFVGKD
51 FLPRGSGIVT RRPLILQLIN GVTEYGEFLH IKGKKFSSFD EIRKEIEDET
101 DRVTGSNKGI SNIPINLRVY SPHVLNLTLI DLPGLTKVAI GDQPVDIEQQ
151 IKQMIFQFIR KETCLILAVT PANTDLANSD ALKLAEVDP QGVRTIGVIT
201 KLDLMDEGTD ARDILENKLL PLRRGYIGVV NRSQKDIEGR KDIHQALAAE
251 RKFFLSHPSY RHMADRLGTP YLQRVLNQQL TNHIRDTLPG LRDKLQKQML
301 TLEKEVEEFK HFQPGDASIK TKAMLQMIQQ LQSDFERIE GSGSALVNTN
351 ELSGGAKINR IFHERLRFEI VKMACDEKEL RREISFAIRN IHGIRVGLFT
401 PDMAFEAIVK RQIALLKEPV IKCVDLVVQE LSVVVRMCTA KMSRYPRLRE
451 ETERIITTHV RQREHSCKEQ ILLLIDFELA YMNTNHEDFI GFANAQNKSE
501 NANKTGTRQL GNQVIRKGHM VIQNLGIMKG GSRPYWFVLT SESISWYKDE
551 DEKEKKFMLP LDGLKLRDIE QGFMSMSRRV TFALFSPDGR NVYKDYKQLE
601 LSCETVEDVE SWKASFLRAG VYPEKQETQE NGDESASEES SSDPQLERQV
651 ETIRNLVDSY MKIVTKTTRD MVPKAIMMLI INNAKDFING ELLAHLYASG
701 DQAQMMEESA ESATRREEML RMYRACKDAL QIIGDVSMAT VSSPLPPPVK
751 NDWLPSGLDN PRLSPPSPGG VRGKPGPPAQ SSLGGRNPPL PPSTGRPAPA
801 IPNRPGGGAP PLPGGRPGGS LPPPMLPSRR

Fig. 33 Dynamin interacts with BRP
A) A schematic overview of the three major BRP-isoforms. The epitopes of three BRP antibodies are indicated (arrows). The exon clusters are annotated. **B**) A silver stained SDS-gel of BRP co-immunoprecipitates that were obtained after elution from three different BRP antibodies. The arrows indicate the excised bands that uncovered Dynamin. **C**) Dynamin peptides identified via MS/MS are highlighted in magenta.

To further confirm a direct interaction of BRP and Dynamin, Schneider S2+ cells were double transfected (together with Harald Depner) with Dynamin-Myc and the N-terminal aa 1-617 of BRP tagged with GFP. Supporting the BRP-Dynamin interaction uncovered from *in vivo*-immunoprecipitations (Fig. 33), Dynamin and BRP reciprocally co-immunoprecipitated from lysed cells (Fig. 34B).

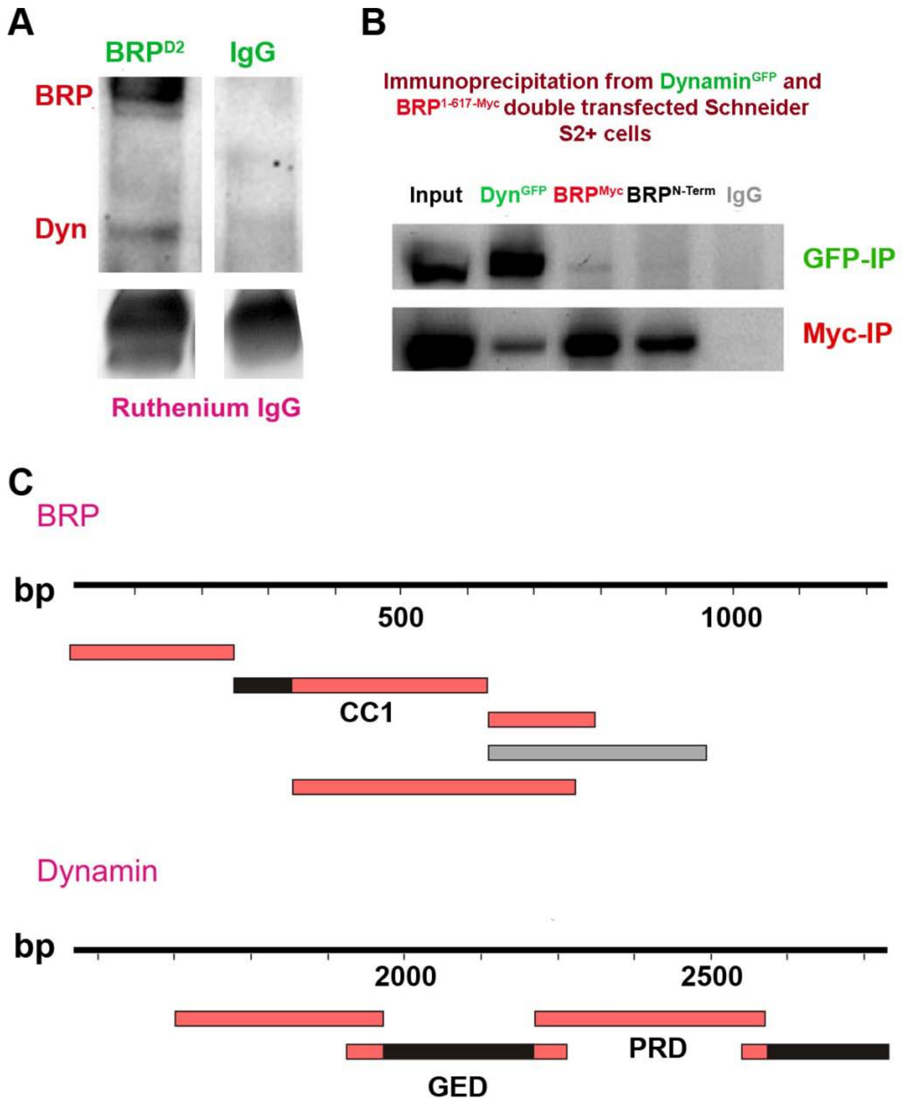
A
BRPD2
IgG
BRP
Dyn
Ruthenium IgG
B
Immunoprecipitation from DynaminGFP and BRP1-617-Myc double transfected Schneider S2+ cells
Input
DynGFP
BRPMyc
BRPN-Term
IgG
GFP-IP
Myc-IP
C
BRP
bp
500
1000
CC1
Dynamin
bp
2000
2500
GED
PRD

Fig. 34 The GED of Dynamin interacts with an N-terminal BRP domain
A) A western blot of BRP^{D2} and control co-immunoprecipitates from adult fly head extract. The membrane was first probed with BRP^{D2} (double band at 190 and 170 kDa) and afterwards with the Dynamin antibody (band at 100 kDa). The in-gel ruthenium stained IgG heavy chains served as loading control. **B**) A western blot shows co-immunoprecipitates of BRP$^{1\text{-}617}$–Myc and Dynamin-GFP. The immunoprecipitations were obtained from co-transfected Schneider S2+ cell lysates. The membranes were probed with an anti-GFP and an anti-Myc antibody. **C**) A yeast two-hybrid-based interaction domain mapping. The N-terminal part of the BRP fragment CC1 was identified to interact with the Dynamin fragments comprising the GED and a C-terminal domain (CS). Interacting domains are indicated in black. An auto-activating construct is marked grey.

Dynamin is known to physically interact with several proteins. These interactions are, however, primarily mediated via its proline rich domain [PRD, (Praefcke and McMahon, 2004)]. In order to investigate which domain of Dynamin would interact with BRP, a yeast two-hybrid-based interaction-domain mapping was performed. Four overlapping BRP domains (Fouquet et al., 2009; Owald et al., 2010) were tested against three overlapping Dynamin fragments, which taken together, covered the complete protein. The N-term of BRP and the C-terminal domain of Dynamin were found to associate, while all other combinations were negative for interactions. While the N-term of BRP comprises multiple coiled coil domains and shows high degrees of identities to mammalian CAST/ELKS/ERC (Wagh et al., 2006), the Dynamin fragment comprised a GTPase effector domain (GED), the PRD, and a C-terminal stretch without clear domain annotation (CS).

In order to get a precise idea of the interacting sequences, positive fragments were divided into smaller overlapping domains (Fig. 34C). Surprisingly, a fragment comprising the PRD did not show positive for interaction with BRP. The GED, however, along with the CS, interacted with a BRP fragment comprising the first coiled coil domain (CC) along with a 30 aa stretch preceding this. A BRP fragment covering solely the first coiled coil domain did not show positive. This argues that the 30 aa preceding the motive are necessary for the protein-protein interaction (Fig. 34C).

Thus, the interaction site of BRP was mapped down to the amino acids 84-113, which directly precede a coiled coil motif. On the other side, two domains of Dynamin were positive for interaction with BRP (Fig. 34C, indicated by arrows and black boxes). Future analysis will have to address the physiological implications of this interaction.

4. Discussion

Starting from a proteomics-based screen for interaction partners of the AZ protein BRP, this study dissects early assembly processes of synapses. BRP is found to be a structural component of, and to shape, the CAZ.

A further AZ protein, DSyd-1, is identified as a physical interactor of BRP. DSyd-1 is needed for the establishment of a sufficient number of synapses at the *Drosophila* NMJ. Likely as a consequence of reduced synapse numbers, loss of *dsyd-1* reduces the amplitude of evoked junctional currents. DSyd-1 is essential for shaping the morphology of AZs, with *dsyd-1* electron dense ensembles appearing misshapen, and for suppressing ectopic accumulation of CAZ material. This function is DLiprin-α-dependent, as inferred from *dliprin-α; dsyd-1* double mutant analysis. DSyd-1 is required for the proper localization as well as mobility of DLiprin-α at AZs, and both proteins localize to a distinct compartment towards the AZ-edge.

Intravital imaging at single synapse resolution uncovers an early step in AZ assembly, which (temporarily upstream from practically irreversible accumulation of postsynaptic glutamate receptors) involves DLiprin-α and DSyd-1. Although many DSyd-1 and DLiprin-α clusters develop into mature (BRP positive) AZs, they often disassemble again, indicating that an initial step of AZ assembly can still be reversible.

Independent of DLiprin-α, postsynaptic receptor levels and composition are dependent on presynaptic DSyd-1. Similar to *dsyd-1* deficient animals, mutants for postsynaptic PSD-edge localized DNlg1 show elevated glutamate receptor levels as well as orphan boutons, comprising presynaptic, however no postsynaptic differentiation. Interestingly, DNlg1 levels are severely reduced in *dsyd-1* mutants. It is proposed that DSyd-1 executes its functions via a presynaptic substrate (potentially DNrx), which then interacts with postsynaptic DNlg1.

Finally, as a result of a proteomics screen, BRP is shown to interact with Dynamin, a protein implicated in the SV exo/endo-cycle.

BRP is thus suggested to be a master organizer of AZ structure and function.

4.1. The BRP Protein Shapes the Electron Dense Specialization at *Drosophila* Synapses

BRP is shown to be an integral part of the electron dense projection at AZs [Fig. 7, (Fouquet et al., 2009)], a structure characterized by high protein content (Owald and Sigrist, 2009). Loss of *brp* has prominent phenotypical consequences, likely interfering with Ca^{2+} nanodomain to SV coupling (Schneggenburger and Neher, 2005), and thus impairing SV release (Kittel et al., 2006). As the localization of different proteins (including Ca^{2+} channels, but also DSyd-1, Fig. 23F) seems to be dependent on the presence of BRP, it appears conceivable that several phenotypes sum up when ablating BRP. Proteins that govern multiple interactions with other proteins may be considered as interaction network knots or “hubs” in a given interactome (Schmid and McMahon, 2007). Thus, BRP appears to be a prime candidate to perform as a central protein-protein interaction hub at the presynaptic AZ. This hub might be involved in stabilizing the synaptic protein scaffold. So, synaptic protein exchange rates could be regulated, conferring synaptic tenacity to proteins of the exo/endo-cycle.

The N-terminal half of BRP shows high degrees of identities with the coiled coil-rich ELKS/CAST family of proteins (Wagh et al., 2006). Although loss of the worm as well as the mammalian (Deken et al., 2005; Kaeser et al., 2009) homologues of BRP have rather subtle consequences on overall SV release or AZ morphology, ELKS family members have been shown to interact with further AZ proteins (Ko et al., 2003; Ohtsuka et al., 2002; Takao-Rikitsu et al., 2004). Interaction partners include: the priming factor Rim (Castillo et al., 2002; Schoch et al., 2002), the transport module Liprin-α (Dai et al., 2006; Ko et al., 2003), as well as the large AZ proteins Piccolo and Bassoon (Cases-Langhoff et al., 1996; tom Dieck et al., 1998), and the RhoGap Syd-1 (this study and Patel and Shen, 2009). Moreover, AZ proteins appear to build a dense meshwork (Harlow et al., 2001; Jin and Garner, 2008; Phillips et al., 2001), as seen for example for Rim, Piccolo, Bassoon and CAST interactions with Munc 13 (Wang et al., 2009). Notably, neither Piccolo nor Bassoon has homologues in *Drosophila* or *C. elegans* (Owald and Sigrist, 2009).

Mammalian ELKS 1 has been shown to be involved in endosome to trans-Golgi network trafficking (Monier et al., 2002). The C-terminal half of BRP, also rich in coiled coil motives, indeed shares similarities in domain organization with Golgi tethering factors, such as Uso1p or GM130. These coiled coils typically form rod-like structures, where 100 amino acid residues extend about 15 nm when dimerized, and proteins as, e.g., Uso1p (Yamakawa et al., 1996) extend over 150 nm (Sztul and Lupashin, 2006). In fact, the N-term of the 1744 aa BRP protein is localized rather close to the plasma membrane, while the C-term on average reaches 70 nm into the cytosol (Fouquet et al., 2009). Moreover, immunoelectron microscopy localizes the $\mathrm{BRP}^{\text{N-Term}}$ to the T bar pedestal, while C-terminal $\mathrm{BRP}^{\text{Nc82}}$ is found to localize to the cytosolic filaments emerging from the T bar (Fouquet et al., 2009).

Golgi-resident rod-like proteins are believed to act prior to SNARE protein assembly by forming contacts between membranes at a distance, thereby increasing the specificity, or the efficiency, of the initial attachment of vesicles. GM130 (Sztul and Lupashin, 2006, 2009) interacts with p115 in mammals, while both proteins seem to be “fused” in yeast [Uso1p, (Gillingham and Munro, 2003; Nakamura et al., 1997)]. It might be intriguing to draw parallels at this stage, with BRP possibly taking over functions that in mammals are distributed to ELKS and potential AZ tethers, e.g. Piccolo or Bassoon.

High pressure freeze/freeze substitution preparation of specimen has improved ultrastructural analysis, avoiding shrinkage artifacts due to aldehyde fixation and dehydration. Using this technique, the T bar appears to be comprised of multiple filaments emerging from the plasma membrane to the cytosol (Fouquet et al., 2009). These filaments seem to be connected to, or at least in close proximity to SVs (Carolin Wichmann and Stephan Sigrist, personal communication). Similarly, ultrastructural studies from mammalian synapses show filaments emanating from the AZ plasma membrane, appearing to “tether” SVs (Siksou et al., 2007). Indeed, while Bassoon mutants show a decrease in the readily releasable pool size of hair cell synapses (Khimich et al., 2005), Piccolo has been implicated in coupling SV mobilization from the reserve pool to events within the AZ (Leal-Ortiz et al., 2008). Taken together, large coiled coil proteins might play a crucial role in recruitment of SVs to release sites.

Along with functional implications, a BRP-based T bar appears to be necessary for overall structural integrity and maturation of AZs. BRP seems responsible for effectively clustering Ca^{2+} channels beneath the T bar density late in a protracted AZ formation process, potentially through a direct molecular interaction with intracellular Ca^{2+} channel domains (Fouquet et al., 2009). Electron tomography of frog NMJs suggested that the cytoplasmic domains of Ca^{2+} channels, reminiscent of pegs, are concentrated directly beneath a component of an electron dense AZ matrix resembling ribs [(Harlow et al., 2001), compare Fig. 1]. In addition, freeze-fracture electron microscopy identified membrane-associated particles at flesh fly AZs, which, as judged by their dimensions, might well be Ca^{2+} channels (Feeney et al., 1998). In line with these observations, peg-like structures are observable beneath the T bar pedestal (Fouquet et al., 2009). Similar to fly T bars, the frog CAZ extends up to 75 nm into the presynaptic cytoplasm. Based on the amount of cytoplasmic Ca^{2+} channel protein (Catterall, 1998), Harlow et al. concluded that Ca^{2+} channels are likely to extend into parts of the ribs. Thus, physical interactions between cytoplasmic domains of Ca^{2+} channels and components of ribs/T bars might well control the formation of Ca^{2+} channel clusters at the AZ membrane (Fouquet et al., 2009). This might guarantee tight coupling of Ca^{2+} channel clusters and presynaptic release sites. Interestingly, Ca^{2+} microdomain amplitudes have recently been correlated to the size of individual ribbons of mammalian hair cells (Frank et al., 2009b).

Following MS/MS analysis, *Drosophila* Syd-1 was identified as interactor of BRP. Work on en passant synapses of the *C. elegans* HSNL motoneuron implies that in genetic terms, Syd-1 (Synapse defective 1) operates upstream of another AZ protein, Syd-2/Liprin-α [which had been recovered in the same *C. elegans* screen as Syd-1 (Zhen and Jin, 1999)]. Indeed, a Syd-2/Liprin-α dominant allele (Dai et al., 2006) can bypass the requirement of *syd-1*, indicating that the essential role of Syd-1 in AZ assembly at HSNL synapses appears to be mediated via the transport factor (Shin et al., 2003; Wagner et al., 2009; Wyszynski et al., 2002) Syd-2/Liprin-α.

4.2. DSyd-1 Stalls DLiprin-α at Nascent AZs

As demonstrated by direct *in vivo* imaging of single release sites in intact living *Drosophila* larvae (Fig. 21-23), DLiprin-α and DSyd-1 mark presynaptic sites where subsequently AZs (and PSDs) originate and mature (Fig. 21-23). These "nascent AZs" later incorporate further synaptic proteins, such as BRP and Ca^{2+} channels (Fouquet et al., 2009; Owald et al., 2010). DLiprin-α has previously been described to be important for proper AZ formation (Kaufmann et al., 2002). Thus, consistent with reduced numbers of AZs forming at developing and expanding *Drosophila* NMJs of *dsyd-1* and *dliprin-α* mutants (Kaufmann et al., 2002), the accumulation of DLiprin-α and DSyd-1 at nascent AZs appears instrumental for a process transforming selected sites into AZs. Moreover, DSyd-1 is essential to properly target DLiprin-α to AZs (Fig. 23A-C). In the absence of DSyd-1, DLiprin-α distributes unevenly at NMJ terminals, sparing many AZs. Additionally, DLiprin-α cluster mobility was largely elevated, compared to controls, in *dsyd-1* mutants (Fig. 23H). Thus, the RhoGAP DSyd-1 operates upstream of DLiprin-α in AZ assembly: DSyd-1 seemingly stalls DLiprin-α at developing AZs (Owald et al., 2010).

Protein mobility can be regulated through cytoskeletal proteins, such as Actin. A DSyd-1-mediated "clamp" (mediating the stabilization of local protein mobility) could be executed through local Actin remodeling (Cingolani and Goda, 2008; Pawson et al., 2008), potentially via members of the Rho GTPase family (Luo, 2000). Interestingly, the Rho Cdc42 has recently been shown to mediate DGluRIIA-dependent increases in presynaptic release at the *Drosophila* NMJ (Frank et al., 2009a). Whether the RhoGAP domain of DSyd-1 is functional will need to be addressed in the future. The presence of a specific arginine residue (arginine finger) is regarded as a prerequisite for functionality of a RhoGAP domain. While DSyd-1 comprises this arginine, *C. elegans* Syd-1 lacks the crucial arginine finger and is likely to be nonfunctional. Furthermore, function is not (re)constituted by introducing an arginine (Hallam et al., 2002). Nonetheless, non-functional RhoGAP domains are thought to at least be able to bind GTPases (Hallam et al., 2002), and might anyway play a role in Rho signaling pathways.

Notably, synapse assembly deficits do not *per se* affect DLiprin-α mobility, as a *dgluRIIA* mutant [known to provoke deficits in synapse assembly (Frank et al., 2006; Petersen et al., 1997; Sigrist et al., 2002)] neither changes DLiprin-α distribution nor mobility (Fig. 23H). Despite being rate limiting for synapse formation or proliferation, DGluRIIA is a key player in a synaptic homeostasis network at the *Drosophila* NMJ. Thus, impaired receptor function is balanced by increased presynaptic neurotransmitter release (Davis and Goodman, 1998; Frank et al., 2006; Frank et al., 2009a). As both DSyd-1 and DLiprin-α mobility are not markedly changed in *dgluRIIA* mutants, early protein dynamics might well be regulated independently of homeostasis-based dynamics. One could thus speculate that DSyd-1 and DLiprin-α may rather be involved in activity-based synaptic plasticity as opposed to spontaneous (meaning activity-independent) homeostatic remodeling (Minerbi et al., 2009).

4.3. Premature "Precipitation" of BRP in *dsyd-1* Mutants

What processes are downstream of the DSyd-1 mediated DLiprin-α activity at nascent AZs? In biochemical studies, Liprin-family proteins are described to steer protein transport in axons and dendrites (e.g. of AMPA receptors) supporting synaptic specializations (Shin et al., 2003; Wagner et al., 2009; Wyszynski et al., 2002). Notably, large ectopic accumulations of DLiprin-α are observed (Fig. 23A-C) in *dsyd-1* mutants, while many AZs lack proper amounts of DLiprin-α. At the same time, ectopic BRP/electron density is observed in the absence of DSyd-1 (Fig. 17C-F and 19B-C). It is tempting to speculate that these ectopic pools of DLiprin-α provoke the ectopic accumulation of BRP in *dsyd-1*, consistent with the proposed transport function for DLiprin-α (Miller et al., 2005) and the direct interaction of DLiprin-α/Syd-2 and ELKS/BRP (Patel and Shen, 2009). Indeed, large BRP accumulations as observed in *dsyd-1* embryos are no longer present in *dsyd-1*; *dliprin-α* double mutants. This indicates that in fact the presence of DLiprin-α is needed to provoke the over-accumulations of BRP when DSyd-1 is missing (Fig. 19B and C). Hence, DSyd-1 appears to control the DLiprin-α mediated transport of BRP and potentially other proteins.

In the absence of DSyd-1, BRP seems to "precipitate" at inappropriate positions, even within the cytoplasm, forming ectopic electron dense material (consistent with its role as a building block of the electron dense T bars). Such precipitations also occur at and close to non-AZ membranes. Moreover, at *dsyd-1*

AZs, large malformed dense bodies form (Fig. 17B). Consequently, it appears plausible that DSyd-1 keeps BRP “in solution” to organize its proper consumption at assembling AZs. The presence of several binding interfaces between BRP and DSyd-1 may be considered as a basis for regulating their interplay. Additionally, AZs with strikingly small dense bodies are observed (Fig. 17B’) in *dsyd-1* mutants. DSyd-1 might regulate the distribution of CAZ material amongst individual AZs throughout the NMJ, and thus steer the balance and release characteristics between individual release sites. In-depth (opto)physiological analysis will be needed to address this issue.

Recently, *Drosophila* Rab3 was found to be important for effective “nucleation” of BRP at AZs; only a fraction of AZs is decorated with electron dense projections in *rab3* mutants. Similar to *dsyd-1* mutants, remaining AZs appeared enlarged (Graf et al., 2009). Thus, the defects seen in *dsyd-1* mutants, with increased fractions of both small and large T bars, could correspond to a weaker version of the defects observed after *rab3* loss. However, instead of overgrown T bars, as observed in *dsyd-1* mutants, *rab3* mutants rather showed multiple T bars per AZ (Graf et al., 2009), indicating that both proteins might act along different pathways (which, however, might converge). It could be promising to place the Rab3 effector Rim (Castillo et al., 2002; Schoch et al., 2002) into context at the *Drosophila* NMJ.

Rab3 is known to play a role in regulating the SV cycle (Schluter et al., 2004; Sudhof, 2004), while residing on SVs (Takamori et al., 2006). However, Rab3 has also been reported to reside on dense core vesicles positive for the AZ markers Piccolo and Bassoon [PTVs, (Zhai et al., 2001)]. Thus, Rab3 may deliver cargo (including BRP) to early maturing AZs that have already incorporated DSyd-1. It will be interesting to test whether synapses lacking demonstrable levels of BRP are positive for DSyd-1 in *rab3* mutants.

PTVs have been suggested to be added to AZs of hippocampal neurons in a quantal manner, with AZs forming by unitary assembly of two or three PTVs (Dresbach et al., 2006; Shapira et al., 2003; Tao-Cheng, 2007). Such PTV-type vesicles might be delivered in conjunction with SV precursors reflecting preformed packages. These seem to be interlinked by electron dense material (Tao-Cheng, 2007). In contrast, non membranous electron dense precursor spheres have been observed at mammalian ribbon synapses (Regus-Leidig et al., 2009). Interestingly, loss of *dsyd-1* provokes electron dense “spheres” which do not show the typical mature T bar morphology, but rather appeared amorphous (Fig. 17E). These spheres are often decorated with SVs throughout the axonal cytoplasm. As BRP corresponds to the T bar meshwork, this might further indicate a direct role of BRP in SV tethering, analogous to the mentioned Golgi tethering factors (see 4.1.). Indeed, immunoreactivity to Bassoon was not found directly associated with dense core vesicles, but rather at dense material in close proximity to PTVs, but also to SV precursors (Tao-Cheng, 2007).

Direct *in vivo* imaging demonstrates that BRP spots appear to grow gradually with AZ maturation at individual sites (Fouquet et al., 2009; Owald et al., 2010). This scenario would favor addition of diffuse BRP molecules rather than that of a small number of preformed modules (e.g. PTVs). However, DSyd-1 and DLiprin-α localize to discrete clusters at the edge of individual AZs. With synapse maturation (as judged by increasing BRP area), the number of these entities increases from one at small nascent AZs to five at mature large AZs (Owald et al., 2010). Thus, the amount of these proteins per AZ appears to be added in a quantal manner and might well be delivered in preformed modules. Whether the dense body is preassembled, or whether precursor modules add up *in situ* will need to be addressed in more detail.

BRP accumulation in the center of the AZ is also in the center of the functional and structural AZ assembly process (Fouquet et al., 2009; Kittel et al., 2006; Wagh et al., 2006). It appears likely that BRP assembly is regulated on multiple levels. For example, BRP transport, and thus accumulation, is not fully eliminated, but severely compromised in mutants for the kinesin *imac* (Pack-Chung et al., 2007). Moreover, the serine/arginine protein kinase SRPK79D was recently shown to associate with BRP and to repress premature T bar formation in the axon (Johnson et al., 2009; Nieratschker et al., 2009). Thus, similar to DSyd-1 (Fig. 17C-F), SRPK79D is needed to prevent CAZ material from nucleating ectopically. Additionally, mutants for the serine/threonine kinase *unc 51* have recently been shown to suffer from BRP targeting defects (Wairkar et al., 2009). It is tempting to speculate that phosphorylation of DSyd-1 (e.g. within serine-rich stretches towards the C-term) might be involved in regulating proper transport (“blocking precipitation on the way”) as well as proper delivery of BRP to nascent

AZ sites.

While synaptic ribbon formation *per se* has not been shown to depend on a single protein in mammals, heterologously expressed RIBEYE [a CtBP2 family member (Schmitz et al., 2000)] provokes ectopic electron density in COS cells (Magupalli et al., 2008). Loss of Bassoon, however, leads to floating electron dense projections no longer anchored to the AZ (Khimich et al., 2005; tom Dieck et al., 1998).

It cannot be ruled out that the ectopic CAZ material observed in *dsyd-1* mutants (Fig. 17C-F), which appears capable of "tethering" SVs (Fig. 17D-E and 18), represents detached T bars, rather than prematurely assembled material. This issue should be addressed in the future.

4.4. Both DSyd-1 and DLiprin-α promote synapse assembly but are not fully essential

Although at reduced rates, synapses were still able to form in both *dliprin-α* and *dsyd-1* mutants. It seems possible that DLiprin-α-mediated functions could, for example, be mediated via other Liprin family members [e.g. Liprin-β (CG10743) and Liprin-γ (CG11206)] in *dliprin-α* mutants. Likewise, initial targeting of DLiprin-α, and thus initial synapse formation, might still proceed in *dsyd-1* animals [despite the overall DLiprin-α distribution being disturbed and mobility being elevated in the absence of DSyd-1 (Fig. 23G-H)]. Indeed, the reduction in release site numbers is more pronounced in *dliprin-α* than in *dsyd-1* animals (see 3.2.5.). This would be consistent with DLiprin-α partially being able to execute its initial role during synapse assembly in *dsyd-1* mutants, potentially defining nascent synaptic sites. Why eEJC amplitudes are reduced to comparable levels in *dsyd-1* and *dliprin-α* mutants, despite *dliprin-α* mutants forming less synapses than *dsyd-1* mutants, will need to be studied in more detail.

Transmembrane molecules, such as the receptor tyrosine phosphatase LAR (Kaufmann et al., 2002), may play a role in early recruitment of DLiprin-α. However, Liprin-α can influence the subcellular localization of LAR which would place Liprin-α upstream of LAR (Wyszynski et al., 2002). Even so, at *C. elegans* HSNL synapses (Patel et al., 2006) Syg1 and Syg2 seem to operate upstream of

Syd-2/Liprin-α. In the fly, postsynaptic N-cadherin appears to interact with presynaptic DLAR, and seems to negatively regulate DLiprin-α in photoreceptor-to-target contact formation, as inferred by genetic analysis (Choe et al., 2006; Prakash et al., 2009). In line with this, DLiprin-α has been shown to operate, at least partially, independent of DLAR. Thus, the genetic hierarchy between transmembrane proteins and factors, such as Liprin-α, does not at all seem to follow a simple linear scheme. This may start with different postsynaptic interaction partners which for LAR also include NGL family members (Woo et al., 2009), and Neuroligins (Lim et al., 2009).

4.5. DSyd-1 and DLiprin-α Define a Novel Subcompartment at the AZs Edge

DLiprin-α and DSyd-1 closely co-localize at AZs (Fig. 12C). Moreover, STED revealed that DLiprin-α and DSyd-1 appeared to form a novel AZ "subcompartment", which is located towards the edge of mature AZs coordinating the AZ central BRP-organized T bar (Owald et al., 2010). This discrete modular nature might reflect an underlying quantal building principle for the AZ of reciprocally stabilizing interactions (Ko et al., 2003; Patel and Shen, 2009; Schoch and Gundelfinger, 2006), for example in a BRP/ELKS, DSyd-1/Syd-1 and DLiprin-α/Syd-2 trias. Such modular AZ architecture has recently been proposed for mammalian synapses on the basis of tomographic analysis (Zampighi et al., 2008).

It is tempting to speculate that AZ edge-localized DLiprin-α and DSyd-1 clusters might promote the incorporation of membrane proteins diffusing at the surrounding plasma membrane [as seen on the postsynaptic site (Renner et al., 2008)], and eventually colliding with the AZ. Interestingly enough, Rsy-1, which was uncovered as a repressor of Syd-1 function in *C. elegans*, has also been reported to localize to the edge of AZs (Patel and Shen, 2009).

4.6. Timing of Synaptic Assembly

Getting a realistic impression of molecular processes mediating assembly and plastic changes of synapse populations in functional circuits seems inevitable for a deeper understanding of learning and memory. Time course and coordination of synapse assembly in intact nervous systems is thus under intense investigation.

Somewhat different from expectations based on cell culture experiments suggesting a rapid assembly leading to mature synapses in one to two hours or less (Friedman et al., 2000; Okabe et al., 2001), *in vivo* synapse assembly has recently been suggested to protract over many hours (Owald and Sigrist, 2009; Fouquet et al., 2009; Owald et al., 2010).

In intact developing *Drosophila* larvae, new synapses form over several hours in physical separation from pre-existing synapses, and retrieve their glutamate receptors from diffuse, non synaptic pools (Rasse et al., 2005; Schmid et al., 2006). Moreover, on the presynaptic side, addition of BRP to initially DSyd-1 only positive sites takes place within a time frame of 12 hours (Fig. 21A). Early events of AZ assembly, however, appear to occur more rapidly and are difficult to visualize on a 30 minute time scale, as judged from DSyd-1 and DLiprin-α co-imaging (Fig. 22B-C). Thus, in order to get a reliable impression of the time-course of synapse assembly, it appears important to carefully dissect markers for early processes from those involved in synapse maturation in future studies.

For mammalian brains, retrospective serial section electron microscopy (SSEM) of previously imaged dendritic spines in the adult rodent neocortex showed that spine growth precedes the growth of synapses *in vivo* (Knott and Holtmaat, 2008). In line with this, newly formed spines became functional within a day after induction of long-term potentiation (LTP) in hippocampal slices (De Roo et al., 2008). A further SSEM study found that new spines would form synapses, judged by morphological means (such as SV filled boutons and a synaptic cleft) after 15-19 hours after outgrowth, induced by tetanic stimulation (Nagerl et al., 2007). Recently, however, electrophysiological analysis coupled with electron microscopy (EM) suggested that synapses form within hours after spontaneous spine formation (Zito et al., 2009), matching the findings from dissociated cell culture (Friedman et al., 2000; Okabe et al., 2001) and cultured slices (Zito et al., 2009) more closely. The synapse assembly program might hence differ between situations of “high activity” (LTP-induction) and “low activity” [spontaneous, (Owald and Sigrist, 2009)].

4.7. Early AZ Assembly Appears Reversible at *Drosophila* NMJs

Small clusters of DLiprin-α and DSyd-1 appear at presynaptic sites before any other sign of AZ or synapse assembly (BRP or DGluRIIA; Fig. 20-22). Such clusters are spatio-temporally coherent with matured AZs characterized by glutamate receptors, BRP and the Ca^{2+} channel Cac (Fouquet et al., 2009). Notably, however, a high percentage of these clusters dissolve again (Fig. 22D). In this context, DSyd-1 has the tendency to leave the clusters before DLiprin-α . It appears likely that synapse assembly can be divided into an early assembly step, which is still reversible, and a later (mostly) irreversible maturation phase (for a model see Fig. 35). DLiprin-α and DSyd-1 might explore new non-synaptic membrane patches for assembly (Fig. 35). That AZ formation efficacy is reduced in *dsyd-1*, could thus be causally linked to elevated dynamics (and thus reversibility of assembly) of DLiprin-α clusters. This would, however, not explain the residual AZs forming in *dliprin-α* mutants (see 4.4.). In control settings, the mobility of DLiprin-α clusters was somewhat larger than that of DSyd-1 (Fig. 22D). It therefore seems as though a fraction of DLiprin-α clusters disassembles prior to the arrival of DSyd-1 to nascent sites (see model, Fig. 35). The arrival of DSyd-1 clusters would hence increase the probability of a nascent site to mature and form a stable synapse. Which signal steers DSyd-1 to remain at a nascent site (and thus to stabilize it) will need to be investigated (see 4.8.).

Testing for the role of the *Drosophila* homologue of Rsy-1, which directly binds Syd-2/Liprin-α and Syd-1, weakening the interaction of Syd-1 with ELKS (Patel and Shen, 2009), may provide some answers. Reversibility of the DSyd-1 mediated processes could require local action of Rsy-1, loosening the DSyd-1-clamp and revoking further synaptic differentiation. Indeed, DLiprin-α has been implicated as an effector of the E3 ubiquitin ligase APC/C (van Roessel et al., 2004).

In contrast to DLiprin-α and DSyd-1 clusters, BRP positive AZs disappear at very low rates (Fig. 23H), which might be in line with synaptic disassembly processes (Eaton et al., 2002) that probably occur temporarily downstream of presynaptic nascent site assembly processes.

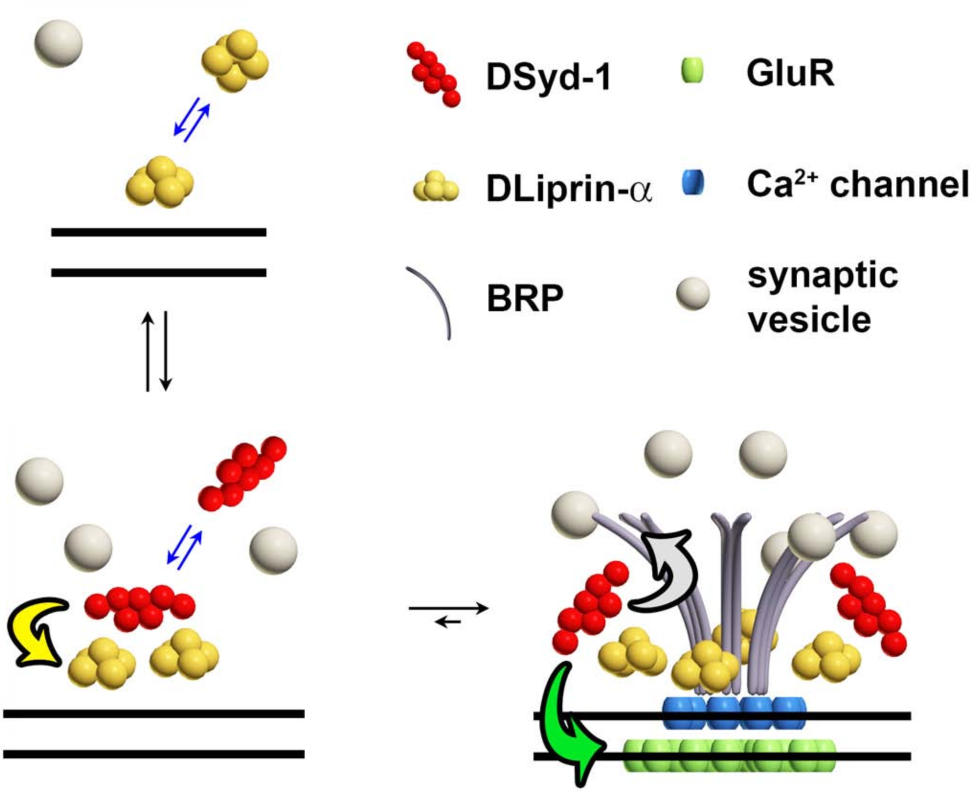

Fig. 35 Model of early AZ formation in *Drosophila*
A model of early AZ assembly [modified from Owald et al. (2010)]. DLiprin-α arrives early at nascent AZs and is closely followed by DSyd-1. Initial DLiprin-α is highly reversible and DLiprin-α clusters often disassemble at nascent sites. After initial appearance, DSyd-1 either leaves nascent sites again or clamps DLiprin-α to early AZs. This clamp potentially transfers the early reversible nascent, to a practically irreversible phase of AZ assembly (yellow arrow). This later, largely irreversible phase comprises postsynaptic accumulation of glutamate receptors as well as presynaptic incorporation of Ca^{2+} channels and BRP. Green arrow: DSyd-1 regulates glutamate receptor field size. Grey arrow: DSyd-1 binds BRP and regulates BRP supply.

Early synapses appear to lack the tenacity later conferred to them after addition of BRP. This later maturation step seems crucial for Ca^{2+} channel clustering at AZs. In line with this, impaired Ca^{2+} channel clustering at AZs lacking BRP becomes apparent only from a certain synapse size onwards. Maturation including the late, BRP-dependent formation of the T bar, seems to be required for maintaining high Ca^{2+} channel levels at maturing AZs but apparently not for initializing Ca^{2+} channel clustering at newly forming sites (Fouquet et al., 2009).

It appears possible that signals promoting synaptogenesis (Aberle et al., 2002; Ataman et al., 2008; McCabe et al., 2003; Packard et al., 2003) execute their function by regulating the transition from early stages into later maturation.

Pathways converging on DLiprin-α and DSyd-1 remain to be characterized. Notably, floating electron dense material was observed in mutants for the BMP factor *wishful thinking* (Aberle et al., 2002).

On an ultrastructural level, 15-23% of the NMJ synapses do not show an EM detectable T bar (Atwood et al., 1993; Reiff et al., 2002). Likewise approximately 5% of sites showing a postsynaptic compartment lack BRP on a light microscopic level (Rasse et al., 2005). It might well be that minor amounts of BRP, just enough to be demonstrated with the high-affinity monoclonal antibody Nc82, do not yet lead to the assembly of an ultrastructurally visible CAZ. Nonetheless, sites lacking BRP or T bars may well represent early synapses positive for DLiprin-α and DSyd-1, however not yet for BRP. Whether nascent AZs are already active will need to be addressed in the future.

4.8. Potential Modes of DSyd-1 Regulation

Whether synaptic activity is needed for synapse development *per se*, or at least for fast execution of synapse assembly programs is debatable (Hiesinger et al., 2006; Katz and Shatz, 1996). At the fly NMJ, presynaptic electrical activity is needed for proper clustering of postsynaptic glutamate receptors (Broadie and Bate, 1993a, b, c; Saitoe et al., 1997), which, however, seems independent of SV release. Neither mutating SNARES or *Drosophila unc 13* nor expressing TNT, which all result in largely ablating synaptic transmission, affects postsynaptic glutamate receptor field formation (Aravamudan et al., 1999; Broadie, 1995).

Synapse proliferation at the *Drosophila* NMJ seems to be regulated by Ca^{2+} influx through the AZ-resident N-type Ca^{2+} channel Cac (Rieckhof et al., 2003). BRP recruitment to AZs, however, still persists in *cac* embryos (Fouquet et al., 2009). So, Ca^{2+} influx through Cac seems to be needed for the refinement of AZ/synapse numbers rather than for AZ assembly *per se*. It remains to be tested whether DSyd-1 mediated processes are AP-dependent, and whether DSyd-1 might be regulated via binding of Ca^{2+} to its C2 domain.

Interestingly, DSyd-1 expression is high in freshly hatched first instar larvae and decreases at later stages (Fig. 13). However, immunoreactivity remains high at certain synapses. Moreover, as synapses mature (as judged by BRP immunoreactivity), distinct quanta of DLiprin-α/DSyd-1 are added to AZs (Owald et al., 2010). It thus may be intriguing that DSyd-1 not only plays a prominent role during AZ formation, but also during AZ rearrangement. Hence, DSyd-1 levels might be high at newly forming, or remodeling synapses, anchoring dynamic material (such as DLiprin-α), and thus be involved in regulating synaptic plasticity. Indeed, levels of DSyd-1 at individual synapses in the *Drosophila* adult CNS appear synapse-type and potentially synapse status dependent (Frauke Christiansen and Stephan Sigrist, Berlin, personal communication). Along these lines, levels of BRP in the adult fly CNS have been demonstrated to be altered after sleep deprivation (Gilestro et al., 2009).

4.9. DSyd-1 Regulates the Postsynaptic Compartment

Unexpected from the analyses in *C. elegans* so far, presynaptic DSyd-1 (but apparently not DLiprin-α) plays an important role for proper postsynaptic assembly. Embryos and larvae single mutant for *dsyd-1* and, importantly, also *dliprin-α; dsyd-1* double mutant embryos (the double mutant is embryonic lethal), but neither *dliprin-α* single mutant embryos (Fig. 19B and C) nor larvae (data not shown), show severely increased overall amounts of postsynaptic glutamate receptors. These increased amounts of glutamate receptors in *dsyd-1* mutants vanish after presynaptic re-expression of UAS-*dsyd-1*^{cDNA}, indicating that DSyd-1 would regulate PSD size in a transsynaptic manner. That *dliprin-α; dsyd-1* double mutants are embryonic lethal furthermore indicated divergent functions for both DSyd-1 and DLiprin-α.

Drosophila NMJs express two functionally distinct glutamate receptor complexes (DGluRIIA and IIB), whose levels influence the number of release sites forming (DiAntonio, 2006). Individual PSDs form distinct from pre-existing ones, and mature over hours, switching from DGluRIIA to IIB incorporation throughout maturation in dependence of presynaptic signals (Rasse et al., 2005; Schmid et al., 2008). Notably, DSyd-1 might mediate such a maturation signal, as *dsyd-1* mutants show excessive amounts of DGluRIIA incorporating at their PSDs (Fig. 24D and H). This regulation is likely not (or only partially) due to compensation for reduced presynaptic glutamate release, as *dliprin-α* mutants (with similarly reduced transmission levels) do not show this dramatic increase in glutamate receptor levels (Fig. 19B and C).

Despite enlarged receptor fields and specifically elevated DGluRIIA levels, average miniature event amplitudes are only slightly shifted towards elevated values in *dsyd-1* animals (Fig. 14B; however, see Fig.25A), which at this stage cannot be accounted for. A possible explanation might comprise regulatory processes rendering populations of receptors non/partially functional. Nonetheless, EJC decay time constants (Fig. 25B-D) of *dsyd-1* mutants resemble those found at *dgluRIIB* deficient (and thus DGluRIIA-dominated) NMJs (Schmid et al., 2008). Importantly, regulating the postsynaptic receptor composition might be a way of regulating synaptic strength.

4.10. *Drosophila* Neurexin is a Potential Second Substrate for DSyd-1

How does presynaptic DSyd-1 regulate the composition of the postsynaptic compartment? In addition to DLiprin-α, a second presynaptic substrate protein of DSyd-1 might exist at (e.g. nascent) synapses. It was tempting to speculate that DSyd-1 helps the AZ localization of an adhesion protein, which via transsynaptic interaction might steer the incorporation of postsynaptic glutamate receptors. Moreover, besides DSyd-1, *Drosophila* Neurexin was recovered from BRP immunoprecipitations (Schmidt, 2006). This provides grounds to speculate upon the existence of a BRP-DSyd-1-DNrx complex at the presynaptic site.

When comparing phenotypic consequences of the loss of DSyd-1 (Fig. 24A and G) and DNrx [Fig. 29B and (Li et al., 2007)], both lead to large assemblies of postsynaptic glutamate receptors. Moreover, the same holds true for the potential postsynaptic binding partner of DNrx, *Drosophila* Nlg1 (Fig. 29A and B). Indeed, genetic evidence points towards a direct interaction of DNrx and DNlg1 in *Drosophila* (Omid Khorramshahi and Stephan Sigrist, personal communication). In addition, although a transsynaptic interaction of DNrx with DNlg1 awaits direct demonstration in *Drosophila*, it appears reasonable to deduce from overwhelming evidence coming from studies on the mammalian orthologues (Sudhof, 2008). Consequently, it seems plausible that DSyd-1 could stall DNrx, analogous to DLiprin-α at AZs (see 4.2.) in order to keep the protein in place (for a model see

Fig. 36).

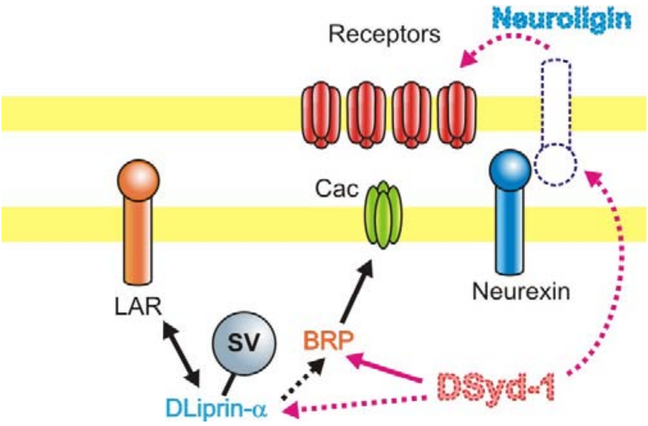

Fig. 36 Model of AZ formation and transsynaptic communication in *Drosophila*
DSyd-1 (physically) interacts with BRP at the AZ, while regulating the localization and motility of DLiprin-α. Furthermore, *Drosophila* Neuroligin is regulated by DSyd-1, which in turn might regulate postsynaptic receptor fields. *Drosophila* Neurexin is proposed as a potential direct substrate for DSyd-1.

Potentially bridging the gap, PSD-close clustering of DNlg-1 is dramatically down-regulated at *dsyd-1* mutant NMJs (Fig. 31), and nearly absent in *dnrx* mutants (Omid Khorramshahi, David Owald and Stephan Sigrist, unpublished observation). Via interaction with postsynaptic DNlg1, a DSyd-1/DNrx complex might regulate dynamics and composition of the postsynaptic compartment. DNlg1 might constrain populations of receptors within a certain radius, as seen at wild type NMJs. It, however, cannot be ruled out that reduced DNlg1 levels in *dsyd-1* are due to secondary effects, e.g. as a consequence of (rather than a cause for) deregulated glutamate receptor fields.

As for *dsyd-1* mutants, eEJC decay constants are elevated by approximately 50% compared to controls in *dnlg1* mutants (Fig. 30B). Whether this is correlated to an increase in DGluRIIA levels [eEJCs recorded from DGluRIIA-dominated NMJs also show slow decay constants (Schmid et al., 2008)] should be investigated, along with further potential functional implications of the loss of *dnlg1*, e.g. via short-term plasticity and high frequency stimulation protocols. Functional read-out of the loss of *dnlg1* might, however, be masked by structural synaptic deficits (Fig. 29A), and will need to be analyzed in more depth in the future.

dsyd-1 mutants show a specific increase in DGluRIIA complexes. Interestingly, mammalian Nlg isoforms have been shown to function neurotransmitter system-specific (Sudhof, 2008). Moreover, on a synapse level, they appear to recruit specific subtypes of receptor complexes (Heine et al., 2008). It remains to be tested, whether DNlg1 specifically recruits DGluRIIA complexes.

Both *dsyd-1* and *dnlg1* mutants comprise orphan boutons, showing pre- and lacking postsynaptic differentiation. Surprisingly, *dnrx* mutants do not seem to exhibit orphan boutons (Omid Khorramshahi, personal communication), although otherwise similar to *dnlg1* and *dsyd-1* on morphological grounds (Fig. 29B). One could speculate that deregulated DNrx might be responsible for orphan bouton outgrowth in *dnlg1* and *dsyd-1*. Interestingly, orphan boutons lacking postsynaptic specializations do not seem to be a consequence of synapse retraction processes, as these boutons form *de novo* and persist throughout larval development (Omid Khorramshahi, Stephan Sigrist and Hermann Aberle, personal communication), arguing that these effects are a consequence of disturbed synapse assembly.

In spite of phenotypic similarities, *dnlg1* mutants show a much higher penetrance of postsynaptic abnormalities (as seen in Fig. 29A) than *dsyd-1* or *dnrx* single mutants do. It thus seems likely that DNlg1, despite its involvement in fine-tuning of synaptic morphology, has an autonomous and DNrx-independent function in defining the postsynaptic compartment.

On a functional level, *dsyd-1* and *dnlg1* mutants show a marked reduction in eEJC amplitudes at both 0.5 mM and 1 mM extracellular [Ca^{2+}] (Fig. 14A, C and 30A-B). In contrast, evoked junctional potentials appear to be comparable to controls at 1 mM extracellular [Ca^{2+}], but reduced at lower Ca^{2+} concentrations in *dnrx* mutants (Li et al., 2007). Double or triple mutant combinations, might well help in dissecting potentially segregated functions.

4.11. A Possible Link to Autism Spectrum Diseases?

Mutations in Neurexin- and Neuroligin-type proteins have recently been linked to autism spectrum diseases [ASDs, (Garber, 2007; Varoqueaux et al., 2006)]. ASDs are classified as developmental disorders and typical phenotypes include disturbed social interactions coupled to impaired language acquisition and repetitive or ritualistic behavior (Varoqueaux et al., 2006). Especially impaired synaptic connectivity has been postulated to cause ASDs in this context (Herbert, 2005; Polleux and Lauder, 2004). In line with this, Neuroligin 4 deficient mice have been shown to exhibit deficits in reciprocal social interactions and communication, which are apparently similar to ASDs in humans (Jamain et al., 2008). Generally, it appears likely that other AZ proteins might contribute in a similar way here (Garber, 2007). Thus, the role of synaptic refinement mediated via a potential Syd-1-Nrx-Nlg axis should be considered in this context. Moreover the postsynaptic scaffold Shank 3 has been linked to ASD (Durand et al., 2007). Whether Shank 3 might link Neuroligin to postsynaptic receptors in *Drosophila* remains an important question.

4.12. Does the CAZ Interact with the Exo/Endo-Cycle?

Proteomics indicate that BRP physically interacts with Dynamin, linking the CAZ to the exo/endo-cycle (Fig. 33 and 34).

Dynamins make up a superfamily of large GTPases, typically characterized by an approximately 300 aa spanning GTPase domain, a middle domain and a GTPase effector (GED) domain (Praefcke and McMahon, 2004). Oligomerization, mediated via these three domains (Praefcke and McMahon, 2004), stimulates the GTPase activity of the protein, which favors the Dynamin mediated lipid fission reaction over that of membrane tubulation (Sweitzer and Hinshaw, 1998).

The BRP-Dynamin interaction domain was mapped down to the N-terminal region of BRP (Fig. 34C), which is located close to the presynaptic membrane (Fouquet et al., 2009). In turn, the GED of Dynamin interacted with BRP (Fig. 34C). Suppressor screens targeting a temperature-sensitive mutation (*shibire*^{TS2}) located to the GTPase domain of Dynamin (Narayanan et al., 2005) identified mutations in the GED. It thus seems possible that the GED might be involved in regulating an early rate-limiting step of Dynamin function via a modulation of the ratio of bound GTP to GDP (Narayanan et al., 2005); it might be of use to locally inhibit Dynamin function via the GED, keeping the concentration of GTP-bound Dynamin molecules high. Stimulus-mediated disinhibition would then ensure rapid action of GTP-bound Dynamin. Binding of the GED of Dynamin by BRP may thus inhibit GTP hydrolization and locally enrich GTP-bound Dynamin at AZ.

What might be the function of enriched GTP-bound Dynamin at fusion sites? Interestingly, the t-SNARE Vam3p has been proposed to bind the Dynamin-like Vps-1p in vacuolar fission and fusion in yeast (Peters et al., 2004). Via this interaction, Vps-1p appears to silence the t-SNARES, which allows for fission reactions to take place. Thereafter, Vps-1p seems to be released from Vam3p by Sec 18p/NSF, activating the SNARE for further fusion events to take place, and inhibiting fission activity. As deletion of Vps-1p also leads to a block of vacuolar fusion, Vps-1p appears necessary for t-SNARE association, potentially defining hot-spots for fusion (Peters et al., 2004). For fusion of vacuoles, Dynamin might thus (together with NSF) regulate the definition of fusion sites.

Studies from *shibire*^{TS} adult NMJs have shown that upon stimulation, synapses with a full set of SVs exhibit fast fatigue on a 20 ms time scale (Kawasaki et al., 2000). Moreover, studies from the Calyx of Held have demonstrated that block of endocytosis delays the recruitment of readily releasable vesicles. These effects are observed on time scales too small to be accounted for by the non-availability of recycled SVs (Hosoi et al., 2009). It was hence postulated that a step linking endo- and exocytosis is required for efficient vesicle docking at specialized release sites. This step likely involves release site replenishment (Hosoi et al., 2009). Along with Dynamin, both the adaptor protein AP2 and the Ca^{2+} sensor Synaptotagmin 2 are needed in this process (Hosoi et al., 2009). Thus, Dynamin might well be involved in the clearance of release sites (Fig. 3A) from SV material – independent of fission activity – to guarantee the rapid reuse of these sites at AZs.

Koenig and Ikeda have published several papers (Koenig and Ikeda, 1996; Koenig et al., 1983; Koenig et al., 1998), focusing on the morphology of AZs after recovery from temperature sensitive Dynamin-blockade. They observed local invaginations in close proximity to the AZ center marked by the BRP-formed T bar (Fouquet et al., 2009). This process appears to be Ca^{2+} dependent, and furthermore high levels of extracellular $[Mg^{2+}]$ seem sufficient to suppress such phenotypes (Koenig and Ikeda, 1996). In an interesting parallel, tubular invaginations are observable in *br*p^{c04298} mutants that still comprise the N-terminal Dynamin-interacting domain (data not shown). Dynamins have been shown to exert several functions. As mentioned above, amongst those are tubulation and fission reactions. The fission reaction is believed to depend on GTP hydrolysis (Praefcke and McMahon, 2004). The residual BRP detected in *br*p^{c04298} mutants does not seem to target properly to the AZ center and is not sufficient for T-bar formation (Fig. 7C). It might be intriguing to explain the tubule observed in these *brp* alleles in relation to misguided Dynamin function.

Thus, BRP might enrich GTP-Dynamin locally at AZs, which might be released after stimulus [e.g. stimulus-mediated Ca^{2+} influx (Daly and Ziff, 2002)], to either take a role in e.g. Syntaxin recycling (Peters et al., 2004), release-site replenishment (Neher and Sakaba, 2008; Hosoi et al., 2009), or local kiss and run-like endocytosis [for a model see Fig. 37, (He and Wu, 2007; Zhang et al., 2009)]. Clearly, future work is needed to critically evaluate this hypothesis.

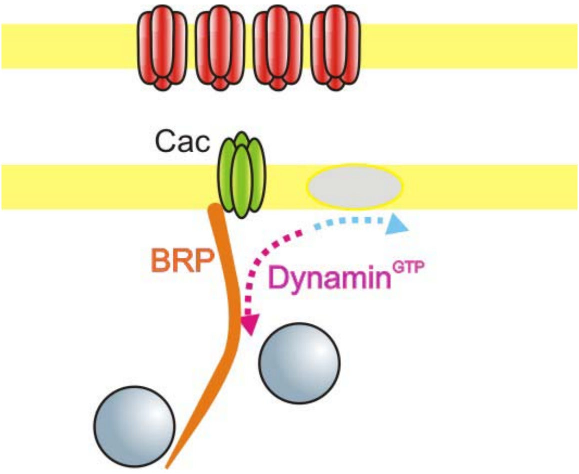

Fig. 37 Hypothesis: Dynamin and BRP interact physically
BRP might bind GTP-bound Dynamin via its GED, and thus inhibit hydrolization of GTP to GDP, keeping Dynamin in its active conformation. Stimuli (e.g. Ca^{2+}) might release $Dynamin^{GTP}$, which could then take its action either in slot clearance (blue arrow) or local endocytosis (magenta arrow).

5. Summary

The dissection of presynaptic assembly processes has proven difficult in the past. Apart from genetic redundancies, this likely reflects a highly cooperative and regulated nature of synapse assembly, complicating the straightforward deduction of linear molecular models. This study genetically dissects defined event hierarchies and assembly intermediates and complements these with biochemical, electrophysiological, ultrastructural and *in vivo* protein trafficking data.

Analysis of chemically-induced alleles of the active zone (AZ) protein BRP, positions it as a direct building block of the electron dense cytomatrix at the AZ (CAZ). An unbiased proteomics screen reveals that the RhoGAP DSyd-1 physically interacts with BRP and localizes to AZs. Moreover, DSyd-1 closely co-localizes with a further AZ protein, DLiprin-α.

Using transposon-based genetics two *dsyd-1* deficient alleles were synthesized. *dsyd-1* mutant animals elicit impaired locomotive behavior and a reduced life span, while NMJ synapse numbers and evoked synaptic currents are reduced. Furthermore, AZ morphology appears abnormal in *dsyd-1* deficient animals with the CAZ often appearing misshapen. Floating electron dense material is, moreover, found at ectopic positions.

In vivo imaging reveals that DSyd-1 and DLiprin-α accumulate early during synapse development, preceding postsynaptic glutamate receptor accumulation, as well as presynaptically localized BRP. Analysis of *dliprin-α; dsyd-1* double mutants indicates that overgrown BRP accumulations found in *dsyd-1* mutants are dependent on the presence of *dliprin-α*. In fact, defining a hierarchy of the two proteins, DLiprin-α localization is largely impaired in *dsyd-1* mutant animals, while DSyd-1 localizes normally in mutants for *dliprin-α*.

Unlike BRP, DLiprin-α and DSyd-1 clusters appear to be able to decompose again, indicating that early AZ assembly is still reversible. Thus, AZ assembly can be divided into an early, reversible step at nascent site and a later, largely irreversible maturation phase. DLiprin-α mobility is largely elevated in *dsyd-1* mutants, specifically indicating a clamping function of DSyd-1, which possibly shapes the transition between nascent and maturing synapses. Presynaptic DSyd-1 is further shown to regulate postsynaptic receptor field composition, increasing the amount of slow desensitizing IIA subunit-containing glutamate receptor complexes. This process is independent of DLiprin-α. Following phenotypic similarities, *Drosophila* Neurexin is proposed as a further DSyd-1 substrate. Indeed, postsynaptic Neuroligin1, a potential DNrx interactor, is identified as localizing towards the edge of postsynaptic densities here. Mutants in *dnlg1* exhibit aberrant NMJ morphology with increased sizes of postsynaptic densities, impaired neurotransmission and boutons lacking postsynaptic receptor fields. Such “orphan” boutons are also occasionally found in *dsyd-1* mutants. Moreover, DNlg1 immunoreactivity is drastically reduced in the absence of DSyd-1. It thus appears likely that presynaptic DSyd-1 regulates the levels of postsynaptic DNlg1, potentially via presynaptic DNrx.

In a proteomics approach, the GTPase Dynamin is uncovered as a potential interactor of BRP. This physical interaction is confirmed *in vitro*. The interaction platform is fine-mapped to an N-terminal 30 aa of BRP and the GTPase effector domain along with a domain towards the very C-term of Dynamin. This interaction might link the BRP-based CAZ to the SV exo/endo-cycle.

6. References

Aberle, H., Haghighi, A.P., Fetter, R.D., McCabe, B.D., Magalhaes, T.R., and Goodman, C.S. (2002). wishful thinking encodes a BMP type II receptor that regulates synaptic growth in Drosophila. Neuron *33*, 545-558.

Adams, M.D., Celniker, S.E., Holt, R.A., Evans, C.A., Gocayne, J.D., Amanatides, P.G., Scherer, S.E., Li, P.W., Hoskins, R.A., Galle, R.F., *et al.* (2000). The genome sequence of Drosophila melanogaster. Science *287*, 2185-2195.

Akaaboune, M., Culican, S.M., Turney, S.G., and Lichtman, J.W. (1999). Rapid and reversible effects of activity on acetylcholine receptor density at the neuromuscular junction in vivo. Science *286*, 503-507.

Akins, M.R., and Biederer, T. (2006). Cell-cell interactions in synaptogenesis. Curr Opin Neurobiol *16*, 83-89.

Aravamudan, B., Fergestad, T., Davis, W.S., Rodesch, C.K., and Broadie, K. (1999). Drosophila UNC-13 is essential for synaptic transmission. Nat Neurosci *2*, 965-971.

Ataman, B., Ashley, J., Gorczyca, M., Ramachandran, P., Fouquet, W., Sigrist, S.J., and Budnik, V. (2008). Rapid activity-dependent modifications in synaptic structure and function require bidirectional Wnt signaling. Neuron *57*, 705-718.

Atwood, H.L., Govind, C.K., and Wu, C.F. (1993). Differential ultrastructure of synaptic terminals on ventral longitudinal abdominal muscles in Drosophila larvae. J Neurobiol *24*, 1008-1024.

Atwood, H.L., and Karunanithi, S. (2002). Diversification of synaptic strength: presynaptic elements. Nat Rev Neurosci *3*, 497-516.

Banovic, D., Korramshahi, O., Owald, D., Wichmann, C., Riedt, T., Tian, R., Sigrist, S.J., and Aberle, H. (2010). Drosophila Neuroligin 1 coordinates pre- and postsynaptic assembly. submitted.

Barry, M.F., and Ziff, E.B. (2002). Receptor trafficking and the plasticity of excitatory synapses. Curr Opin Neurobiol *12*, 279-286.

Bate, M., Rushton, E., and Frasch, M. (1993). A dual requirement for neurogenic genes in Drosophila myogenesis. Dev Suppl, 149-161.

Bellen, H.J., Levis, R.W., Liao, G., He, Y., Carlson, J.W., Tsang, G., Evans-Holm, M., Hiesinger, P.R., Schulze, K.L., Rubin, G.M.*, et al.* (2004). The BDGP gene disruption project: single transposon insertions associated with 40% of Drosophila genes. Genetics *167*, 761-781.

Bennett, M.R. (1999). The early history of the synapse: from Plato to Sherrington. Brain Res Bull *50*, 95-118.

Betz, A., Ashery, U., Rickmann, M., Augustin, I., Neher, E., Sudhof, T.C., Rettig, J., and Brose, N. (1998). Munc13-1 is a presynaptic phorbol ester receptor that enhances neurotransmitter release. Neuron *21*, 123-136.

Bliss, T.V., and Lomo, T. (1973). Long-lasting potentiation of synaptic transmission in the dentate area of the anaesthetized rabbit following stimulation of the perforant path. J Physiol *232*, 331-356.

Brand, A.H., and Perrimon, N. (1993). Targeted gene expression as a means of altering cell fates and generating dominant phenotypes. Development *118*, 401-415.

Broadie, K., and Bate, M. (1993a). Activity-dependent development of the neuromuscular synapse during Drosophila embryogenesis. Neuron *11*, 607-619.

Broadie, K., and Bate, M. (1993b). Innervation directs receptor synthesis and localization in Drosophila embryo synaptogenesis. Nature *361*, 350-353.

Broadie, K., and Bate, M. (1993c). Muscle development is independent of innervation during Drosophila embryogenesis. Development *119*, 533-543.

Broadie, K.S. (1995). Genetic dissection of the molecular mechanisms of transmitter vesicle release during synaptic transmission. J Physiol Paris *89*, 59-70.

Calakos, N., Schoch, S., Sudhof, T.C., and Malenka, R.C. (2004). Multiple roles for the active zone protein RIM1alpha in late stages of neurotransmitter release. Neuron *42*, 889-896.

Caroni, P., and Scheiffele, P. (2008). Neuronal polarity, the establishment and function of neuronal subdomains, and how these are prominent targets of disease. Editorial overview. Curr Opin Neurobiol *18*, 469-471.

Cases-Langhoff, C., Voss, B., Garner, A.M., Appeltauer, U., Takei, K., Kindler, S., Veh, R.W., De Camilli, P., Gundelfinger, E.D., and Garner, C.C. (1996). Piccolo, a novel 420 kDa protein associated with the presynaptic cytomatrix. Eur J Cell Biol *69*, 214-223.

Castillo, P.E., Schoch, S., Schmitz, F., Sudhof, T.C., and Malenka, R.C. (2002). RIM1alpha is required for presynaptic long-term potentiation. Nature *415*, 327-330.

Catterall, W.A. (1998). Structure and function of neuronal Ca2+ channels and their role in neurotransmitter release. Cell Calcium *24*, 307-323.

Chao, D.L., and Shen, K. (2008). Functional dissection of SYG-1 and SYG-2, cell adhesion molecules required for selective synaptogenesis in C. elegans. Mol Cell Neurosci *39*, 248-257.

Cingolani, L.A., and Goda, Y. (2008). Actin in action: the interplay between the actin cytoskeleton and synaptic efficacy. Nat Rev Neurosci *9*, 344-356.

Collingridge, G.L., and Bliss, T.V. (1995). Memories of NMDA receptors and LTP. Trends Neurosci *18*, 54-56.

Collins, C.A., and DiAntonio, A. (2007). Synaptic development: insights from Drosophila. Curr Opin Neurobiol *17*, 35-42.

Colon-Ramos, D.A., Margeta, M.A., and Shen, K. (2007). Glia promote local synaptogenesis through UNC-6 (netrin) signaling in C. elegans. Science *318*, 103-106.

Couteaux, R., and Pecot-Dechavassine, M. (1970). [Synaptic vesicles and pouches at the level of "active zones" of the neuromuscular junction]. C R Acad Sci Hebd Seances Acad Sci D *271*, 2346-2349.

Dai, Y., Taru, H., Deken, S.L., Grill, B., Ackley, B., Nonet, M.L., and Jin, Y. (2006). SYD-2 Liprin-alpha organizes presynaptic active zone formation through ELKS. Nat Neurosci *9*, 1479-1487.

Dalva, M.B., Takasu, M.A., Lin, M.Z., Shamah, S.M., Hu, L., Gale, N.W., and Greenberg, M.E. (2000). EphB receptors interact with NMDA receptors and regulate excitatory synapse formation. Cell *103*, 945-956.

Daly, C., and Ziff, E.B. (2002). Ca2+-dependent formation of a dynamin-synaptophysin complex: potential role in synaptic vesicle endocytosis. J Biol Chem *277*, 9010-9015.

Daniels, R.W., Collins, C.A., Gelfand, M.V., Dant, J., Brooks, E.S., Krantz, D.E., and DiAntonio, A. (2004). Increased expression of the Drosophila vesicular glutamate transporter leads to excess glutamate release and a compensatory decrease in quantal content. J Neurosci *24*, 10466-10474.

Davis, G.W., and Goodman, C.S. (1998). Genetic analysis of synaptic development and plasticity: homeostatic regulation of synaptic efficacy. Curr Opin Neurobiol *8*, 149-156.

De Roo, M., Klauser, P., and Muller, D. (2008). LTP promotes a selective long-term stabilization and clustering of dendritic spines. PLoS Biol *6*, e219.

Deken, S.L., Vincent, R., Hadwiger, G., Liu, Q., Wang, Z.W., and Nonet, M.L. (2005). Redundant localization mechanisms of RIM and ELKS in Caenorhabditis elegans. J Neurosci *25*, 5975-5983.

Del Castillo, J., and Katz, B. (1954). Quantal components of the end-plate potential. J Physiol *124*, 560-573.

Delgado, R., Maureira, C., Oliva, C., Kidokoro, Y., and Labarca, P. (2000). Size of vesicle pools, rates of mobilization, and recycling at neuromuscular synapses of a Drosophila mutant, shibire. Neuron *28*, 941-953.

DiAntonio, A. (2006). Glutamate receptors at the Drosophila neuromuscular junction. Int Rev Neurobiol *75*, 165-179.

Dickman, D.K., Horne, J.A., Meinertzhagen, I.A., and Schwarz, T.L. (2005). A slowed classical pathway rather than kiss-and-run mediates endocytosis at synapses lacking synaptojanin and endophilin. Cell *123*, 521-533.

Dresbach, T., Torres, V., Wittenmayer, N., Altrock, W.D., Zamorano, P., Zuschratter, W., Nawrotzki, R., Ziv, N.E., Garner, C.C., and Gundelfinger, E.D. (2006). Assembly of active zone precursor vesicles: obligatory trafficking of presynaptic cytomatrix proteins Bassoon and Piccolo via a trans-Golgi compartment. J Biol Chem *281*, 6038-6047.

Durand, C.M., Betancur, C., Boeckers, T.M., Bockmann, J., Chaste, P., Fauchereau, F., Nygren, G., Rastam, M., Gillberg, I.C., Anckarsater, H.*, et al.* (2007). Mutations in the gene encoding the synaptic scaffolding protein SHANK3 are associated with autism spectrum disorders. Nat Genet *39*, 25-27.

Eaton, B.A., and Davis, G.W. (2003). Synapse disassembly. Genes Dev *17*, 2075-2082.

Eaton, B.A., Fetter, R.D., and Davis, G.W. (2002). Dynactin is necessary for synapse stabilization. Neuron *34*, 729-741.

Eissenberg, J.C., Wong, M., and Chrivia, J.C. (2005). Human SRCAP and Drosophila melanogaster DOM are homologs that function in the notch signaling pathway. Mol Cell Biol *25*, 6559-6569.

Estes, P.S., Roos, J., van der Bliek, A., Kelly, R.B., Krishnan, K.S., and Ramaswami, M. (1996). Traffic of dynamin within individual Drosophila synaptic boutons relative to compartment-specific markers. J Neurosci *16*, 5443-5456.

Fang, Q., Berberian, K., Gong, L.W., Hafez, I., Sorensen, J.B., and Lindau, M. (2008). The role of the C terminus of the SNARE protein SNAP-25 in fusion pore opening and a model for fusion pore mechanics. Proc Natl Acad Sci U S A *105*, 15388-15392.

Featherstone, D.E., and Broadie, K. (2000). Surprises from Drosophila: genetic mechanisms of synaptic development and plasticity. Brain Res Bull *53*, 501-511.

Feeney, C.J., Karunanithi, S., Pearce, J., Govind, C.K., and Atwood, H.L. (1998). Motor nerve terminals on abdominal muscles in larval flesh flies, Sarcophaga bullata: comparisons with Drosophila. J Comp Neurol *402*, 197-209.

Fiala, J.C. (2005). Reconstruct: a free editor for serial section microscopy. J Microsc *218*, 52-61.

Foster, M. (1897). with Sherrington, C. S. A textbook of physiology, part 116 BENNETT three: The central nervous system. Macmillan and Co Ltd 7th ed.

Fouquet, W., Owald, D., Wichmann, C., Mertel, S., Depner, H., Dyba, M., Hallermann, S., Kittel, R.J., Eimer, S., and Sigrist, S.J. (2009). Maturation of active zone assembly by Drosophila Bruchpilot. J Cell Biol *186*, 129-145.

Frank, C.A., Kennedy, M.J., Goold, C.P., Marek, K.W., and Davis, G.W. (2006). Mechanisms underlying the rapid induction and sustained expression of synaptic homeostasis. Neuron *52*, 663-677.

Frank, C.A., Pielage, J., and Davis, G.W. (2009a). A presynaptic homeostatic signaling system composed of the Eph receptor, ephexin, Cdc42, and CaV2.1 calcium channels. Neuron *61*, 556-569.

Frank, T., Khimich, D., Neef, A., and Moser, T. (2009b). Mechanisms contributing to synaptic Ca2+ signals and their heterogeneity in hair cells. Proc Natl Acad Sci U S A *106*, 4483-4488.

Friedman, A.H. (1971). Circumstances influencing Otto Loewi's discovery of chemical transmission in the nervous system. Pflugers Arch *325*, 85-86.

Friedman, H.V., Bresler, T., Garner, C.C., and Ziv, N.E. (2000). Assembly of new individual excitatory synapses: time course and temporal order of synaptic molecule recruitment. Neuron *27*, 57-69.

Frischknecht, R., Heine, M., Perrais, D., Seidenbecher, C.I., Choquet, D., and Gundelfinger, E.D. (2009). Brain extracellular matrix affects AMPA receptor lateral mobility and short-term synaptic plasticity. Nat Neurosci *12*, 897-904.

Fuger, P., Behrends, L.B., Mertel, S., Sigrist, S.J., and Rasse, T.M. (2007). Live imaging of synapse development and measuring protein dynamics using two-color fluorescence recovery after photo-bleaching at Drosophila synapses. Nat Protoc *2*, 3285-3298.

Galvani, L. (1791). De viribus electricitatis in motu musculari commentarius. De Bononiensi Scientiarum Artium Instituto Academia Commentarii *7*, 363– 418.

Garber, K. (2007). Neuroscience. Autism's cause may reside in abnormalities at the synapse. Science *317*, 190-191.

Garner, C.C., Waites, C.L., and Ziv, N.E. (2006). Synapse development: still looking for the forest, still lost in the trees. Cell Tissue Res *326*, 249-262.

Gerrow, K., Romorini, S., Nabi, S.M., Colicos, M.A., Sala, C., and El-Husseini, A. (2006). A preformed complex of postsynaptic proteins is involved in excitatory synapse development. Neuron *49*, 547-562.

Gilestro, G.F., Tononi, G., and Cirelli, C. (2009). Widespread changes in synaptic markers as a function of sleep and wakefulness in Drosophila. Science *324*, 109-112.

Gillingham, A.K., and Munro, S. (2003). Long coiled-coil proteins and membrane traffic. Biochim Biophys Acta *1641*, 71-85.

Goda, Y., and Davis, G.W. (2003). Mechanisms of synapse assembly and disassembly. Neuron *40*, 243-264.

Gottmann, K., Mittmann, T., and Lessmann, V. (2009). BDNF signaling in the formation, maturation and plasticity of glutamatergic and GABAergic synapses. Exp Brain Res *199*, 203-234.

Graf, E.R., Daniels, R.W., Burgess, R.W., Schwarz, T.L., and DiAntonio, A. (2009). Rab3 dynamically controls protein composition at active zones. Neuron *64*, 663-677.

Graf, E.R., Zhang, X., Jin, S.X., Linhoff, M.W., and Craig, A.M. (2004). Neurexins induce differentiation of GABA and glutamate postsynaptic specializations via neuroligins. Cell *119*, 1013-1026.

Gray, N.W., Weimer, R.M., Bureau, I., and Svoboda, K. (2006). Rapid redistribution of synaptic PSD-95 in the neocortex in vivo. PLoS Biol *4*, e370.

Guan, R., Dai, H., and Rizo, J. (2008). Binding of the Munc13-1 MUN domain to membrane-anchored SNARE complexes. Biochemistry *47*, 1474-1481.

Hallam, S.J., Goncharov, A., McEwen, J., Baran, R., and Jin, Y. (2002). SYD-1, a presynaptic protein with PDZ, C2 and rhoGAP-like domains, specifies axon identity in C. elegans. Nat Neurosci *5*, 1137-1146.

Harlow, M.L., Ress, D., Stoschek, A., Marshall, R.M., and McMahan, U.J. (2001). The architecture of active zone material at the frog's neuromuscular junction. Nature *409*, 479-484.

He, L., and Wu, L.G. (2007). The debate on the kiss-and-run fusion at synapses. Trends Neurosci *30*, 447-455.

Heine, M., Thoumine, O., Mondin, M., Tessier, B., Giannone, G., and Choquet, D. (2008). Activity-independent and subunit-specific recruitment of functional AMPA receptors at neurexin/neuroligin contacts. Proc Natl Acad Sci U S A *105*, 20947-20952.

Heisenberg, M. (2003). Mushroom body memoir: from maps to models. Nat Rev Neurosci *4*, 266-275.

Hell, S.W. (2007). Far-field optical nanoscopy. Science *316*, 1153-1158.

Helmholtz, H. (1850). Messungen uber den zeitlichen Verlauf der Zuchung animalischer Muskeln und die Fortpflanzungsgeschwindigkeit der Reizung in den Nerven. Arch Anat Physiol, 277–364.

Herbert, M.R. (2005). Large brains in autism: the challenge of pervasive abnormality. Neuroscientist *11*, 417-440.

Heuser, J.E., and Reese, T.S. (1973). Evidence for recycling of synaptic vesicle membrane during transmitter release at the frog neuromuscular junction. J Cell Biol *57*, 315-344.

Hiesinger, P.R., Zhai, R.G., Zhou, Y., Koh, T.W., Mehta, S.Q., Schulze, K.L., Cao, Y., Verstreken, P., Clandinin, T.R., Fischbach, K.F., *et al.* (2006). Activity-independent prespecification of synaptic partners in the visual map of Drosophila. Curr Biol *16*, 1835-1843.

Hodgkin, A.L., and Huxley, A.F. (1952). A quantitative description of membrane current and its application to conduction and excitation in nerve. J Physiol *117*, 500-544.

Hofbauer, A., Ebel, T., Waltenspiel, B., Oswald, P., Chen, Y.C., Halder, P., Biskup, S., Lewandrowski, U., Winkler, C., Sickmann, A.*, et al.* (2009). The Wuerzburg hybridoma library against Drosophila brain. J Neurogenet *23*, 78-91.

Holt, M., Riedel, D., Stein, A., Schuette, C., and Jahn, R. (2008). Synaptic vesicles are constitutively active fusion machines that function independently of Ca2+. Curr Biol *18*, 715-722.

Hormuzdi, S.G., Filippov, M.A., Mitropoulou, G., Monyer, H., and Bruzzone, R. (2004). Electrical synapses: a dynamic signaling system that shapes the activity of neuronal networks. Biochim Biophys Acta *1662*, 113-137.

Hosoi, N., Holt, M., and Sakaba, T. (2009). Calcium dependence of exo- and endocytotic coupling at a glutamatergic synapse. Neuron *63*, 216-229.

Hubel, D.H., and Wiesel, T.N. (1959). Receptive fields of single neurones in the cat's striate cortex. J Physiol *148*, 574-591.

Ichtchenko, K., Hata, Y., Nguyen, T., Ullrich, B., Missler, M., Moomaw, C., and Sudhof, T.C. (1995). Neuroligin 1: a splice site-specific ligand for beta-neurexins. Cell *81*, 435-443.

Jamain, S., Radyushkin, K., Hammerschmidt, K., Granon, S., Boretius, S., Varoqueaux, F., Ramanantsoa, N., Gallego, J., Ronnenberg, A., Winter, D.*, et al.* (2008). Reduced social interaction and ultrasonic communication in a mouse model of monogenic heritable autism. Proc Natl Acad Sci U S A *105*, 1710-1715.

Jin, Y., and Garner, C.C. (2008). Molecular mechanisms of presynaptic differentiation. Annu Rev Cell Dev Biol *24*, 237-262.

Johnson, E.L., 3rd, Fetter, R.D., and Davis, G.W. (2009). Negative regulation of active zone assembly by a newly identified SR protein kinase. PLoS Biol *7*, e1000193.

Kaeser, P.S., Deng, L., Chavez, A.E., Liu, X., Castillo, P.E., and Sudhof, T.C. (2009). ELKS2alpha/CAST deletion selectively increases neurotransmitter release at inhibitory synapses. Neuron *64*, 227-239.

Kalla, S., Stern, M., Basu, J., Varoqueaux, F., Reim, K., Rosenmund, C., Ziv, N.E., and Brose, N. (2006). Molecular dynamics of a presynaptic active zone protein studied in Munc13-1-enhanced yellow fluorescent protein knock-in mutant mice. J Neurosci *26*, 13054-13066.

Katz, B., and Miledi, R. (1965). The Effect of Calcium on Acetylcholine Release from Motor Nerve Terminals. Proc R Soc Lond B Biol Sci *161*, 496-503.

Katz, L.C., and Shatz, C.J. (1996). Synaptic activity and the construction of cortical circuits. Science *274*, 1133-1138.

Kaufmann, N., DeProto, J., Ranjan, R., Wan, H., and Van Vactor, D. (2002). Drosophila liprin-alpha and the receptor phosphatase Dlar control synapse morphogenesis. Neuron *34*, 27-38.

Kawasaki, F., Collins, S.C., and Ordway, R.W. (2002). Synaptic calcium-channel function in Drosophila: analysis and transformation rescue of temperature-sensitive paralytic and lethal mutations of cacophony. J Neurosci *22*, 5856-5864.

Kawasaki, F., Hazen, M., and Ordway, R.W. (2000). Fast synaptic fatigue in shibire mutants reveals a rapid requirement for dynamin in synaptic vesicle membrane trafficking. Nat Neurosci *3*, 859-860.

Kawasaki, F., and Ordway, R.W. (2009). Molecular mechanisms determining conserved properties of short-term synaptic depression revealed in NSF and SNAP-25 conditional mutants. Proc Natl Acad Sci U S A *106*, 14658-14663.

Khimich, D., Nouvian, R., Pujol, R., Tom Dieck, S., Egner, A., Gundelfinger, E.D., and Moser, T. (2005). Hair cell synaptic ribbons are essential for synchronous auditory signalling. Nature *434*, 889-894.

Kittel, R.J., Wichmann, C., Rasse, T.M., Fouquet, W., Schmidt, M., Schmid, A., Wagh, D.A., Pawlu, C., Kellner, R.R., Willig, K.I.*, et al.* (2006). Bruchpilot promotes active zone assembly, Ca2+ channel clustering, and vesicle release. Science *312*, 1051-1054.

Kiyonaka, S., Wakamori, M., Miki, T., Uriu, Y., Nonaka, M., Bito, H., Beedle, A.M., Mori, E., Hara, Y., De Waard, M.*, et al.* (2007). RIM1 confers sustained activity and neurotransmitter vesicle anchoring to presynaptic Ca2+ channels. Nat Neurosci *10*, 691-701.

Klein, R. (2009). Bidirectional modulation of synaptic functions by Eph/ephrin signaling. Nat Neurosci *12*, 15-20.

Knott, G., and Holtmaat, A. (2008). Dendritic spine plasticity--current understanding from in vivo studies. Brain Res Rev *58*, 282-289.

Ko, J., Na, M., Kim, S., Lee, J.R., and Kim, E. (2003). Interaction of the ERC family of RIM-binding proteins with the liprin-alpha family of multidomain proteins. J Biol Chem *278*, 42377-42385.

Koenig, J.H., and Ikeda, K. (1996). Synaptic vesicles have two distinct recycling pathways. J Cell Biol *135*, 797-808.

Koenig, J.H., Saito, K., and Ikeda, K. (1983). Reversible control of synaptic transmission in a single gene mutant of Drosophila melanogaster. J Cell Biol *96*, 1517-1522.

Koenig, J.H., Yamaoka, K., and Ikeda, K. (1998). Omega images at the active zone may be endocytotic rather than exocytotic: implications for the vesicle hypothesis of transmitter release. Proc Natl Acad Sci U S A *95*, 12677-12682.

Korkut, C., Ataman, B., Ramachandran, P., Ashley, J., Barria, R., Gherbesi, N., and Budnik, V. (2009). Trans-synaptic transmission of vesicular Wnt signals through Evi/Wntless. Cell *139*, 393-404.

Krueger, S.R., Kolar, A., and Fitzsimonds, R.M. (2003). The presynaptic release apparatus is functional in the absence of dendritic contact and highly mobile within isolated axons. Neuron *40*, 945-957.

Leal-Ortiz, S., Waites, C.L., Terry-Lorenzo, R., Zamorano, P., Gundelfinger, E.D., and Garner, C.C. (2008). Piccolo modulation of Synapsin1a dynamics regulates synaptic vesicle exocytosis. J Cell Biol *181*, 831-846.

Li, J., Ashley, J., Budnik, V., and Bhat, M.A. (2007). Crucial role of Drosophila neurexin in proper active zone apposition to postsynaptic densities, synaptic growth, and synaptic transmission. Neuron *55*, 741-755.

Liebl, F.L., Chen, K., Karr, J., Sheng, Q., and Featherstone, D.E. (2005). Increased synaptic microtubules and altered synapse development in Drosophila sec8 mutants. BMC Biol *3*, 27.

Lim, B.K., Matsuda, N., and Poo, M.M. (2008). Ephrin-B reverse signaling promotes structural and functional synaptic maturation in vivo. Nat Neurosci *11*, 160-169.

Lim, S.H., Kwon, S.K., Lee, M.K., Moon, J., Jeong, D.G., Park, E., Kim, S.J., Park, B.C., Lee, S.C., Ryu, S.E., *et al.* (2009). Synapse formation regulated by protein tyrosine phosphatase receptor T through interaction with cell adhesion molecules and Fyn. EMBO J *28*, 3564-3578.

Littleton, J.T., Chapman, E.R., Kreber, R., Garment, M.B., Carlson, S.D., and Ganetzky, B. (1998). Temperature-sensitive paralytic mutations demonstrate that synaptic exocytosis requires SNARE complex assembly and disassembly. Neuron *21*, 401-413.

Luo, L. (2000). Rho GTPases in neuronal morphogenesis. Nat Rev Neurosci *1*, 173-180.

Magupalli, V.G., Schwarz, K., Alpadi, K., Natarajan, S., Seigel, G.M., and Schmitz, F. (2008). Multiple RIBEYE-RIBEYE interactions create a dynamic scaffold for the formation of synaptic ribbons. J Neurosci *28*, 7954-7967.

Mahr, A., and Aberle, H. (2006). The expression pattern of the Drosophila vesicular glutamate transporter: a marker protein for motoneurons and glutamatergic centers in the brain. Gene Expr Patterns *6*, 299-309.

Margeta, M.A., Shen, K., and Grill, B. (2008). Building a synapse: lessons on synaptic specificity and presynaptic assembly from the nematode C. elegans. Curr Opin Neurobiol *18*, 69-76.

Marrus, S.B., Portman, S.L., Allen, M.J., Moffat, K.G., and DiAntonio, A. (2004). Differential localization of glutamate receptor subunits at the Drosophila neuromuscular junction. J Neurosci *24*, 1406-1415.

Mayford, M., Mansuy, I.M., Muller, R.U., and Kandel, E.R. (1997). Memory and behavior: a second generation of genetically modified mice. Curr Biol *7*, R580-589.

McCabe, B.D., Marques, G., Haghighi, A.P., Fetter, R.D., Crotty, M.L., Haerry, T.E., Goodman, C.S., and O'Connor, M.B. (2003). The BMP homolog Gbb provides a retrograde signal that regulates synaptic growth at the Drosophila neuromuscular junction. Neuron *39*, 241-254.

Meinrenken, C.J., Borst, J.G., and Sakmann, B. (2003). Local routes revisited: the space and time dependence of the Ca2+ signal for phasic transmitter release at the rat calyx of Held. J Physiol *547*, 665-689.

Micheva, K.D., Buchanan, J., Holz, R.W., and Smith, S.J. (2003). Retrograde regulation of synaptic vesicle endocytosis and recycling. Nat Neurosci *6*, 925-932.

Miller, K.E., DeProto, J., Kaufmann, N., Patel, B.N., Duckworth, A., and Van Vactor, D. (2005). Direct observation demonstrates that Liprin-alpha is required for trafficking of synaptic vesicles. Curr Biol *15*, 684-689.

Minerbi, A., Kahana, R., Goldfeld, L., Kaufman, M., Marom, S., and Ziv, N.E. (2009). Long-term relationships between synaptic tenacity, synaptic remodeling, and network activity. PLoS Biol *7*, e1000136.

Missler, M., Zhang, W., Rohlmann, A., Kattenstroth, G., Hammer, R.E., Gottmann, K., and Sudhof, T.C. (2003). Alpha-neurexins couple Ca2+ channels to synaptic vesicle exocytosis. Nature *423*, 939-948.

Moebius, J., Denker, K., and Sickmann, A. (2007). Ruthenium (II) tris-bathophenanthroline disulfonate is well suitable for Tris-Glycine PAGE but not for Bis-Tris gels. Proteomics *7*, 524-527.

Monier, S., Jollivet, F., Janoueix-Lerosey, I., Johannes, L., and Goud, B. (2002). Characterization of novel Rab6-interacting proteins involved in endosome-to-TGN transport. Traffic *3*, 289-297.

Nagerl, U.V., Kostinger, G., Anderson, J.C., Martin, K.A., and Bonhoeffer, T. (2007). Protracted synaptogenesis after activity-dependent spinogenesis in hippocampal neurons. J Neurosci *27*, 8149-8156.

Nakamura, N., Lowe, M., Levine, T.P., Rabouille, C., and Warren, G. (1997). The vesicle docking protein p115 binds GM130, a cis-Golgi matrix protein, in a mitotically regulated manner. Cell *89*, 445-455.

Narayanan, R., Leonard, M., Song, B.D., Schmid, S.L., and Ramaswami, M. (2005). An internal GAP domain negatively regulates presynaptic dynamin in vivo: a two-step model for dynamin function. J Cell Biol *169*, 117-126.

Neher, E., and Sakaba, T. (2008). Multiple roles of calcium ions in the regulation of neurotransmitter release. Neuron *59*, 861-872.

Neher, E., and Sakmann, B. (1976). Single-channel currents recorded from membrane of denervated frog muscle fibres. Nature *260*, 799-802.

Nicoll, R.A., and Schmitz, D. (2005). Synaptic plasticity at hippocampal mossy fibre synapses. Nat Rev Neurosci *6*, 863-876.

Nieratschker, V., Schubert, A., Jauch, M., Bock, N., Bucher, D., Dippacher, S., Krohne, G., Asan, E., Buchner, S., and Buchner, E. (2009). Bruchpilot in ribbon-like axonal agglomerates, behavioral defects, and early death in SRPK79D kinase mutants of Drosophila. PLoS Genet *5*, e1000700.

Ohtsuka, T., Takao-Rikitsu, E., Inoue, E., Inoue, M., Takeuchi, M., Matsubara, K., Deguchi-Tawarada, M., Satoh, K., Morimoto, K., Nakanishi, H.*, et al.* (2002). Cast: a novel protein of the cytomatrix at the active zone of synapses that forms a ternary complex with RIM1 and munc13-1. J Cell Biol *158*, 577-590.

Okabe, S., Miwa, A., and Okado, H. (2001). Spine formation and correlated assembly of presynaptic and postsynaptic molecules. J Neurosci *21*, 6105-6114.

Owald, D., Fouquet, W., Schmidt, M., Wichmann, C., Mertel, S., Depner, H., Christiansen, F., Zube, C., Quentin, C., Korner, J.*, et al.* (2010). A Syd-1 homologue regulates pre- and postsynaptic maturation in Drosophila. J Cell Biol *188*, 565-579.

Owald, D., and Sigrist, S.J. (2009). Assembling the presynaptic active zone. Curr Opin Neurobiol *19*, 311-318.

Pack-Chung, E., Kurshan, P.T., Dickman, D.K., and Schwarz, T.L. (2007). A Drosophila kinesin required for synaptic bouton formation and synaptic vesicle transport. Nat Neurosci *10*, 980-989.

Packard, M., Mathew, D., and Budnik, V. (2003). Wnts and TGF beta in synaptogenesis: old friends signalling at new places. Nat Rev Neurosci *4*, 113-120.

Parks, A.L., Cook, K.R., Belvin, M., Dompe, N.A., Fawcett, R., Huppert, K., Tan, L.R., Winter, C.G., Bogart, K.P., Deal, J.E.*, et al.* (2004). Systematic generation of high-resolution deletion coverage of the Drosophila melanogaster genome. Nat Genet *36*, 288-292.

Patel, M.R., Lehrman, E.K., Poon, V.Y., Crump, J.G., Zhen, M., Bargmann, C.I., and Shen, K. (2006). Hierarchical assembly of presynaptic components in defined C. elegans synapses. Nat Neurosci *9*, 1488-1498.

Patel, M.R., and Shen, K. (2009). RSY-1 is a local inhibitor of presynaptic assembly in C. elegans. Science *323*, 1500-1503.

Pawlu, C., DiAntonio, A., and Heckmann, M. (2004). Postfusional control of quantal current shape. Neuron *42*, 607-618.

Pawson, C., Eaton, B.A., and Davis, G.W. (2008). Formin-dependent synaptic growth: evidence that Dlar signals via Diaphanous to modulate synaptic actin and dynamic pioneer microtubules. J Neurosci *28*, 11111-11123.

Peters, C., Baars, T.L., Buhler, S., and Mayer, A. (2004). Mutual control of membrane fission and fusion proteins. Cell *119*, 667-678.

Petersen, S.A., Fetter, R.D., Noordermeer, J.N., Goodman, C.S., and DiAntonio, A. (1997). Genetic analysis of glutamate receptors in Drosophila reveals a retrograde signal regulating presynaptic transmitter release. Neuron *19*, 1237-1248.

Phillips, G.R., Huang, J.K., Wang, Y., Tanaka, H., Shapiro, L., Zhang, W., Shan, W.S., Arndt, K., Frank, M., Gordon, R.E.*, et al.* (2001). The presynaptic particle web: ultrastructure, composition, dissolution, and reconstitution. Neuron *32*, 63-77.

Pilling, A.D., Horiuchi, D., Lively, C.M., and Saxton, W.M. (2006). Kinesin-1 and Dynein are the primary motors for fast transport of mitochondria in Drosophila motor axons. Mol Biol Cell *17*, 2057-2068.

Polleux, F., and Lauder, J.M. (2004). Toward a developmental neurobiology of autism. Ment Retard Dev Disabil Res Rev *10*, 303-317.

Praefcke, G.J., and McMahon, H.T. (2004). The dynamin superfamily: universal membrane tubulation and fission molecules? Nat Rev Mol Cell Biol *5*, 133-147.

Prakash, S., McLendon, H.M., Dubreuil, C.I., Ghose, A., Hwa, J., Dennehy, K.A., Tomalty, K.M., Clark, K.L., Van Vactor, D., and Clandinin, T.R. (2009). Complex interactions amongst N-cadherin, DLAR, and Liprin-alpha regulate Drosophila photoreceptor axon targeting. Dev Biol *336*, 10-19.

Prokop, A. (2006). Organization of the efferent system and structure of neuromuscular junctions in Drosophila. Int Rev Neurobiol *75*, 71-90.

Prokop, A., Landgraf, M., Rushton, E., Broadie, K., and Bate, M. (1996). Presynaptic development at the Drosophila neuromuscular junction: assembly and localization of presynaptic active zones. Neuron *17*, 617-626.

Qin, G., Schwarz, T., Kittel, R.J., Schmid, A., Rasse, T.M., Kappei, D., Ponimaskin, E., Heckmann, M., and Sigrist, S.J. (2005). Four different subunits are essential for expressing the synaptic glutamate receptor at neuromuscular junctions of Drosophila. J Neurosci *25*, 3209-3218.

Rasse, T.M., Fouquet, W., Schmid, A., Kittel, R.J., Mertel, S., Sigrist, C.B., Schmidt, M., Guzman, A., Merino, C., Qin, G.*, et al.* (2005). Glutamate receptor dynamics organizing synapse formation in vivo. Nat Neurosci *8*, 898-905.

Regus-Leidig, H., Tom Dieck, S., Specht, D., Meyer, L., and Brandstatter, J.H. (2009). Early steps in the assembly of photoreceptor ribbon synapses in the mouse retina: the involvement of precursor spheres. J Comp Neurol *512*, 814-824.

Reiff, D.F., Thiel, P.R., and Schuster, C.M. (2002). Differential regulation of active zone density during long-term strengthening of Drosophila neuromuscular junctions. J Neurosci *22*, 9399-9409.

Renner, M., Specht, C.G., and Triller, A. (2008). Molecular dynamics of postsynaptic receptors and scaffold proteins. Curr Opin Neurobiol *18*, 532-540.

Rheuben, M.B., Yoshihara, M., and Kidokoro, Y. (1999). Ultrastructural correlates of neuromuscular junction development. Int Rev Neurobiol *43*, 69-92.

Rieckhof, G.E., Yoshihara, M., Guan, Z., and Littleton, J.T. (2003). Presynaptic N-type calcium channels regulate synaptic growth. J Biol Chem *278*, 41099-41108.

Ritzenthaler, S., Suzuki, E., and Chiba, A. (2000). Postsynaptic filopodia in muscle cells interact with innervating motoneuron axons. Nat Neurosci *3*, 1012-1017.

Rizo, J., and Rosenmund, C. (2008). Synaptic vesicle fusion. Nat Struct Mol Biol *15*, 665-674.

Rizzoli, S.O., and Betz, W.J. (2005). Synaptic vesicle pools. Nat Rev Neurosci *6*, 57-69.

Rizzoli, S.O., and Jahn, R. (2007). Kiss-and-run, collapse and 'readily retrievable' vesicles. Traffic *8*, 1137-1144.

Rosenmund, C., Rettig, J., and Brose, N. (2003). Molecular mechanisms of active zone function. Curr Opin Neurobiol *13*, 509-519.

Rostaing, P., Real, E., Siksou, L., Lechaire, J.P., Boudier, T., Boeckers, T.M., Gertler, F., Gundelfinger, E.D., Triller, A., and Marty, S. (2006). Analysis of synaptic ultrastructure without fixative using high-pressure freezing and tomography. Eur J Neurosci *24*, 3463-3474.

Saitoe, M., Tanaka, S., Takata, K., and Kidokoro, Y. (1997). Neural activity affects distribution of glutamate receptors during neuromuscular junction formation in Drosophila embryos. Dev Biol *184*, 48-60.

Sambrook, J., Fritsch, E.F., and Maniatis, T. (1989). Molecular cloning: a laboratory manual, Vol 3, 2 edn (Cold Spring Harbor Laboratory, New York).

Sanyal, S., Tolar, L.A., Pallanck, L., and Krishnan, K.S. (2001). Genetic interaction between shibire and comatose mutations in Drosophila suggest a role for snap-receptor complex assembly and disassembly for maintenance of synaptic vesicle cycling. Neurosci Lett *311*, 21-24.

Satzler, K., Sohl, L.F., Bollmann, J.H., Borst, J.G., Frotscher, M., Sakmann, B., and Lubke, J.H. (2002). Three-dimensional reconstruction of a calyx of Held and its postsynaptic principal neuron in the medial nucleus of the trapezoid body. J Neurosci *22*, 10567-10579.

Scheiffele, P., Fan, J., Choih, J., Fetter, R., and Serafini, T. (2000). Neuroligin expressed in nonneuronal cells triggers presynaptic development in contacting axons. Cell *101*, 657-669.

Schluter, O.M., Schmitz, F., Jahn, R., Rosenmund, C., and Sudhof, T.C. (2004). A complete genetic analysis of neuronal Rab3 function. J Neurosci *24*, 6629-6637.

Schmid, A., Hallermann, S., Kittel, R.J., Khorramshahi, O., Frolich, A.M., Quentin, C., Rasse, T.M., Mertel, S., Heckmann, M., and Sigrist, S.J. (2008). Activity-dependent site-specific changes of glutamate receptor composition in vivo. Nat Neurosci *11*, 659-666.

Schmid, A., Qin, G., Wichmann, C., Kittel, R.J., Mertel, S., Fouquet, W., Schmidt, M., Heckmann, M., and Sigrist, S.J. (2006). Non-NMDA-type glutamate receptors are essential for maturation but not for initial assembly of synapses at Drosophila neuromuscular junctions. J Neurosci *26*, 11267-11277.

Schmid, E.M., and McMahon, H.T. (2007). Integrating molecular and network biology to decode endocytosis. Nature *448*, 883-888.

Schmidt, M. (2006). Characterization of synaptic protein complexes in Drosophila melanogaster. PhD thesis *Universitaet Goettingen*.

Schmitz, F., Konigstorfer, A., and Sudhof, T.C. (2000). RIBEYE, a component of synaptic ribbons: a protein's journey through evolution provides insight into synaptic ribbon function. Neuron *28*, 857-872.

Schneggenburger, R., and Neher, E. (2005). Presynaptic calcium and control of vesicle fusion. Curr Opin Neurobiol *15*, 266-274.

Schoch, S., Castillo, P.E., Jo, T., Mukherjee, K., Geppert, M., Wang, Y., Schmitz, F., Malenka, R.C., and Sudhof, T.C. (2002). RIM1alpha forms a protein scaffold for regulating neurotransmitter release at the active zone. Nature *415*, 321-326.

Schoch, S., and Gundelfinger, E.D. (2006). Molecular organization of the presynaptic active zone. Cell Tissue Res *326*, 379-391.

Schuster, C.M. (2006). Experience-dependent potentiation of larval neuromuscular synapses. Int Rev Neurobiol *75*, 307-322.

Seeburg, P.H. (1993). The TINS/TiPS Lecture. The molecular biology of mammalian glutamate receptor channels. Trends Neurosci *16*, 359-365.

Shapira, M., Zhai, R.G., Dresbach, T., Bresler, T., Torres, V.I., Gundelfinger, E.D., Ziv, N.E., and Garner, C.C. (2003). Unitary assembly of presynaptic active zones from Piccolo-Bassoon transport vesicles. Neuron *38*, 237-252.

Shen, K., Fetter, R.D., and Bargmann, C.I. (2004). Synaptic specificity is generated by the synaptic guidepost protein SYG-2 and its receptor, SYG-1. Cell *116*, 869-881.

Shi, S.H., Hayashi, Y., Petralia, R.S., Zaman, S.H., Wenthold, R.J., Svoboda, K., and Malinow, R. (1999). Rapid spine delivery and redistribution of AMPA receptors after synaptic NMDA receptor activation. Science *284*, 1811-1816.

Shin, H., Wyszynski, M., Huh, K.H., Valtschanoff, J.G., Lee, J.R., Ko, J., Streuli, M., Weinberg, R.J., Sheng, M., and Kim, E. (2003). Association of the kinesin motor KIF1A with the multimodular protein liprin-alpha. J Biol Chem *278*, 11393-11401.

Siddiqi, O., and Benzer, S. (1976). Neurophysiological defects in temperature-sensitive paralytic mutants of Drosophila melanogaster. Proc Natl Acad Sci U S A *73*, 3253-3257.

Sigrist, S.J., Reiff, D.F., Thiel, P.R., Steinert, J.R., and Schuster, C.M. (2003). Experience-dependent strengthening of Drosophila neuromuscular junctions. J Neurosci *23*, 6546-6556.

Sigrist, S.J., Thiel, P.R., Reiff, D.F., Lachance, P.E., Lasko, P., and Schuster, C.M. (2000). Postsynaptic translation affects the efficacy and morphology of neuromuscular junctions. Nature *405*, 1062-1065.

Sigrist, S.J., Thiel, P.R., Reiff, D.F., and Schuster, C.M. (2002). The postsynaptic glutamate receptor subunit DGluR-IIA mediates long-term plasticity in Drosophila. J Neurosci *22*, 7362-7372.

Siksou, L., Rostaing, P., Lechaire, J.P., Boudier, T., Ohtsuka, T., Fejtova, A., Kao, H.T., Greengard, P., Gundelfinger, E.D., Triller, A.*, et al.* (2007). Three-dimensional architecture of presynaptic terminal cytomatrix. J Neurosci *27*, 6868-6877.

Sorensen, J.B., Wiederhold, K., Muller, E.M., Milosevic, I., Nagy, G., de Groot, B.L., Grubmuller, H., and Fasshauer, D. (2006). Sequential N- to C-terminal SNARE complex assembly drives priming and fusion of secretory vesicles. EMBO J *25*, 955-966.

Sotelo, C. (2003). Viewing the brain through the master hand of Ramon y Cajal. Nat Rev Neurosci *4*, 71-77.

Spangler, S.A., and Hoogenraad, C.C. (2007). Liprin-alpha proteins: scaffold molecules for synapse maturation. Biochem Soc Trans *35*, 1278-1282.

Stewart, B.A., Atwood, H.L., Renger, J.J., Wang, J., and Wu, C.F. (1994). Improved stability of Drosophila larval neuromuscular preparations in haemolymph-like physiological solutions. J Comp Physiol A *175*, 179-191.

Sudhof, T.C. (2004). The synaptic vesicle cycle. Annu Rev Neurosci *27*, 509-547.

Sudhof, T.C. (2008). Neuroligins and neurexins link synaptic function to cognitive disease. Nature *455*, 903-911.

Sweitzer, S.M., and Hinshaw, J.E. (1998). Dynamin undergoes a GTP-dependent conformational change causing vesiculation. Cell *93*, 1021-1029.

Sztul, E., and Lupashin, V. (2006). Role of tethering factors in secretory membrane traffic. Am J Physiol Cell Physiol *290*, C11-26.

Sztul, E., and Lupashin, V. (2009). Role of vesicle tethering factors in the ER-Golgi membrane traffic. FEBS Lett *583*, 3770-3783.

Takamori, S., Holt, M., Stenius, K., Lemke, E.A., Gronborg, M., Riedel, D., Urlaub, H., Schenck, S., Brugger, B., Ringler, P*., et al.* (2006). Molecular anatomy of a trafficking organelle. Cell *127*, 831-846.

Takao-Rikitsu, E., Mochida, S., Inoue, E., Deguchi-Tawarada, M., Inoue, M., Ohtsuka, T., and Takai, Y. (2004). Physical and functional interaction of the active zone proteins, CAST, RIM1, and Bassoon, in neurotransmitter release. J Cell Biol *164*, 301-311.

Tao-Cheng, J.H. (2006). Activity-related redistribution of presynaptic proteins at the active zone. Neuroscience *141*, 1217-1224.

Tao-Cheng, J.H. (2007). Ultrastructural localization of active zone and synaptic vesicle proteins in a preassembled multi-vesicle transport aggregate. Neuroscience *150*, 575-584.

Thompson, V. (1977). Recombination and response to selection in Drosophila melanogaster. Genetics *85*, 125-140.

tom Dieck, S., Sanmarti-Vila, L., Langnaese, K., Richter, K., Kindler, S., Soyke, A., Wex, H., Smalla, K.H., Kampf, U., Franzer, J.T*., et al.* (1998). Bassoon, a novel zinc-finger CAG/glutamine-repeat protein selectively localized at the active zone of presynaptic nerve terminals. J Cell Biol *142*, 499-509.

Toonen, R.F., and Verhage, M. (2007). Munc18-1 in secretion: lonely Munc joins SNARE team and takes control. Trends Neurosci *30*, 564-572.

Tsuriel, S., Fisher, A., Wittenmayer, N., Dresbach, T., Garner, C.C., and Ziv, N.E. (2009). Exchange and redistribution dynamics of the cytoskeleton of the active zone molecule bassoon. J Neurosci *29*, 351-358.

van Roessel, P., Elliott, D.A., Robinson, I.M., Prokop, A., and Brand, A.H. (2004). Independent regulation of synaptic size and activity by the anaphase-promoting complex. Cell *119*, 707-718.

Varoqueaux, F., Aramuni, G., Rawson, R.L., Mohrmann, R., Missler, M., Gottmann, K., Zhang, W., Sudhof, T.C., and Brose, N. (2006). Neuroligins determine synapse maturation and function. Neuron *51*, 741-754.

Verstreken, P., Kjaerulff, O., Lloyd, T.E., Atkinson, R., Zhou, Y., Meinertzhagen, I.A., and Bellen, H.J. (2002). Endophilin mutations block clathrin-mediated endocytosis but not neurotransmitter release. Cell *109*, 101-112.

Wadel, K., Neher, E., and Sakaba, T. (2007). The coupling between synaptic vesicles and Ca2+ channels determines fast neurotransmitter release. Neuron *53*, 563-575.

Wagh, D.A., Rasse, T.M., Asan, E., Hofbauer, A., Schwenkert, I., Durrbeck, H., Buchner, S., Dabauvalle, M.C., Schmidt, M., Qin, G*., et al.* (2006). Bruchpilot, a protein with homology to ELKS/CAST, is required for structural integrity and function of synaptic active zones in Drosophila. Neuron *49*, 833-844.

Wagner, O.I., Esposito, A., Kohler, B., Chen, C.W., Shen, C.P., Wu, G.H., Butkevich, E., Mandalapu, S., Wenzel, D., Wouters, F.S*., et al.* (2009). Synaptic scaffolding protein SYD-2 clusters and activates kinesin-3 UNC-104 in C. elegans. Proc Natl Acad Sci U S A *106*, 19605-19610.

Wairkar, Y.P., Toda, H., Mochizuki, H., Furukubo-Tokunaga, K., Tomoda, T., and Diantonio, A. (2009). Unc-51 controls active zone density and protein composition by downregulating ERK signaling. J Neurosci *29*, 517-528.

Wang, X., Hu, B., Zieba, A., Neumann, N.G., Kasper-Sonnenberg, M., Honsbein, A., Hultqvist, G., Conze, T., Witt, W., Limbach, C*., et al.* (2009). A protein interaction node at the neurotransmitter release site: domains of Aczonin/Piccolo, Bassoon, CAST, and rim converge on the N-terminal domain of Munc13-1. J Neurosci *29*, 12584-12596.

Weimer, R.M., Gracheva, E.O., Meyrignac, O., Miller, K.G., Richmond, J.E., and Bessereau, J.L. (2006). UNC-13 and UNC-10/rim localize synaptic vesicles to specific membrane domains. J Neurosci *26*, 8040-8047.

Woehler, A., and Ponimaskin, E.G. (2009). G protein--mediated signaling: same receptor, multiple effectors. Curr Mol Pharmacol *2*, 237-248.

Woo, J., Kwon, S.K., Choi, S., Kim, S., Lee, J.R., Dunah, A.W., Sheng, M., and Kim, E. (2009). Trans-synaptic adhesion between NGL-3 and LAR regulates the formation of excitatory synapses. Nat Neurosci *12*, 428-437.

Wu, Y., Kawasaki, F., and Ordway, R.W. (2005). Properties of short-term synaptic depression at larval neuromuscular synapses in wild-type and temperature-sensitive paralytic mutants of Drosophila. J Neurophysiol *93*, 2396-2405.

Wyszynski, M., Kim, E., Dunah, A.W., Passafaro, M., Valtschanoff, J.G., Serra-Pages, C., Streuli, M., Weinberg, R.J., and Sheng, M. (2002). Interaction between GRIP and liprin-alpha/SYD2 is required for AMPA receptor targeting. Neuron *34*, 39-52.

Xue, M., Lin, Y.Q., Pan, H., Reim, K., Deng, H., Bellen, H.J., and Rosenmund, C. (2009). Tilting the balance between facilitatory and inhibitory functions of mammalian and Drosophila Complexins orchestrates synaptic vesicle exocytosis. Neuron *64*, 367-380.

y Cajal, S.R. (1894). The Croonian Lecture: La Fine Structure des Centres Nerveux. Proceedings of the Royal Society of London *55*, 444-468.

Yamakawa, H., Seog, D.H., Yoda, K., Yamasaki, M., and Wakabayashi, T. (1996). Uso1 protein is a dimer with two globular heads and a long coiled-coil tail. J Struct Biol *116*, 356-365.

Yeh, E., Gustafson, K., and Boulianne, G.L. (1995). Green fluorescent protein as a vital marker and reporter of gene expression in Drosophila. Proc Natl Acad Sci U S A *92*, 7036-7040.

Yoshihara, M., Adolfsen, B., Galle, K.T., and Littleton, J.T. (2005). Retrograde signaling by Syt 4 induces presynaptic release and synapse-specific growth. Science *310*, 858-863.

Zampighi, G.A., Fain, N., Zampighi, L.M., Cantele, F., Lanzavecchia, S., and Wright, E.M. (2008). Conical electron tomography of a chemical synapse: polyhedral cages dock vesicles to the active zone. J Neurosci *28*, 4151-4160.

Zhai, R.G., and Bellen, H.J. (2004). The architecture of the active zone in the presynaptic nerve terminal. Physiology (Bethesda) *19*, 262-270.

Zhai, R.G., Vardinon-Friedman, H., Cases-Langhoff, C., Becker, B., Gundelfinger, E.D., Ziv, N.E., and Garner, C.C. (2001). Assembling the presynaptic active zone: a characterization of an active one precursor vesicle. Neuron *29*, 131-143.

Zhang, Q., Li, Y., and Tsien, R.W. (2009). The dynamic control of kiss-and-run and vesicular reuse probed with single nanoparticles. Science *323*, 1448-1453.

Zhen, M., and Jin, Y. (1999). The liprin protein SYD-2 regulates the differentiation of presynaptic termini in C. elegans. Nature *401*, 371-375.

Zito, K., Parnas, D., Fetter, R.D., Isacoff, E.Y., and Goodman, C.S. (1999). Watching a synapse grow: noninvasive confocal imaging of synaptic growth in Drosophila. Neuron *22*, 719-729.

Zito, K., Scheuss, V., Knott, G., Hill, T., and Svoboda, K. (2009). Rapid functional maturation of nascent dendritic spines. Neuron *61*, 247-258.

7. Figure Index

Fig. 1 AZ ultrastructure **9**

Fig. 2 Proteins implicated in AZ assembly **12**

Fig. 3 The SV exo/endo-cycle **17**

Fig. 4 The larval nervous system **23**

Fig. 5 The *Drosophila* NMJ **24**

Fig. 6 Genomic analysis of the *brp* locus **40**

Fig. 7 AZ organization of different *brp* alleles **41**

Fig. 8 *brp*^{c04298} physiology **43**

Fig. 9 Identification of *Drosophila* Syd-1 as an interactor of BRP **44**

Fig. 10 The DSyd-1 protein **45**

Fig. 11 *dsyd-1* deficient flies **46**

Fig. 12 DSyd-1 localizes to AZs **47**

Fig. 13 High DSyd-1 levels in young larvae **48**

Fig. 14 Physiological analysis of *dsyd-1* and *dliprin-*α mutant NMJs **50**

Fig. 15 SV distribution and size is mildly affected, while NMJ size is reduced in *dsyd-1* **52**

Fig. 16 Abnormal BRP clusters at *dsyd-1* mutant NMJs 54

Fig. 17 Abnormal organization of T bar and electron dense material in *dsyd-1* mutant animals 55

Fig. 18 Ectopic BRP and DVGlut co-localize in *dsyd-1* mutant axons 57

Fig. 19 DSyd-1 regulates AZ size dependent on, and PSD size independent of DLiprin-α 58

Fig. 20 Temporal model of DLiprin-α, BRP and glutamate receptor assembly at *Drosophila* NMJs 60

Fig. 21 DSyd-1 accumulates early during AZ formation 62

Fig. 22 Reversible assembly of nascent AZs 63

Fig. 23 DLiprin-α is highly mobile in *dsyd-1* mutants 66

Fig. 24 DSyd-1 controls postsynaptic glutamate receptor field size and composition 69

Fig. 25 Decay constants in *dsyd-1* animals resemble those of DGluRIIA-dominated NMJs 70

Fig. 26 Individual boutons lack postsynaptic receptor fields in *dsyd-1* mutants 71

Fig. 27 *Drosophila* Neuroligin 1 72

Fig. 28 DNlg1 localizes adjacent to postsynaptic glutamate receptor fields 73

Fig. 29 *dnlg1* and *dnrx* mutans show elevated levels of postsynaptic glutamate receptors 74

Fig. 30 Impaired neurotransmission in *dnlg1* mutants 76

Fig. 31 DNlg1 immunoreactivity is reduced in *dsyd-1* animals 77

Fig. 32 Optimization of BRP solubilization 78

Fig. 33 Dynamin interacts with BRP 79

Fig. 34 The GED of Dynamin interacts with an N-terminal BRP domain 80

Fig. 35 Model of early AZ formation 94

Fig. 36 Model of AZ formation and transsynaptic communication in *Drosophila* 98

Fig. 37 Hypothesis: Dynamin and BRP interact physically 102

8. Abbreviations

a.u.	arbitrary units
aa	amino acid
AB	antibody
AChE	acetylcholine esterase
AMPA	α-amino-3-hydroxyl-5-methyl-4-isoxazole-propionate
AP	action potential
AP2	adaptor protein 2
ASD	autism spectrum disorders
AZ	active zone
B.C.	before christ
BRP	Bruchpilot
C. elegans	*Caenorhabditis elegans*
C1	phorbol ester/diacylglycerol binding domain
C2	calcium-binding motif
Cac	Cacophony
CamKII	calcium/calmodulin-dependent protein kinase II
cAMP	cyclic adenosine monophosphate
CAST	CAZ-associated structural protein
CAZ	cytomatrix at the AZ
CC	coiled coil
Cd8GFP-Sh	Cd8GFP-Shaker
CS	C-terminal sequence
CtBP2	C-terminal-binding protein 2
cx	cortex
DCC	Deleted in Colorectal Cancer
DOC	deoxycholate
DVGlut	*Drosophila* vesicular glutamate transporter
eEJC	evoked excitatory junctional current
EKO	KCNA/Kv1
ELKS	Glutamate, Leucine, Lysine, Serine-rich protein
EM	electron microscopy
EMS	ethyl methanesulfonate
endo	endocytosis
ERC	ELKS–Rab6-interacting protein CAST
exo	exocytosis
GABA	γ-aminobutyric acid
GDP	Guanosine diphosphate
GED	GTPase effector domain
gf	gain of function
GFP	green fluorescent protein
GluR	glutamate receptor

GM130	Golgi matrix protein 130
G-protein	GTP-binding protein
GTP	Guanosine triphosphate
HL3	hemolymph-like solution
HPF/FS	High pressure frozen/freeze substituted
HRP	horseradish peroxidase
IgCAM	immunoglobulin cell adhesion molecule family
IgG	Immunoglobulin G
imac	immaculate connections
kDa	kilo Dalton
LAR	Leukocyte-antigen-related-like
LC	liquid chromatography
LTD	long-term depression
LTP	long-term potentiation
ME	micro electrode
mEJC	miniature excitatory junctional current
MS/MS	tandem mass spectrometry
mStraw	monomeric strawberry
Munc	Mammalian Unc
ne	nerve
Neph1	Nephrin 1
NGL	netrin-G ligand
NGS	normal goat serum
Nlg1	Neuroligin-1
NMDA	N-methyl-D-aspartic acid
NMJ	neuromuscular junction
np	neuropil
Nrx	Neurexin
NSF	N-ethylmaleimide-sensitive factor
PAA	polyacrylamide
PAGE	polyacrylamide gel electrophoresis
PBS	phosphate buffered saline
PBT	PBS with Triton
PCR	polymerase chain reaction
PRD	Proline-rich domain
PSD	postsynaptic density
PTV	Piccolo and Bassoon transport vesicle
RhoGAP	Rho GTPase activating protein
RIM	Rab3a-interacting molecule
RSy-1	Regulator of synaptogenesis–1
RT	room temperature
SAM	sterile-alpha-motif
SDS	sodium dodecyl sulfate
SerRR	Serine-rich region

SM	Sec1/Unc18/Munc18-1
SNAP-25	Synaptosomal-associated protein 25
SNARE	soluble NSF attachment protein receptors
SRPK79D	serine-threonine protein kinase
SSEM	serial section electron microscopy
SSR	sub synaptic reticulum
STED	stimulated emission depletion microscopy
SV	synaptic vesicle
Syb	Synaptobrevin
Syd-1	Synapse defective 1
Syd-2	Synapse defective 2
Syg	synaptogenesis abnormal
SynCAM1	Synaptic Cell Adhesion Molecule 1
TEVC	two electrode voltage clamp
TMD	transmembrane domain
TNT	tetanus toxin
t-SNARE	target membrane SNARE
UAS	upstream activating sequence
Unc	uncoordinated mutants
v-SNARE	Vesicle SNARE
Wnt	wingless
Y2H	yeast two-hybrid assay

9. *Curriculum Vitae*

David Owald was born on March 29th 1983 in Wolfenbüttel, Germany. He currently lives and works in Berlin.

Contact: david.owald@charite.de

2002	Allgemeine Hochschulreife (Abitur), Gymnasium Neue Oberschule, Braunschweig
2002 – 2005	Bachelor of Science (BSc) in Molecular Biotechnology, University of Heidelberg
2005 – present	MSc/PhD studies in Neurosciences at the University of Göttingen
2006 – 2008	European Neuroscience Institute and the Max-Planck-Institute for Biophysical Chemistry, Göttingen; Lab of Stephan Sigrist at the Rudolf-Virchow Center for Biomedical Research, Würzburg
2008 – present	Lab of Stephan Sigrist at the Charité and the Free University Berlin

10. Scientific Abstracts at International Conferences

Owald D., M. Schmidt, C. Wichmann, S. Mertel, W. Fouquet, F. Christiansen, K. Mechtler, M. Heckmann, S. J. Sigrist. *The Bruchpilot Protein in Assembly of Active Zone Structure and Function*. Molecular Dynamics of the Chemical Synapse, 20-23 August 2007, Westerburg, Germany

Owald D., M. Schmidt, C. Wichmann, S. Mertel, W. Fouquet, F. Christiansen, K. Mechtler, R. J. Kittel, M. Heckmann, S. J. Sigrist. *The Bruchpilot Protein in Assembly of Active Zone Structure and Function*. Neurobiology of *Drosophila*, 03-07 October 2007, Cold Spring Harbor, NY, USA

Owald D., W. Fouquet, M. Schmidt, C. Wichmann, F. Christiansen, H. Depner, J. Körner, S. Mertel and S. J. Sigrist. *Analysis of the Active Zone Protein DSyd-1*. Neurofly, 06-10 September 2008, Würzburg, Germany
Journal of Neurogenetics, 2009, Vol. 23, No. s1, Pages S1-S102, DOI 10.1080/01677060902742364

Owald D., W. Fouquet, M. Schmidt, C. Wichmann, F. Christiansen, H. Depner, S. Mertel and S. J. Sigrist. Spatio-Temporal Analysis of Active Zone Assembly in *Drosophila.* Axon Guidance, Synaptogenesis and Synaptic Plasticity, 10-14 September 2008, Cold Spring Harbor, NY, USA

11. Publications

Owald, D., and Sigrist, S.J. (2009). Assembling the presynaptic active zone. Curr Opin Neurobiol *19*, 311-318.

Fouquet, W.*, Owald, D.*, Wichmann, C., Mertel, S., Depner, H., Dyba, M., Hallermann, S., Kittel, R.J., Eimer, S., and Sigrist, S.J. (2009). Maturation of active zone assembly by Drosophila Bruchpilot. J Cell Biol *186*, 129-145.
** equal contribution*

Owald, D.*, Fouquet, W.*, Schmidt, M., Wichmann, C., Mertel, S., Depner, H., Christiansen, F., Zube, C., Quentin, C., Korner, J., Urlaub, H., Mechtler, K., and Sigrist, S.J. (2010). A Syd-1 homologue regulates pre- and postsynaptic maturation in Drosophila. J Cell Biol *188, 565-579*.
**equal contribution*

Banovic, D., Korramshahi, O., Owald, D., Wichmann, C., Riedt, T., Tian, R., Sigrist, S.J., and Aberle, H. (2010). Drosophila Neuroligin 1 coordinates pre- and postsynaptic assembly. *Submitted.*

Hallermann S., Kittel, R.J., Wichmann, C., Weyhersmüller, A., Fouquet, W., Mertel, S., Owald, D., Eimer, S., Depner, H., Schwärzel, M., Sigrist, S.J., and Heckmann, M. (2010). Naked dense bodies provoke depression within milliseconds. *Submitted.*